AD-A207 806

REPORT DOCUMENTATION PAGE

1a. REPORT SECURITY CLASSIFICATION	1b. RESTRICTIVE MARKINGS
U	NA

2a. SECURITY CLASSIFICATION AUTHORITY	3. DISTRIBUTION / AVAILABILITY OF REPORT
NA	Distribution Unlimited
2b. DECLASSIFICATION / DOWNGRADING SCHEDULE	
NA	

4. PERFORMING ORGANIZATION REPORT NUMBER(S)	5. MONITORING ORGANIZATION REPORT NUMBER(S)
NA	NA

6a. NAME OF PERFORMING ORGANIZATION	6b. OFFICE SYMBOL (If applicable)	7a. NAME OF MONITORING ORGANIZATION
National Institute of Standards and Technology	NIST	Office of Naval Research

6c. ADDRESS (City, State, and ZIP Code)	7b. ADDRESS (City, State, and ZIP Code)
Bldg. 245/B-119 Gaithersburg, MD 20899	800 N. Quincy Street Arlington, VA 22217-5000

8a. NAME OF FUNDING / SPONSORING ORGANIZATION Strategic Defense Initiative Organization	8b. OFFICE SYMBOL (If applicable)	9. PROCUREMENT INSTRUMENT IDENTIFICATION NUMBER
		N00014-87-F-0066

8c. ADDRESS (City, State, and ZIP Code)	10. SOURCE OF FUNDING NUMBERS

	PROGRAM ELEMENT NO.	PROJECT NO.	TASK NO.	WORK UNIT ACCESSION NO
Washington, DC 20301-7100	63222C			

11. TITLE (Include Security Classification)
Annual Report to the Strategic Defense Initiative Organization on the Free-Electron Laser Driven by the NIST CW Microtron

12. PERSONAL AUTHOR(S) Johnson, Ronald G.

13a. TYPE OF REPORT	13b. TIME COVERED	14. DATE OF REPORT (Year, Month, Day)	15. PAGE COUNT
Annual	FROM 4/1/88 TO 3/31/89	5/5/89	

16. SUPPLEMENTARY NOTATION

17. COSATI CODES			18. SUBJECT TERMS (Continue on reverse if necessary and identify by block number)
FIELD	GROUP	SUB-GROUP	Free electron laser, racetrack microtron

19. ABSTRACT (Continue on reverse if necessary and identify by block number)
Excellent progress has been made during the past year on all areas critical to the NIST-NRL FEL project. A contract for the construction of a wiggler was signed early in this reporting period. The contractor has completed the engineering design of the wiggler and is well along in construction. Several methods to increase the peak current in the RTM were studied. The conceptual design of the injector for the method selected was completed. A study on the problem of mirror damage has been completed, and commercial suppliers of mirrors that can withstand the high intracavity power of the FEL have been identified. The design of the room in which the FEL is located has been improved, and the design of the users area has been completed. Calculations of FEL performance have been extended to include short-pulse effects and the effects of wiggler magnetic field errors. A major activity in this period has been preparation of the RTM for one-pass acceleration to 17 MeV. One-pass tests were started, and preliminary measurements of beam quality were better than design goals by a factor of two.

20. DISTRIBUTION / AVAILABILITY OF ABSTRACT	21. ABSTRACT SECURITY CLASSIFICATION
[X] UNCLASSIFIED/UNLIMITED [ ] SAME AS RPT [ ] DTIC USERS	(U)

22a. NAME OF RESPONSIBLE INDIVIDUAL	22b. TELEPHONE (Include Area Code)	22c. OFFICE SYMBOL
Dr. Nick Montanarelli	(202) 693-1556	SDIO

DD FORM 1473, 84 MAR   83 APR edition may be used until exhausted.   SECURITY CLASSIFICATION OF THIS PAGE
All other editions are obsolete.

89 5 11 016

Annual Report

to the

Strategic Defense Initiative Organization

on the

Free-Electron Laser Driven by the NIST CW Microtron

for the period

April 1, 1988 to March 31, 1989

by the

U.S. Department of Commerce
National Institute of Standards and Technology*

and the

U.S. Department of Defense
Naval Research Laboratory

*formerly the National Bureau of Standards

May 5, 1989

TABLE OF CONTENTS

1. Project Goals

For this project we will construct and commission a free-electron laser (FEL) which will be driven by the NIST racetrack-microtron (RTM) electron accelerator. The RTM, radiation-shielded areas for the RTM and FEL, and experimental areas are being provided by NIST. Major elements of the project include: modifying the RTM injector for increased peak current; developing electron-beam transport from the RTM to the FEL; developing a wiggler and optical cavity; and developing optical-beam transport and diagnostics. An updated plan for the facility is shown in Figure 1.

2. Activities and Accomplishments

In general, excellent progress has been made during the past year on all areas critical to the project. This progress is summarized here and is presented in more detail in the following sections.

A contract for the construction of a wiggler was signed early in this reporting period. The contractor has completed the engineering design of the wiggler and is well along in construction. Several methods to increase the peak current in the RTM were studied. The conceptual design of the injector for the method selected was completed, and a detailed design was started. A study on the problem of mirror damage has been completed, and commercial suppliers of mirrors that can withstand the high intracavity power of the FEL have been identified. The design of the room in which the FEL is located has been improved, and design of the users area has been completed.

Calculations of FEL performance have been extended to include short-pulse effects and the effects of wiggler magnetic field errors. In the

RTM

E1
END MAGNET

12 MeV LINAC

E2
END MAGNET

KLYSTRON

ELECTRON
GUN

CHOPPER
BUNCHER

INJECTOR
LINAC

0   2   4 M
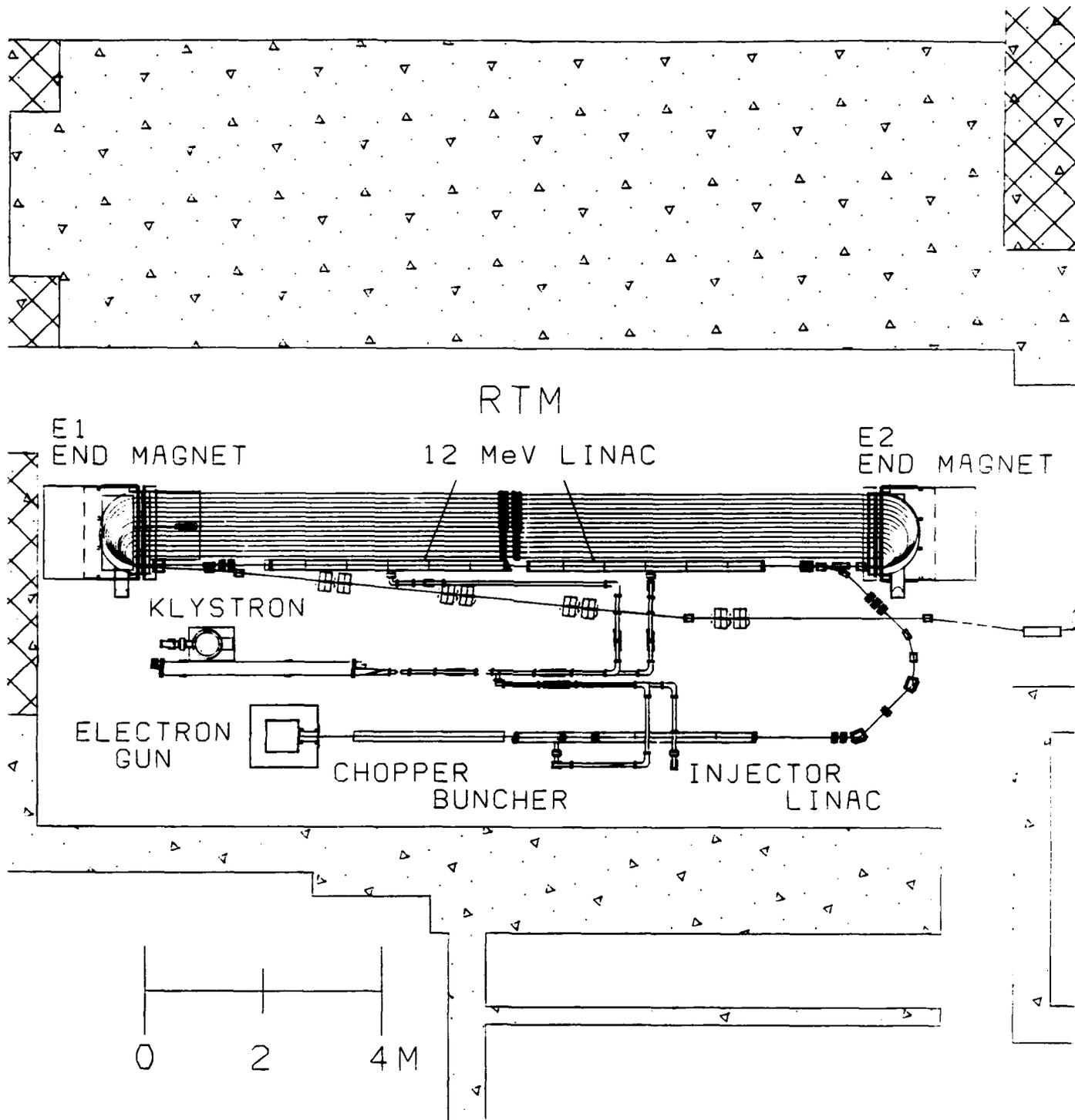
Figure 1.   Plan view of the NIST-NRL Free Electron
Laser facility.   (a.) RTM area.

2

BEAM DUMP

FEL
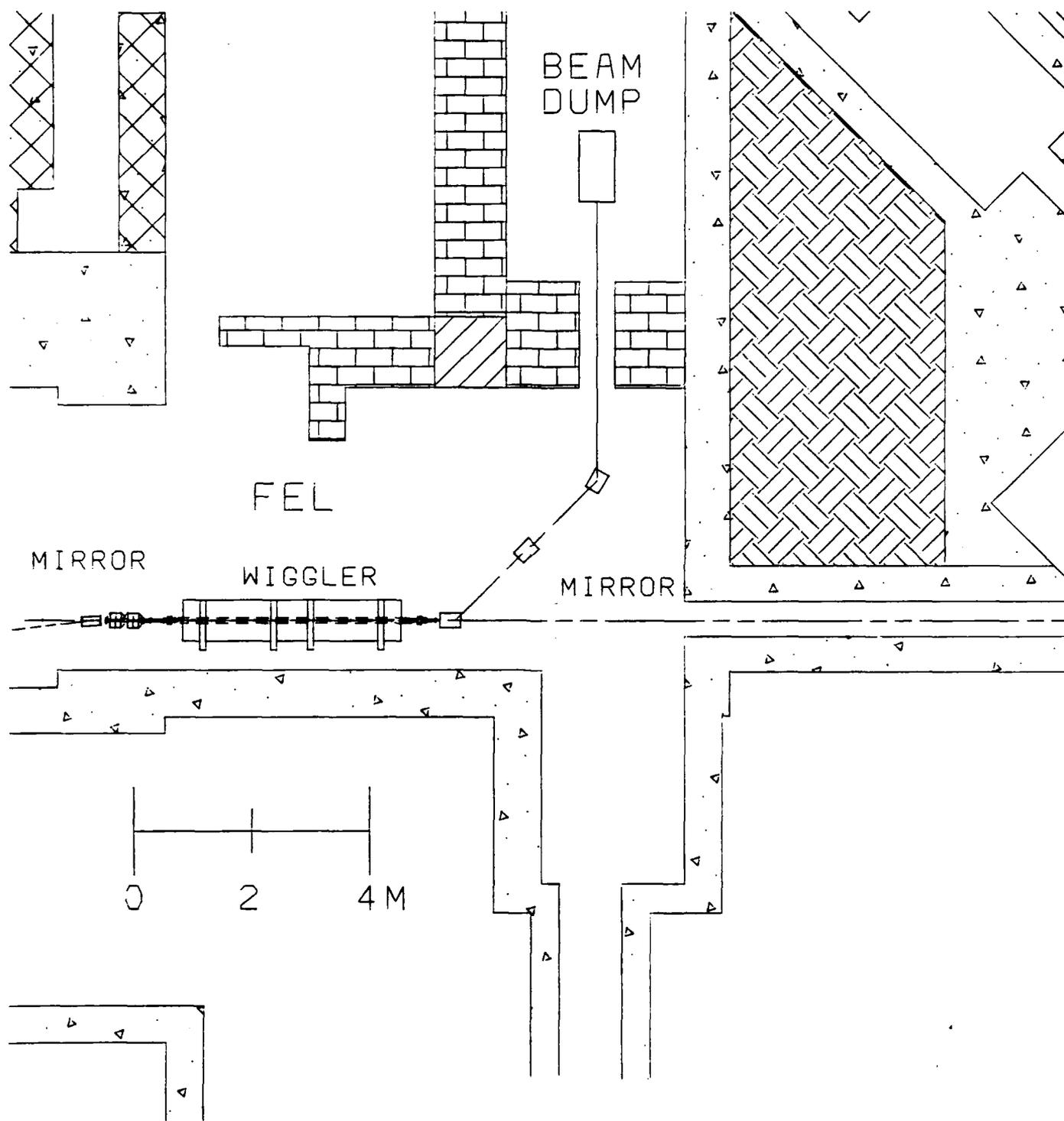
MIRROR   WIGGLER

MIRROR

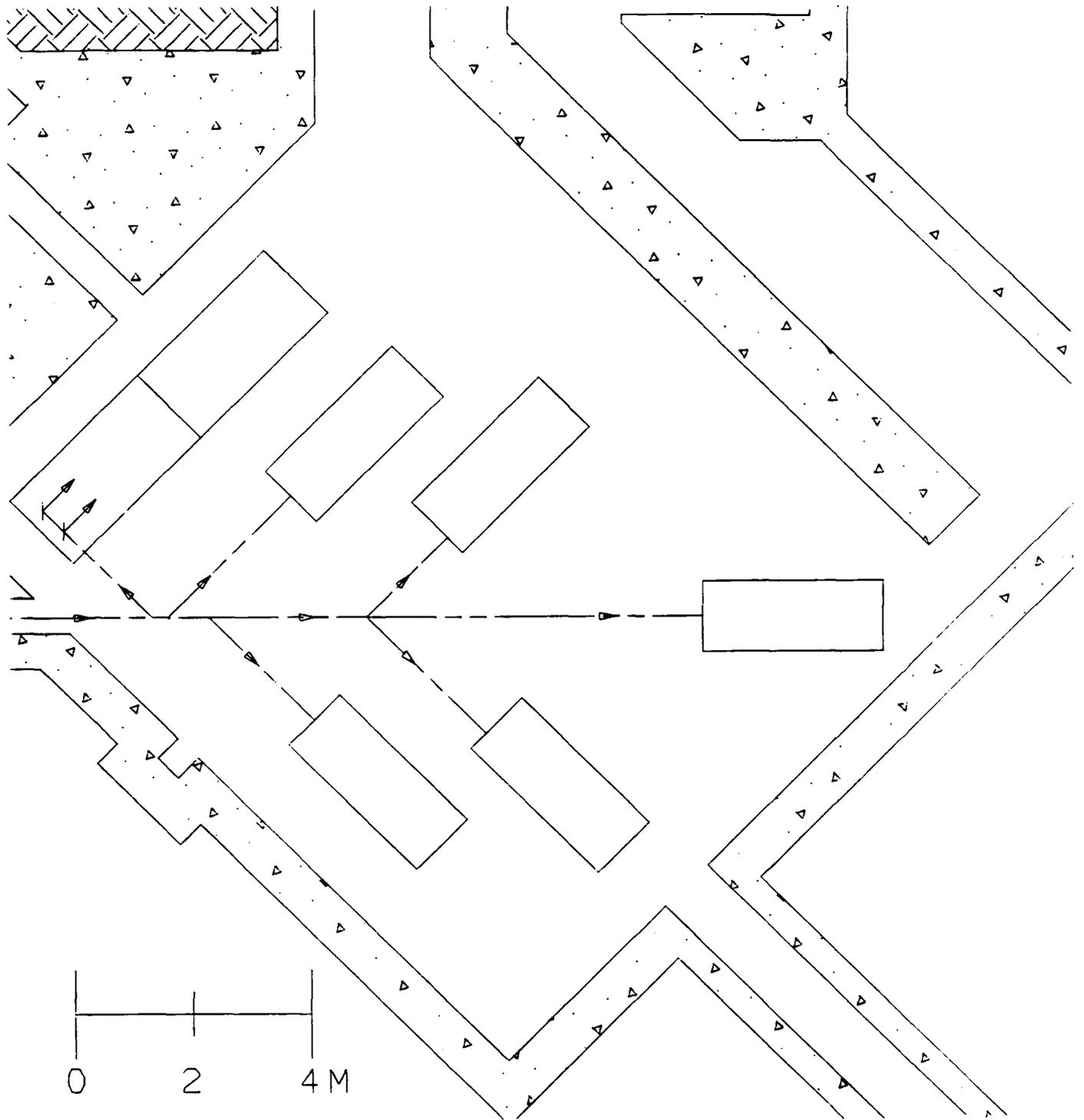0   2   4 M

Figure 1 (b.)   FEL area.

Figure 1 (c.) User area.

latter case the calculations have not yet included the full set of steering coils on the wiggler, but have modeled steering at the entrance of the wiggler.

A major activity in this period has been preparation of the RTM for one-pass acceleration to 17 MeV. One-pass tests were started, and preliminary measurements of beam quality were better than design goals by a factor of two. Completion of these tests has been delayed by the failure of a 1-MW transformer. The transformer has been repaired and completion of the one-pass tests will be done soon.

2.1 RTM and Electron Beam Transport

The RTM, which is described in Appendix E, consists of a 5-MeV injector feeding a microtron. In the microtron, a pair of 180° end magnets are used to recirculate the electron beam through a 12-MeV rf linac up to 15 times for an energy gain of up to 180 MeV. The beam can be extracted from any of 14 separate return lines in 12-MeV steps. The extracted electron beam is then transported to the FEL and then into the beam dump by the beam line shown in Figure 1(b.).

During the past year preparations were completed for one-pass beam tests, preliminary tests of the beam after one pass through the RTM linac were conducted, and fabrication of components on the RTM return lines was well advanced. An invited paper on the preliminary results of the one-pass beam tests was presented at the 1988 Linear Accelerator Conference, Williamsburg, VA, October 3-7, 1988, and a contributed paper on the performance of the rf system during the one-pass tests was presented at the same conference. In addition, designs are nearly complete for most

of the beam-transport elements on the extraction beam line, with procurements scheduled to begin within a month.

Preparation for single-pass acceleration by the RTM linac included completing the installation of all beam-transport elements and installing and leak checking the vacuum envelope on the linac axis. In addition, a temporary eight-meter-long beam line has been installed at the exit of end magnet E1 (Figure 4, Appendix E) with diagnostics for measuring the quality of the electron beam after one pass.

The results of preliminary one-pass tests with a low-average-power pulsed beam are presented in Appendix E. (These tests were performed at 16 MeV because rf conditioning of the linac had not been completed.) The full energy spread of the beam was measured to be only 18 keV, a factor of two better than the design goal of 36 keV. The measured, normalized, transverse emittance was 2.4 μm, a factor of two better than the design goal of 5 μm. The remaining one-pass beam tests are scheduled to begin in April. These tests include completion of beam energy-gain tests, completion of beam-quality measurement after optimizing the beam-transport system for minimum beam emittance and energy spread, and cw operation. Completion of these beam tests has been twice delayed; in December, 1988, and in February, 1989, by the failure of a 1-MW transformer in the power supply for the RTM klystron. (The function of the transformer that failed is to increase the ac voltage from 13 kV to 65 kV. The klystron provides 500 kW of continuous-wave microwave power for the injector linac and the RTM linac.) However, between failures the RTM linac was successfully conditioned to the required accelerating gradient of 1.5 MeV/m. The 1-MW transformer has been successfully repaired.

Delivery and testing of the coils for the return-line quadrupoles Q10 and Q11 (Figure 1, Appendix E) are nearly complete. Fabrication of the yoke and pole pieces by the NIST shops is expected to be completed within a month. Drawings of the return-line steerers, S19-S21, were submitted to the NIST shops at the end of March. The design of the movable deflecting magnet D11 is complete, as is the design of the first dipole magnet D12 on the extraction beam line (Figure 1, Appendix E). Design work is nearing completion on the 2-inch quadrupoles and dipoles D13 and D14 on the extraction line, and design work has begun on the remaining dipoles. In addition, the positions along the extraction line for all the beam-diagnostic devices and corrector coils have been established.

2.2 High Current Injector

The NIST-NRL FEL requires a peak electron current in the electron beam micropulse of 2 amperes twenty times that of the existing peak current, in order to meet the laser design goals. These design goals have also placed quite stringent requirements on the electron-beam emittance in order that reliable, stable FEL output can be achieved. In the past year, the design study for the High Current Injector (HCI) was completed and published[1] and the procurement process for the major components was initiated. The High Current Injector design makes use of known, proven technology similar to the existing RTM injector, and all components are readily available. The HCI design was modeled using the. computer program PARMELA, which simulated the transport of the electron beam from the electron gun through the injector linac taking into account space-charge effects present in a high current beam.

Several factors were considered in the design study of the HCI.
First of all, the beam current and emittance requirements have to be
achieved. Secondly, the HCI has to be reliable for use as a driver for
a FEL to be used in a user-based FEL facility. Third, the HCI must be
able to be constructed on schedule, so as not to delay the project. And
finally, overall cost must be reasonable. Three basic designs were
considered. The first, mentioned in our original proposal, used a laser
driven photocathode. While this design is attractive from a beam quality
standpoint, present research[2] has not shown sufficient lifetime or
average current for our intended use. Development costs to overcome
these problems would be high, and would take too much time. The second
design involved subharmonic bunching, which is used elsewhere[3] to
increase peak currents in a FEL. It was discovered, by modeling with
PARMELA, that this method put too much energy spread on the beam to meet
the longitudinal-emittance goal of the HCI. Also, the subharmonic-
buncher cavity would be large and inefficient, requiring a costly rf
system. The third design, which was adopted, is a new variation of the
system used for the existing RTM injector, and is called subharmonic
chopping. The subharmonic-injector design works as follows: A gridded
thermionic electron gun produces 2-ns long, 300-mA pulses at either
16.528 or 66.111 MHz. These 2-ns pulses are then chopped to 70 ps by a
subharmonic chopping system consisting of a 1/2 by 1/3 fundamental-
frequency deflecting cavity, an aperture located 0.5 meters away, and a
second 1/2 by 1/3 deflecting cavity located a further 0.5 meters away.
The first cavity causes the electron beam pulse to scan a Lissajous
figure (shown in Figure 1, Appendix G) at the aperture plane. Because
the period of the Lissajous figure is 2.5 ns, the Lissajous pattern

8

formed by the 2-ns beam pulse is not closed, and only crosses the center once per beam pulse. A properly sized aperture at the center thus can chop the beam to 70 ps. The beam is then focussed to the second chopping cavity, where the deflections of the first cavity are cancelled. Next, the beam is bunched by a 1/2 fundamental-frequency buncher to 15 ps at the entrance of the injector linac. Further bunching occurs in the two-section injector linac so that the beam emerges from the linac at 5 MeV with a length of 3.5 ps, and peak currents of 2-4 A. This design varies from our existing injector in only two major respects. First, the electron gun is pulsed, and has considerably higher current. This poses no problem, as thermionic guns with such outputs are available commercially. Second, subharmonic-deflecting cavities are used. Again, no problem is anticipated, as the University of Illinois successfully used such cavities at nearly the same frequency (2450 vs 2380 MHz fundamental)[4].

The subharmonic-chopper injector has been extensively modeled using PARMELA and has been found to produce electron beams that meet our design criteria for the FEL, both in current and in emittance. All components are of conventional, proven technology and are readily available. The design is similar enough to our existing system that we can anticipate few design or operational problems, and reliable cost estimates can be made for all components.

2.3 High-Current Effects in the RTM

The maximum beam current in recirculating electron accelerators such as the RTM is limited by beam breakup (BBU), i.e., unwanted deflection of the beam by modes in the rf structure other than the accelerating mode.

9

The design value of maximum average current in the RTM, 550 μA, is less than the estimated BBU limit for a micropulse frequency of 2380 MHz.[5] However, the BBU limit should be recalculated for operation of the RTM as an FEL driver with a micropulse frequency of 66.111 MHz. This is because there may be BBU modes that are resonant with harmonics of 66.111 MHz that are not harmonics of 2380 Mhz. Under a contract with us, Dr. Samuel Penner is developing a model for doing the calculation, as described in Appendix I. Preliminary results of these calculations indicate that average currents of 400 to 600 μA are not significantly affected by BBU for operation at 66.111 MHz. More accurate calculations are underway. Dr. Joseph Bisognano of CEBAF is also collaborating with us on this calculation.

2.4 Wiggler

The contract for construction of a wiggler was signed with Brobeck Division of Maxwell Labs on 12 May 1988. The first requirement of the contract was the design, construction, and testing of a model of the magnetic structure. The model was built and tested on schedule. A model magnet is used to test the magnetic design for the wiggler, i.e., peak field, harmonic content, and transverse uniformity. The results of the test exceeded the specifications for all these quantities. The measured peak field has a margin of 4.6% over the specified 0.54 T. For the harmonic content of the field, the measured values were: third harmonic 3.2%, fifth harmonic 0.5%, and negligible higher harmonics. These results are much better than the specification of 10%. Test results for the transverse uniformity of the field were a variation of less than 0.3% over the central 3.0 cm. Again, the results exceed specifications, which required a variation of less than 0.5% over the central 1.0 cm.

10

The second major requirement of the contract was the submission of engineering and shop drawings of the wiggler and its subsystems. The contractor submitted those drawings last November (considerably ahead of schedule). We reviewed and approved (with minor suggestions) these detailed plans.

Construction of the wiggler is now proceeding. The mechanical structure is approximately 75% complete. The control system has been assembled and the control software written. Testing and debugging of the control system has begun. Vacuum chambers for the full and half length wiggler have been constructed and tested by a subcontractor.

All of the vanadium-permandur pole pieces have been delivered and checked. The contractor has received some of the permanent magnets but that delivery is behind schedule. However the contractor has made plans to speed up the process of measuring, sorting, and assembling magnets such that delivery of the wiggler should remain on schedule.

We have visited the Brobeck plant twice since the start of the contract. Last August we attended a design-review meeting and in March we inspected the mechanical assembly of the wiggler. In our opinion the engineers at Brobeck have produced an excellent design which should result in a wiggler of superior performance.

2.5 Optical Cavity and Optical Alignment

Mirror Damage in FELs

Estimates were made for minimum values of the intracavity optical power at the fundamental wavelength for a saturated FEL with the NIST operating parameters. These data, which are given in Design Note 10 (Appendix A), demonstrate that thermally-induced distortion of the cavity

11

end mirrors can destroy the well-defined spatial modes of the resonator, so that lasing in the fundamental TEM_{00} mode is not possible. The critical parameters are the average intracavity power and the amount of absorption in the cavity end mirrors. The NIST-NRL FEL will have the highest average power of any FEL in the world. We have identified suppliers for cavity mirrors that have 10-20 ppm absorption in the visible spectral region. These mirrors will perform well in the NIST-NRL FEL.

Unfortunately, the power in the fundamental is not the entire story, as FELs generate substantial amounts of harmonic radiation. Therefore, in Design Note 10, we also calculated the intensity of the spontaneous emission from the undulator at the various harmonics and estimated the intensity of the coherent-harmonic emission, based on other FEL and TOK devices. We estimated the mirror lifetime due to harmonic-radiation damage, when lasing in the visible, to be about a week. The estimates were based on the extensive experience at the LURE/ACO storage ring. We are also coordinating efforts to solve this problem through resources available at the Department of Commerce. This year, we solicited Small Business Innovative Research proposals, and received two outstanding proposals. Awards will be announced on 31 May 1989.

Engineering Design of the Optical Cavity

The engineering design of the optical cavity is underway. Mirror mounts have been specified, and preliminary quotes from vendors have been received. The design of the vacuum system was initiated. After some discussion, we decided to change the length of the optical cavity from 8.062 m to 9.069 m. The new design eliminates clearance problems between

the electron-beam transport system and the cavity end mirrors, reducing the cost of several transport magnets. The extra meter of length in the cavity increases the flexibility of intracavity alignment and diagnostic devices. The design value for the fundamental frequency of the RTM was decreased from 74.375 MHz to 66.111 MHz to accomodate the 9-meter cavity length.

The design of the FEL alignment system is in progress. The magnetic axis of the undulator and the optical axis of the cavity must be parallel to and superimposed on the electron-beam trajectory over the entire length of the undulator. The optical axis of the cavity will be aligned with the magnetic axis of the undulator using mechanical and optical techniques, in the absence of the electron beam. Electron-beam position monitors will be aligned to this axis as well. The goal is to align the three axes well enough so that lasing can begin after the low-power pulsed electron beam is aligned to the beam-position monitors. Fine tuning of the electron-beam position and the optical-cavity axis can then be done remotely, using the full power electron beam and the FEL diagnostics (including spontaneous emission from the undulator).

Optical Beam Transport

The conceptual design of the optical-beam transport is well underway. The transport line will include a horizontal translation in the Magnet Room; this is needed to insure that safe levels of radiation (x rays and neutrons) are present in MR2, even in the event of a major electron-beam spill on the RTM FEL. Using grazing-incidence mirrors, this section of the transport line will have about 80% throughput in the extreme ultraviolet (≈ 300 Å to 1000 Å). With MR2 off-limits to

personnel, and experiments under remote control, conversion to a straight-line optical path will be possible. The location of the FEL diagnostic table and the various user experimental areas in MR2 was determined. The optical-beam transport in this area will consist of several "beam-extraction points", located along a straight line that is parallel to the axis of the undulator, and mounted on a single concrete pier. The users will be located on each side of the transport line. The optical-transport system will be under vacuum.

2.6 Facilities Modification

Significant changes in the facilities plan have been made during the year. In the original plan two user areas were to be provided, an above-ground building addition and a room (MR2) directly in line with the FEL. MR2 was to be shared with users of the RTM electron beam. It has been decided not to build the above-ground addition, and MR2 will be dedicated to users of the FEL. Also affecting the facility planning was a decision to decommission the 100-MeV Electron Linac. Consequently, additional space became available in the room which was to be shared by the wiggler and the linac magnet switchyard (Magnet Room).

Engineering studies of the above-ground building revealed that the type of building originally proposed was inadequate. Considerably thicker walls would be needed to reduce wind-induced vibrations to an acceptable level. Furthermore, since the above-ground building would be directly over MR2, more support would be required. The necessary modifications would increase the costs beyond available funds.

The original proposal for MR2 to be shared by FEL users and users of the RTM electron beam would be inefficient. The electron beam would

produce high levels of radiation. Since it would be impossible to shield the FEL user area adequately, FEL users would have to be excluded from MR2 when the electron beam was present. This would reduce the time available for them to set up experiments. With the space available in the Magnet Room, provision for users of the RTM electron beam can be made in that area. Consequently, MR2 can be used exclusively for FEL users.

With this modification, resources can be concentrated to provide an excellent FEL users facility with 1700 sq ft of area. This is enough room for at least five experimental stations, as shown in Figure 1(c.).

Mirrors and optical benches will be supported on the concrete floor. A false floor will be installed to put the laser beam at waist height for eye safety. Electricity, water, and compressed air will be routed conveniently under the false floor to the experimental stations, and can be accessed by removing floor panels as necessary.

Movable partitions will be used around the experimental stations so that users can safely set up experiments when the laser beam is at another station. Room air temperature and humidity will be controlled with constant, laminar airflow to minimize vibrations.

Plans for the area where the wiggler is located are shown in Figure 1(b.). The shielding wall that was to separate the RTM and the FEL has been removed. Instead a wall will be constructed to shield the FEL from the electron-beam dump. The area behind the beam dump will be used for users of the RTM electron beam. Decommissioning the 100-MeV Electron Linac has also freed the space in the Shielded Equipment Room. This area will be used for electronic equipment for the FEL.

15

All three rooms (MR2, Magnet Room, and Equipment Room) are nearly clear of 100-MeV linac equipment. The false floor for MR2 has been delivered and can be installed when the room is empty.

2.7 Performance Calculations

Wiggler magnetic field errors

Wiggler magnetic field errors affect both the electron-beam propagation and FEL gain. Wiggler field errors can walk the electron beam off the wiggler axis and can alter the phase between the electrons and the radiation, which leads to a loss in gain. These effects have been examined by developing analytical expressions for a statistical ensemble of wigglers with random errors. Expressions have been derived for the mean square displacement of the electron beam both with and without transverse-field gradients. Expressions for the mean deviation and the variance of the relative phase in the absence of transverse gradients have also been derived. Using these expressions the mean gain in the presence of magnetic field errors can be calculated.

It is expected that steering coils along the wiggler can dramatically reduce the effects of field errors. The problem of including such steering in the models is difficult. However the analytical expression derived above have been modified to include a single steering at the entrance to the wiggler. (The NIST wiggler will have steering at each quarter.)

In addition to the analytical calculations, 3D simulations using particle codes were performed to analyze both the electron-beam propagation and the FEL gain in the presence of finite field errors. The results of these simulations were found to support the analytical theory.

The wiggler model that has been used in this development assumes that errors in the magnetic field are random, i.e., no correlation among the errors. If correlations are present, the effects caused by field errors are reduced. Correlations are expected to be high for a hybrid wiggler, such as the NIST wiggler, but a priori determination of the extent of correlations is impossible. Consequently, the model will always be a worst-case estimate, since no correlations are assumed.

Calculated beam displacement and phase deviation are severe for the case of no steering and no transverse gradients, as expected. The improvements caused by steering at the entrance to the wiggler can be predicted exactly, since the difference in the analytical expressions depend only on the length along the wiggler. The maximum deviation of the electron beam is reduced by a factor of four and the maximum phase deviation is reduced by a factor of three when steering at the entrance of the wiggler is added.

The NIST wiggler will have magnetic-field gradients only in the vertical direction. Inclusion of transverse-field gradients considerably reduces the beam walk off in the vertical direction. In addition, errors in the horizontal field (which should be zero in the midplane) are expected to be very small. Consequently, beam displacement in the vertical direction should be negligible.

When the model is modified to include additional steering, it is expected that these calculations will confirm the conclusion that magnetic field errors in the NIST wiggler, as specified, will not severely affect FEL operation.

Short pulse effects

There are two possible effects on FEL operation associated with the short duration (3 ps) of the electron-beam pulse from the NIST microtron. Since the electrons travel at a velocity slightly less than c, they will fall behind the laser pulse. When the pulse slippage becomes comparable to the length of the electron pulse, the gain is reduced. In our case, the slippage is 20% of the pulse length or less and is not significant. The second effect is known as "laser lethargy." In the build-up of the radiation pulse, the growth tends to be on the trailing edge. The result is that the group velocity of the laser pulse is less than c. To maintain synchronism with the electrons the cavity length has to be shortened slightly. This change in length is known as the "detuning length."

To calculate the consequences of short-pulse effects a semi-analytical formulation of the 1-D FEL oscillator in the linearized, small-signal, low-gain limit has been developed. The model includes the effects of arbitrary pulse shape, length detuning, and mirror reflectivity.

This model has been used to simulate the performance of the NIST-NRL FEL. Two conclusions can be drawn from the results. First, the shape of the electron pulse has a very small effect on the gain. Second, the mirror detuning length becomes critical at short wavelengths where a cavity length stability of about 1 μm is required.

2.8 Control Systems

Expansion of the RTM control system

The integration of the RTM and FEL will require the expansion of the computer-based control system. In particular several additional computers will need to be acquired to handle the increased control requirements. During the past year we have been investigating methods to accomplish this task, at minimum cost in both money and time. This investigation has led us to a decision to adopt the control system (both hardware and software) developed at the Continuous Electron Beam Accelerator Facility (CEBAF).

The primary design philosophy of the CEBAF control system is to use commercial hardware and software systems and modules to the maximum extent possible. Hewlett-Packard workstations are connected together by IEEE-802.3 Ethernet Local Area Networks (LANs) to form a hierarchial distributed computer network. The network is composed of two levels, local-control computers and supervisory computers (in the central control room). Local computers are connected to monitor and control devices through Computer Automated Measurement and Control (CAMAC) modules, using the IEEE-488 bus. The CEBAF staff have written software which makes it very easy to develop or modify control systems.

Planning for the details of implementing this control system for the FEL have been started. Three options have been developed. A decision on these options will soon be made and implementation can then be started.

Vacuum control system

The FEL vacuum control system is essentially a duplicate of the system designed for the RTM, with a number of modifications to adapt the

system to the new requirements. It consists of interlocks for the RTM extraction line and FEL vacuum systems, instrumentation for ion gauges and thermocouples, and special control panels to operate beamline and manifold valves. An override capability is designed into the system to permit manual control of beamline and manifold valves during maintenance. This control system is being constructed within two (2) full size electronic racks. Much of the electronics which is contained in this system is custom designed and must be constructed. Since it is very similar to the existing system in the RTM, part of the design was already completed, and only limited changes were necessary.

Presently the racks are wired with electric power, which includes ferromagnetic resonant filtering and dc power supplies for the racks. Custom electronic chassis have been designed, and currently are being assembled. Input/output panels are currently under construction and will be mounted on the rear panel of each rack to permit flexible adaptation of the system's functions as needed by the vacuum system.

This RTM extraction/FEL vacuum control system design has been optimized to reduce the construction details such that a reduction in manpower occurred. Much of this is due to the utilization of low cost computer-automated-design software. It is estimated that the manpower reduction for the design of the input panels alone has reduced the necessary construction time by two (2) man-months. Every system component that will be constructed in-house is being designed to reduce fabrication time to a minimum.

3. References

1. R.I. Cutler, E.R. Lindstrom, S.Penner, "Conceptual Design of a High Current Injector for the NIST-NRL Free Electron Laser", to be published in <u>Proceedings of the 1989 IEEE Particle Accelerator Conference</u>, 1989.

2. R.L. Sheffield, "RF Photoelectron Gun Experimental Performance", to be published in <u>Proceedings of the 1988 Linac Conference</u>, 1988.

3. D.R Shoffstall, "RF Linac FEL Results", to be published in <u>Proceedings of the 1988 Linac Conference</u>, 1988.

4. <u>Nuclear Physics with a 450 MeV Cascade Microtron</u>, a proposal by the Physics Department of the University of Illinois, Champaign, Illinois, March 1986, pp. IV 13-20.

5. Roy E. Rand, <u>Recirculating Electron Accelerators</u>, Harwood, New York, 1984, Chap. 9.

4. **Plans for the Coming Year: April 1989 - March 1990**

In the period April 1, 1989 through March 31, 1990 we plan to:

- Complete the design of and begin procurements for a new high current injector for increasing the charge per micropulse in the RTM to at least 7 pC.

- Complete the one-pass beam tests of the RTM linac.

- Install and align the components for the RTM return beam lines.

- Procure most of the beam-transport components for the extraction line.

- Continue to perform more accurate BBU calculations for high current, subharmonic operation of the RTM as an FEL driver.

- Install the wiggler and perform acceptance tests.

- Prepare an engineering design of the FEL optical cavity, and begin procurement of components.

- Prepare an engineering design of optical-beam transport to the users area.

- Complete the removal of existing equipment from MR2 and begin conversion to an FEL user facility.

- Begin development of the FEL control system.

- Extend the computer model for wiggler field errors to include periodic external steering.

- Develop a 3-D theory and computer simulations to predict the generation of coherent harmonics.

5. Publications

B. Carol Johnson, P.H. Debenham, S. Penner, C-M. Tang, and P. Sprangle, "The NBS Free Electron Laser Facility", Inst. Phys. Conf. Ser. No. 94: Section 6, 247 (1988).

M.A. Wilson, R.L. Ayres, R.I. Cutler, P.H. Debenham, E.R. Lindstrom, D.L. Mohr, S. Penner, J. Rose, and L.M. Young, "NIST-Los Alamos Racetrack Microtron Status", to be published in the Proceedings of the 1988 Linear Accelerator Conference.

R.I. Cutler and L. Young, "Performance of the High Power RF System for the NIST-Los Alamos Racetrack Microtron", to be published in the Proceedings of the 1988 Linear Accelerator Conference.

C.M. Tang, P. Sprangle, S. Penner, and X.K. Maruyama, "Analysis of Free Electron Laser Performance Utilizing the National Bureau of Standards' CW Microtron", J. of Appl. Phys., Vol. 63, NO. 11, (1988).

R.I. Cutler, E.R. Lindstrom, and S. Penner, "Conceptual Design of a High Current Injector for the NIST-NRL Free Electron Laser," to be published in the Proceedings of the 1989 IEEE Particle Accelerator Conference.

P.H. Debenham, R.L. Ayres, J.B. Broberg, R.I. Cutler, B.C. Johnson, R.G. Johnson, E.R. Lindstrom, D.L. Mohr, J.E. Rose, J.K. Whittaker, N.D. Wilkin, M.A. Wilson, C-M. Tang, P. Sprangle, and S. Penner, "The NIST/NRL Free-Electron Laser Facility," to be published in the Proceedings of the 1989 IEEE Particle Accelerator Conference.

S. Penner, "BоU in Microtrons with Subharmonic Injection," to be published in the Proceedings of the 1989 IEEE Particle Accelerator Conference.

6. Talks

B.C. Johnson, "The NBS Free-Electron Laser Facility", Fourth International Symposium on Resonance Ionization Spectroscopy and its Applications, April 10-15, 1988, NIST, Gaithersburg, MD.

B.C. Johnson, "The NBS Free-Electron Laser Facility", Spring meeting of the APS, April 18-20, 1988, Baltimore, MD.

B.C. Johnson, "Progress Report on the NBS-NRL Free-Electron Laser Facility", Third Annual MFEL Contractors Meeting, May 15-18, 1988, University of Utah, Salt Lake City, UT.

C.M. Tang, B. Hafizi, and P. Sprangle, "Effect of Finite Electron and Radiation Pulse Shapes on the NBS-NRL FEL Performance", Third Annual MFEL Contractors Meeting, May 15-18, 1988, University of Utah, Salt Lake City, UT.

M.A. Wilson, "NIST-Los Alamos Racetrack Microtron Status," 1988 Linear Accelerator Conference, October 4, 1988, Williamsburg, VA.

R.I. Cutler, "Performance of the High Power RF System for the NIST-Los Alamos Racetrack Microtron," 1988 Linear Accelerator Conference, October 6, 1988, Williamsburg, VA.

R.I. Cutler, "Design of a High-Current Injector for the NIST-NRL Free-Electron Laser," 1989 IEEE Particle Accelerator Conference, March 20, 1989, Chicago IL.

P.H. Debenham, "The NIST-NRL Free-Electron Laser," 1989 IEEE Particle Accelerator Conference, March 21, 1989, Chicago, IL.

Appendix A

Design Note 10

Mirror Damage

Mirror Damage

C. Johnson

Introduction

The issue of mirror damage is important to us, as FELs are pushing the state of the art for mirror/coating design, and the NIST-FEL will be no exception. The intention of this report is to raise some of the issues that are involved, and to indicate directions for future work. The report is divided into two sections. In the first section, estimates of the radiation fields are made. These values are important for calculating optical effects, although the many possible mechanisms of damage are not considered here. In the second section, thermal effects are considered.

Intracavity Radiation Field

(a) Lasing with the FEL oscillator near threshold

The operating conditions for the NIST-FEL have been described in previous design notes (DN 6 & 9); some of the results are summarized here. Examination of the values near threshold sets a limit on the total loss of the cavity.

The small-signal, single-pass power gain for a infinitely-long electron beam pulse, G_p, has been calculated by Cha-Mei Tang (see Figure 6 in Penner *et al*. 1988), and the results may be used to calculate the round-trip cavity losses that are "acceptable". It is convenient to express the loss as an R_{eff}^2 parameter; the lasing threshold is when $G_p = (1 - R_{eff}^2)/R_{eff}^2$. In Table 1, G_p and the values of R_{eff}^2 at threshold (labeled "t"), and when the round-trip losses, L_p, is $L_p = G_p - 0.03$ (labeled "3%"), are given. The lower limit to the intracavity power is determined by using the threshold value for R_{eff}. Strictly speaking, the laser never saturates when the losses are set to the threshold value, but this approximation illustrates the close relationship

between G_p and the intracavity power at saturation, P_{sat}.

In the one-dimensional model, when the FEL saturates the power gain, g, is equal to $\eta P_{eb}/P_{sat}$, where $\eta = 1/2N$. N is the number of periods in the wiggler and P_{eb} is the average power in the electron beam. At saturation, $L_p = g$, and P_{sat} may be calculated. From the resonator geometry,[1] the radius of the TEM_{00} mode, r_m, on the mirrors is known. The time structure of the laser is taken to be 3-ps wide pulses at a repetition rate of 74.375 MHz. The pulse width is defined as the ratio of total energy in the pulse to the peak power during the pulse. With this information, the average intracavity power, P_{sat}, (Watts), the average and peak intracavity irradiance on the mirrors, I_m and $I_{\blacksquare}$, (Watts cm^{-2}), and the fluence on the mirrors in one pulse, $F_{\blacksquare}$, can be calculated as a function of R_{eff}^2, see Table 1.

Table 1
NIST-FEL Optical Parameters
(a) Full-Length Wiggler, N = 130

λ μm	G_p	R_{eff}^2 t/3%	P_{sat} kW t/3%	r_m mm	A_m cm^2	I_m kW cm^{-2} t/3%	$I_{\blacksquare}$ MW cm^{-2} t/3%	$F_{\blacksquare}$ μJ cm^{-2} t/3%
0.20	0.10	0.91/0.93	3.2/4.6	0.83	0.022	150/215	670/960	2000/2900
0.25	0.12	0.89/0.92	2.5/3.3	0.93	0.027	93/124	420/550	1200/1650
0.35	0.15	0.87/0.89	1.6/2.1	1.10	0.038	44/55	200/250	600/750
0.45	0.18	0.85/0.87	1.2/1.5	1.24	0.048	25/30	110/130	330/390
0.65	0.23	0.81/0.83	0.8/0.9	1.49	0.070	11/13	49/58	150/170
0.75	0.26	0.79/0.81	0.6/0.7	1.60	0.080	8/9	36/40	100/120
0.85	0.28	0.78/0.80	0.5/0.6	1.70	0.091	5.9/6.6	26/30	78/90
1.00	0.32	0.76/0.78	0.4/0.5	1.84	0.107	4.3/4.8	19/22	57/66
2.00	0.52	0.66/0.67	0.2/0.2	2.61	0.215	0.9/1.0	4/4.3	12/13

---

[1]Cavity length = 806.158 cm; Rayleigh length = one-half of the wiggler length; optical waist located at the center of the wiggler.

Table 1, continued
(b) Half-Length Wiggler, N = 65

λ μm	G_p	R^2_{eff} t/3	P_{sat} kW t/3	r_m mm	A_m cm^2	I_m kW cm^{-2} t/3%	I_m MW cm^{-2} t/3%	F_m μJ cm^{-2} t/3%
1.00	0.06	0.94/0.97	4.9/9.9	1.92	0.116	43/85	193/380	580/1100
2.00	0.09	0.92/0.94	2.3/3.4	2.71	0.232	10/15	44/67	130/200
3.00	0.12	0.89/0.92	1.4/1.9	3.33	0.348	4.1/5.5	18/25	54/75
4.00	0.14	0.88/0.90	1.0/1.3	3.84	0.464	2.2/2.8	10/13	30/39
5.00	0.16	0.86/0.88	0.8/1.0	4.30	0.580	1.4/1.7	6.3/7.6	19/23
6.00	0.18	0.85/0.87	0.7/0.8	4.70	0.696	1.0/1.1	4.2/4.9	13/15
7.00	0.20	0.84/0.86	0.6/0.7	5.08	0.812	0.7/0.8	3.1/3.6	9.3/11
8.00	0.21	0.82/0.84	0.5/0.6	5.43	0.928	0.5/0.6	2.3/2.7	6.9/8.1
9.00	0.23	0.81/0.83	0.4/0.5	5.75	1.040	0.4/0.5	1.8/2.1	5.4/6.3
10.0	0.25	0.80/0.82	0.4/0.4	6.08	1.160	0.3/0.4	1.4/1.7	4.2/5.1

It is evident that when G_p is small, the minimum value for the intra-cavity power is high--simply because R^2_{eff} is near unity. The gain is small at the short-wavelength end for each device. This should not present a problem in the 1.0 - 2.0 μm range, because there is good overlap between the full-length and half-length wigglers. However, in the ultraviolet region, the mirrors present a problem. Not only is G_p decreasing, but P_{eb} is increasing and the spot size on the mirrors is decreasing, leading to peak irradiances of about 1 GW cm^{-2} and average powers of about 200 kW cm^{-2}. Absorption in the multi-layers of the mirror coatings will be greater in the ultraviolet than in the visible, increasing the thermal stress on the mirrors.[2] In summary, for efficient operation of this laser, we need to maximize the small-signal power gain while limiting the saturated power in the optical cavity. Factors under

---

[2]According to Bruce Flint of Acton Research (ARC), a leading manufacturer of high-power excimer laser mirrors, it will be difficult to operate the NIST-FEL below 250 nm. His best estimate for absorption in partially transmitting (T = 2%), partially reflecting multi-layer dielectric UV-VUV mirrors is: 1) λ = 172 nm, A = 3-4%; 2) λ = 193 nm, A = 0.5-1.0%; 3) λ = 250 nm, A = 0.3-0.7%; 4) λ = 300 nm, A = 0.25-0.5%; and 5) λ = 350 nm, A = 0.25%.

our control include the average power, the peak current, and the temporal structure. Several combinations for operation at 1.25 μm are illustrated in Table 2. This wavelength was chosen because Tang has calculated the 3-D gain as a function of peak current (Penner *et al.* 1988). Cases b and c have equal power in the electron beam but different power in the optical beam because the 3-D small-signal power gain is nonlinear in peak current.

Table 2
Threshold P_{sat} in FLW at $\lambda=1.25$ μm ($\gamma=150$, $\epsilon_N=10^{-5}$ m-rad)

Case	I,A	G_p(3-D)	$R_{eff}^2(t)$	f_i,MHz	Modulation	P_{eb},kW	P_{sat},W	P_{peak},MW
a	2	0.357	0.737	74.375	none	34.2	368	1.65
b	2	0.357	0.737	18.594	none	8.6	92	1.65
c	4	0.858	0.538	18.594	none	17.1	77	1.38
d	2	0.357	0.737	74.375	100 μs @ 1 kHz	3.4	37	1.65

The R_{eff}^2 parameter includes all of the cavity losses, e.g. absorption and scattering on the mirrors (A + S), outcoupling (T), and diffraction (D). For simplicity, the two mirrors are taken to be identical, so that the output is taken from each end of the oscillator. In the ultraviolet and visible regions, diffraction losses are negligible, so given a value for A + S, the values of T corresponding to the values of R_{eff}^2 listed in Table 1 may be calculated. Commercial suppliers rarely report values for absorption or scattering. Transmission is reported for output couplers, but not for high reflectors, even though the residual transmission may be as high as 1%. See Table 3, where I've also calculated the average output power, $P_{out} = \eta P_{eb}T/(1 - R_{eff})$. In the limit T >> D and T >> (A + S), then $P_{out} = \eta P_{eb}$, which is independent of T.

Table 3
Output Power as a function of R_{eff}^2
Full Length Wiggler

λ μm	R_{eff}^2 t/3%	A + S	D	T t/3%	P_{out} Watts t/3%
0.20	0.91/0.93	0.010	0.000	0.036/0.026	256/239
0.25	0.89/0.92	0.007	0.000	0.050/0.034	259/244
0.35	0.87/0.89	2.5E-3	0.000	0.065/0.053	239/236
0.45	0.85/0.87	2.0E-5	0.000	0.078/0.067	220/220
0.65	0.81/0.83	2.0E-5	0.000	0.100/0.089	180/180
0.75	0.79/0.81	2.0E-5	0.000	0.110/0.100	166/166
0.85	0.78/0.80	2.0E-5	0.000	0.120/0.110	153/153

(b) Undulator Radiation

The spontaneous emission from the undulator is an important diagnostic of the alignment of electron beam and of the quality of the magnetic field (Billardon et al. 1983). The measured wavelength at the peak emission is used to adjust K or γ so that lasing will occur where the mirrors have maximum reflectivity. If K is known, the spontaneous emission can be used to measure absolutely the energy of the electron beam. The undulator radiation is of interest because experiments that require photon energies higher than those available from the FEL oscillator may be possible using the spontaneous emission. Our undulator may also work as a transverse optical klystron (TOK), and this configuration is an excellent source of UV and soft x-ray photons (Kincaid and Freeman 1983). Unfortunately, there is evidence that FEL mirrors are degraded by the spontaneous emission (Deacon 1986, Edighoffer et al. 1988). When a FEL is used as an oscillator, the spontaneous harmonic emission is amplified through the TOK mechanism, and is termed coherent harmonic emission. Our collaborators at NRL will calculate the complete spectrum for an FEL oscillator. This is a very difficult problem because of the nonlinearities involved.

Hofmann (1986) derives the general equations (see Eqn. 58) for the undulator radiation, $P_n(\Omega,\omega) \equiv \partial^2 P_n/\partial\Omega\partial\omega$ (Watts ster^{-1} (rad s^{-1})$^{-1}$) in the limit where the distance from the undulator to the detector is greater than the length of the undulator (far-field limit). Spherical polar coordinates are used, with the z-axis aligned with the longitudinal axis of the undulator. The magnetic field is in the y-direction (vertical), so that the electrons oscillate in the x direction (horizontal). Some of the main results are summarized here.

The spectrum consists of a fundamental frequency, ω_1, and harmonics of this frequency, $n\omega_1$. Even and odd harmonics differ in angular distribution and polarization. Although the polarization for each harmonic is elliptical, the even harmonics are nearly 100% vertically polarized and odd harmonics are nearly 100% horizontally polarized. Since the plane of incidence of the FEL cavity mirrors is horizontal, the even harmonics are $\simeq$ 100% S-polarized and the odd harmonics are $\simeq$ 100% P-polarized. The S and P components of the even harmonics and the S component of the odd harmonics are equal to zero on axis ($\theta = 0$). The P component of the odd harmonics is a maximum for $\theta = 0$ and discrete values of θ (numbering n-1) in the directions $\phi = 0$ and $\phi = \pi$ (see Figure 24 - 26 in Hofmann 1986).

These comments hold for a single electron, or an electron beam that is very cold, i.e., the angular divergence is small. Hence, a measure of $\omega_2 = 2\omega_1$ at $\theta = 0$ can be used to supplement our measurements of the transverse emittance.

The finite number of periods in the undulator, N, broadens each harmonic. The lineshape function scales as $\sin^2 x/x^2$ with an absolute width of ω_1/N and a fractional width of 1/nN (FWHM). I'll call this natural broadening. The

frequency of each harmonic depends on the polar angle through the relation

$$\omega_1(\theta) = 2\gamma^2 k_w c/(1 + \tfrac{1}{2}K^2 + \gamma^2\theta^2)$$

(see Figure 1), which broadens the harmonic on the red side of the line if a detector with a finite aperture is used. This angular broadening is small compared to the natural broadening when the detector accepts radiation from $\theta =$ 0 out to some angle θ_c, where

$$\theta_c \leq ((1 + \tfrac{1}{2}K^2)/(2\gamma^2 nN))^{\tfrac{1}{2}}$$

(Krinsky, Tomlinson, and van Steenbergen 1982). A third source of line broadening is errors in the magnetic field of the undulator (Kincaid 1985), and a fourth source is the longitudinal energy spread.

To evaluate the damage to the FEL cavity mirrors, the angle of interest, θ_m, is defined by the ratio of r_m to L, where L is the distance from the middle of the undulator to the downstream cavity mirror. Writing r_m in terms of the cavity parameters it is easy to see that angular broadening over θ_m is important for $n \geq 3$, independent of the value of the fundamental wavelength.

Hofmann expands the expression for $\partial^2 P_n/\partial\Omega\partial\omega$ for $n = 1$, 2, and 3 in terms of K^*, where

$$K^{*2} = K^2/(1 + \tfrac{1}{2}K^2).$$

The angle-integrated spectral power density, $P_n(\omega) \equiv dP_n/d\omega$, is plotted in Figure 2. $P_n(\omega)$ is often converted from the mks units of $W/(rad\ s^{-1})$ to $\Phi_n(\omega)$ = photons/sec/1% bandwidth by multiplying by the absolute linewidth, dividing by the energy per photon, and then assigning a constant fractional linewidth of 0.01.

Using the relationship between θ and ω, I have also calculated $dP_n/d(\gamma^*\theta)$, where

$$\gamma^{*2} = \gamma^2/(1 + \tfrac{1}{2}K^2),$$

(see Figure 3). Either expression can be integrated up to θ_m to determine a lower limit[3] for the total power incident on the central portion of the mirror from the first, second, and third harmonics. Some examples are given in Table 4. Note that the power in the first three harmonics, $\sum P_n$, is less than the actual power, P_{tot}, and that the agreement improves as K decreases. This is because of the approximations involved in Hofmann's expansion.

Table 4
Undulator Radiation

N	K	γ	$\gamma^*\theta$ rad	$P_1(\gamma^*\theta)$ Watts	$P_2(\gamma^*\theta)$ Watts	$P_3(\gamma^*\theta)$ Watts	$\sum P_n(\gamma^*\theta)$ Watts	P_{tot} Watts	Note
130	1.40	350	$\gamma^*\pi$	3.98E+0	4.41E+0	6.74E+0	1.51E+1	2.12E+1	a
			0.05	3.90E-2	7.69E-4	1.23E+0	1.27E+0		b
			1.00	3.09E+0	3.79E+0	5.68E+0	1.26E+1		
130	0.84	350	$\gamma^*\pi$	3.50E+0	2.23E+0	1.45E+0	7.18E+0	7.62E+0	a
			0.05	4.48E-2	6.62E-4	3.09E-1	3.54E-1		b
			1.00	2.93E+0	2.02E+0	1.28E+0	6.41E+0		
65	1.40	50	$\gamma^*\pi$	1.14E-1	1.26E-1	1.93E-1	4.32E-1	6.05E-1	a
			0.05	1.16E-3	2.36E-4	3.56E-2	3.70E-2		c
			1.00	8.83E-2	1.09E-1	1.62E-1	3.59E-1		
65	0.84	50	$\gamma^*\pi$	3.57E-2	2.28E-2	1.47E-2	7.32E-2	7.78E-2	a
			0.05	4.56E-4	6.75E-6	3.15E-3	3.62E-3		c
			1.00	3.00E-2	2.06E-2	1.31E-2	6.36E-2		

Notes: "a" refers to the angle-integrated (total) power; for "b" and "c", $\theta_m = 0.21$ mrad ($\gamma = 350$) and 1.5 mrad ($\gamma = 50$), respectively.

When $\theta = 0$, the expression for $\partial^2 P_n/\partial\Omega\partial\omega$ simplifies, and by integrating over the natural lineshape and multiplying by the solid angle, it is possible to estimate the flux on axis. Dividing by the photon energy,

$$F_n = \alpha\gamma^2 NIG(n,K)/eL^2 \quad \text{phot s}^{-1} \text{ m}^{-2},$$

where

$$G(n,K) = \frac{nK^2}{1 + \frac{K^2}{2}}\left[J_{\frac{n-1}{2}}\left(\frac{nK^2}{4}\right) - J_{\frac{n+1}{2}}\left(\frac{nK^2}{4}\right)\right]^2 .$$

___

[3]The actual power will be higher because of coherent harmonic emission.

I = electron beam current (A) and α = 1/137. G(n,K) is plotted in Figure 4.

For our range of magnetic field strength, the flux in the fundamental, F_1, does not depend strongly on K: for L $\simeq$ 403 cm, γ = 350, N = 130, and 0.84 $\leq$ K $\leq$ 1.4, $F_1 \simeq 1.6 \cdot 10^{18}$ phot s^{-1} cm^{-2} A^{-1}. However, when K < 1, the function G(n,K) decreases rapidly with increasing values of n (see Figure 4). As an example, the flux at the 19th harmonic for K = 1.4 is equal to the flux in the 5th harmonic for K = 0.84. Therefore, the gap setting for the wiggler will be a compromise between having adequate small-signal gain (large K) and stable mirror performance (low K).

(c) TOK Radiation

A transverse optical klystron (TOK) is a device that produces coherent harmonic emission. An external laser is used to produce energy modulation of the electron beam in an undulator/wiggler; the action of the undulator also acts to modulate the density distribution of the electron beam at harmonics of the laser wavelength; this "bunched" electron beam then radiates coherently at these wavelengths. Since it will be difficult to operate the NIST-FEL as an oscillator in the UV, a TOK configuration may be an attractive alternative. As is the case for the spontaneous emission, radiation generated via the TOK mechanism may be a valuable diagnostic. Finally, in lieu of calculations of the coherent harmonic emission from our oscillator, we can use TOK calculations to estimate the magnitude of this emission.

Kincaid and Freeman (1983) have derived the design requirements for a TOK. I summarize the main design points below. They conclude their paper by citing realistic calculations. In an example with a 130 MW external, pulsed laser (Nd:YAG) at 532 nm driving a uniform, constant-period undulator on the

NSLS VUV storage ring, they show that the coherent harmonic emission exceeds the spontaneous emission of the undulator by a factor of 10^3 to 10^4. Output was estimated up to 40 eV (n = 17). Applying TOK calculations to a saturated FEL is a gross oversimplification, as mentioned before. However, throwing caution to the wind, application of their conversion efficiency of $2.4 \cdot 10^{-5}$ for n = 5 to our anticipated peak power of about 5 MW in the green implies 120 W (peak) at 12 eV. Power levels of this nature will affect the design of the multilayer dielectric coatings for the mirrors.

TOK Design Goals

1) The undulator should have a large K value.

For large K values, the transverse velocity, $\beta_\perp$, becomes large, and the "figure eight" orbit (moving frame) is pronounced (see Hofmann). The multipole content of the spontaneous radiation increases, and the energy modulation, ΔE, due to the laser is more efficient for the higher harmonics. The absolute value of ΔE increases as well ($\Delta E \propto K$). Our maximum value for K, 1.41, is not very robust; values of 2.5 and higher are typical for TOK design values.

2) The undulator should bunch the beam to the optimal value.

The total distance, Δs, that the energy-modulated beam traverses in the momentum-compaction section is proportional to the fractional, laser-induced energy spread, $\Delta E/E$, the length of this section, L_c, and a momentum-compaction factor, α_m. For maximum bunching, $\Delta s = \lambda/\pi$, or

$$\alpha_m = (\lambda/2\pi L_c)(E/\Delta E).$$

For uniform undulators, $\alpha_m = -(1 + K^2)/\gamma^2$, so minimizing L_c requires large values of K and/or large values for $\Delta E/E$.

3) The energy modulation should exceed the natural energy spread.

Kincaid and Freeman show that harmonics will be produced up to some cutoff

value, n_c, where

$$n_c = \Delta E/\sigma_E,$$

and σ_E is the rms value of the energy distribution (Gaussian) of the electron beam. Thus, generation of short wavelengths implies large ΔE (i.e. large peak power in the drive laser) or small energy spread (hence storage rings or the RTM are suitable for TOK drivers).

4) The angular divergence in the electron beam should be small.

Angular spread is negligible when

$$n \leq \lambda/(2\pi L_o \sigma_\theta^2),$$

where L_o is the length of the undulator and σ_θ is the rms value of the angular divergence. Hence it is important to have good transverse emittance and a short undulator.

5) The peak current should be high.

For a bunched beam, the output is proportional to N_e^2, instead of N_e as in the spontaneous emission. The RTM will have about $5 \cdot 10^6$ electrons/bunch, whereas the NSLS storage ring has about 10^{11} electrons/bunch.

6) If the spectral bandwidth doesn't matter, then the bunch should be short.

Assuming that the coherence length of the drive laser is longer than the electron pulse length (300 ps for NSLS; $\approx$3 ps for RTM), then the power scales as $1/\sigma_z$, where σ_z is the one-sigma value of the electron pulse length.

7) If the light is focusable, then the source size should be small.

If you can collect and use the light emitted into all solid angles, then the power scales as $1/(\sigma_x \sigma_y)$, where σ_x and σ_y are the rms values for the electron beam spatial distribution.

8) The laser matters.

Kincaid's calculation examines the effect of varying the size and location

of the laser waist, the Rayleigh length, the wavelength--in particular the relative difference between the laser wavelength and the spontaneous emission wavelength, and the peak power. Actual experiments have shown that the stability of the laser is very important.

9) Overbunching matters.

A bunched electron beam is "de-bunched" in the radiator section of the TOK, limiting the performance of the device. Kincaid suggests that the radiator section should have a transverse gradient designed to preserve the bunching of the electron beam.

Thermal Effects

The discussion in this section is preliminary, but it does indicate that thermal effects will be very important in the design of the FEL resonator.

(a) Instantaneous

The temperature rise due to a single pulse of finite width is equal to the absorbed energy divided by the depth of penetration, the density, and the specific heat. When s, the heat diffusion depth, exceeds the optical absorption depth, d_o, then the depth of penetration is $s = (4\kappa\tau/\rho C)^{1/2}$, where κ is the thermal conductivity, τ is the pulse width, ρ is the density, and C is the specific heat. Then the temperature rise scales as $\tau^{-1/2}$ (Deacon 1986). For metals, $d_o \simeq 10$ nm. For transparent materials, d_o depends on the extinction coefficient and the optical wavelength, but it will always exceed the optical wavelength: $d_o > 200$ nm.

With the 3 ps-wide pulses from the NIST-FEL, and assuming that the optics are at room temperature, s will be about 3 nm (fused silica), 9 nm (quartz), 37 nm (copper and beryllium oxide), and 45 nm (silver). Therefore, for metal mirrors at infrared wavelengths, the scaling law is valid, and the temperature

rise for each pulse is $\Delta T = AF_m/(s\rho C)$. For typical values of $A \approx 0.01$, $F_m \approx$ 100 μJ cm^{-2}, and copper mirrors, then $\Delta T = 8$ °C. For transparent materials, the scaling law is invalid since $s < d_o$, and it is not possible to estimate the temperature rise for an individual pulse. However, the temperature will equilibrate rapidly at our repetition rate, and it is possible to estimate the average temperature rise (see below). The time scale of the micropulses is important, however, as density waves from successive pulses do not have time to propagate out of the irradiated area on the mirrors in the time between pulses. This could lead to nonlinear effects. The repetition rate would have to be decreased by about a factor of about 10 to 100 in order to realize a "single pulse" configuration.

(b) Steady-State

After a short time, a steady state condition will be established so that it is reasonable to ignore the temperature excursion during each pulse. Two sets of boundary conditions are considered.

(i) Radiative Cooling

For this model, the mirror is in vacuum and the temperature gradient at the surface due to thermal conduction is zero, so that radiative cooling is the only loss mechanism. It is assumed that the mirror is a good thermal conductor, so that the temperature distribution is uniform, and that the mirror radiates as a perfect black body. Finally, I'm going to average the incident flux over the entire surface area of the mirror. These assumptions simplify the calculation, and set a lower limit for the temperature.

Then, the average temperature of the mirror is given by

$$T^4 = A \cdot P_{sat}/(\sigma \cdot S_m) + P_{th}/(\sigma S_m),$$

where T is the mirror temperature (°K), A is the absorption coefficient, P_{sat}

is the average power in the intracavity optical field (Watts), P_{th} is the power in the thermal radiation field that is required to maintain the mirror at 300 °K (0.81 W), σ is the Stefan-Boltzmann constant ($5.67 \cdot 10^{-12}$ W cm^{-2} °K^{-4}), and S_m is the surface area of the mirror (cm^{-2}). In the visible region of the spectrum, $P_{sat} \simeq 1$ kW and $S_m = 18$ cm^2 (1" diameter by 3/8" thick). The absorption in the coating varies between $2 \cdot 10^{-3}$ for an average coating (Costich 1987) and $2 \cdot 10^{-5}$ for the best coatings (Ojai 1988). The corresponding black-body temperature would be 410 °K and 302 °K, respectively.

(ii) Perfect Heat Sink

This model assumes that the surface of the cylindrically-shaped mirror is held at constant temperature. The temperature difference in the longitudinal dimension is found by integrating the static heat flow equation. This temperature difference is used to calculate the change in the mirror thickness, and this is used to calculate the angular deflection for plane waves at normal incidence.

Two cases are considered. The longitudinal temperature difference in cylindrical coordinates evaluated at $r = r_m$ is

$$\Delta T(r_m, H) \equiv T(r_m, H) - T(r_m, 0) = AP_{sat} ln(1+2H/r_m)/(2\pi r_m \kappa),$$

where H is the thickness of the mirror. The heat input is P_{sat}, uniformly distributed over area A_m. In the regime where $r_m > H$, $\Delta T(r_m, H) = AP_{sat}H/(A_m \kappa)$. This is the approximation that was used by Deacon (1986). The radial temperature difference in spherical coordinates is

$$\Delta T(H') \equiv T(H') - T(r_m) = AP_{sat}(H' - r_m)/(4\pi \kappa H' r_m),$$

where the surface area of a sphere of radius H' is equal to the surface area of the mirror. The heat input is P_{sat}, uniformly distributed on a spherical surface of radius r_m. When $r_m < H'$, $\Delta T(H') = AP_{sat}r_m/(4A_m \kappa)$. Based on

comparison with unpublished work (Webb 1988), the correct result should lie between the estimates that result from these two models.

I have calculated $\Delta T(r_m, H)$ and $\Delta T(H')$ for several values for P_{sat}, r_m, κ, and H. The temperature rise is highest for poor thermal conductors (fused silica, Zerodur) and appears to eliminate the possibility of operation below about 350 nm based on the absorption values that were quoted by ARC. The near IR, from 2 to 3 μm, may also be troublesome, but I am not sure what are the best possible values for absorption. The temperature rise is less for moderate thermal conductors (sapphire, ZnSe, magnesium fluoride). Metal substrates are also a possibility, but they do not transmit the laser radiation, and another means of outcoupling would be necessary.

The amount of linear expansion is proportional to the coefficient of linear expansion, ξ, divided by the thermal conductivity. The angular deflection is just the change in length divided by r_m, so the ideal substrate material has a value of ξ/κ that is small. Zerodur is the best, followed by Mo, Cu, Al, Al_2O_3, ZnSe, SiO_2, and MgF_2. In the visible and IR the amount of angular deflection is calculated to be small, but again there is a problem in the UV.

Future Work

Most of the points brought up in this design note require elaboration. A listing is:

1) Perform TOK calculations for our system.

2) Calculate the coherent harmonic emission.

3) Broaden knowledge base.

    a. Deacon has/is measuring the coherent harmonic emission on the Stanford/Madey machine.
    b. Jim Wier has an MFEL grant to study FEL mirror damage.
    c. The SDIO program is studying FEL mirror damage.

     d. FELs in the MFEL program have observed mirror damage.

     e. The high power laser community is a resource.

     f. The new generation of light source, a synchrotron ring and a
        wiggler, requires cooled optics.

     g. Information is needed on optical absorption coefficients.

     h. More must be known about MLD coating techniques and materials.

4) Model thermal effects using commercial finite element analysis

software.

Acknowledgements

I want to thank Ron Johnson for the many useful suggestions. I want to
also thank Ron, Bob Madden, Sam Penner, and C.-M. Tang for reading a draft of
this manuscript.

References

M. Billardon *et al.* 1983, *Journal de Physique* C1 29.

V.R. Costich 1987, in *Handbook of Laser Science and Technology*, ed. M.J. Weber, (CRC Press: Boca Raton) vol. V, 405.

D.A.G. Deacon 1986, *Nuc. Instr. and Meth. in Phys. Res.* A250 283.

J.A. Edighoffer *et al.* 1988, *Appl. Phys. Lett.* 52 1569.

A. Hofmann 1986, SSRL ACD-NOTE number 38.

C. Johnson 1987, FEL Design Note 6, unpublished.

C. Johnson 1988, FEL Design Note 9, unpublished.

B. M. Kincaid 1985, *JOSAB* 2 1294.

B. M. Kincaid and R. R. Freeman 1983, Bell Laboratories Memorandum for File.

S. Krinsky, W. Tomlinson, and A. Van Steenbergen 1982, Brookhaven National Laboratory informal report number 31989.

Ojai Research Corporation 1988, personal communication.

S. Penner et al. 1988, *Nuc. Instr. and Meth. in Phys. Res.* A272 73.

Webb, J. 1988, personal communication.

Figure Captions

Figure 1. Photon energy as a function of observation angle θ for n = 1 to 17.

Figure 2. Angle-integrated spectral power density, $\partial P_n/\partial\omega$, as a function of ω (expressed in eV), for K = 1.4, N = 130, γ = 350, and I = 1 Amp.

Figure 3. Rate of change of power, $\partial P_n/\partial(\gamma^*\theta)$, as a function of $\gamma^*\theta$ for K = 1.4, N = 130, γ = 350, and I = 1 Amp.

Figure 4. The function G(n,K) for n = 1 to n = 21 and K = 0 to K = 3.0.

Figure 1

Figure 2

Angle Integrated Spectral Power Density

Phot./s/1% BW

dPn/dw, Watts/rad s-1

Photon energy, eV

Figure 3

Figure 4

G(n,K)

K

n=1

n=3

n=5

n=7

n=21
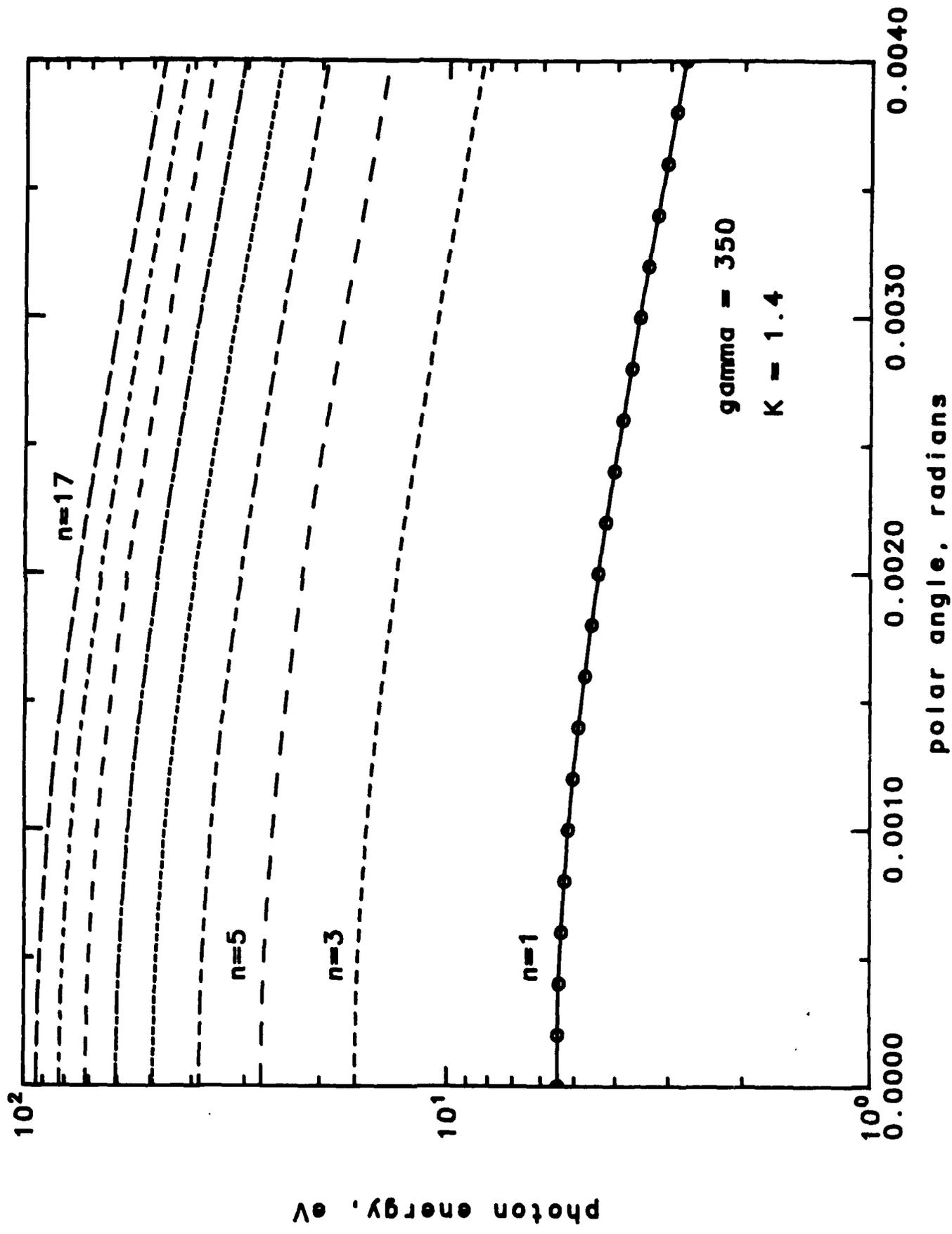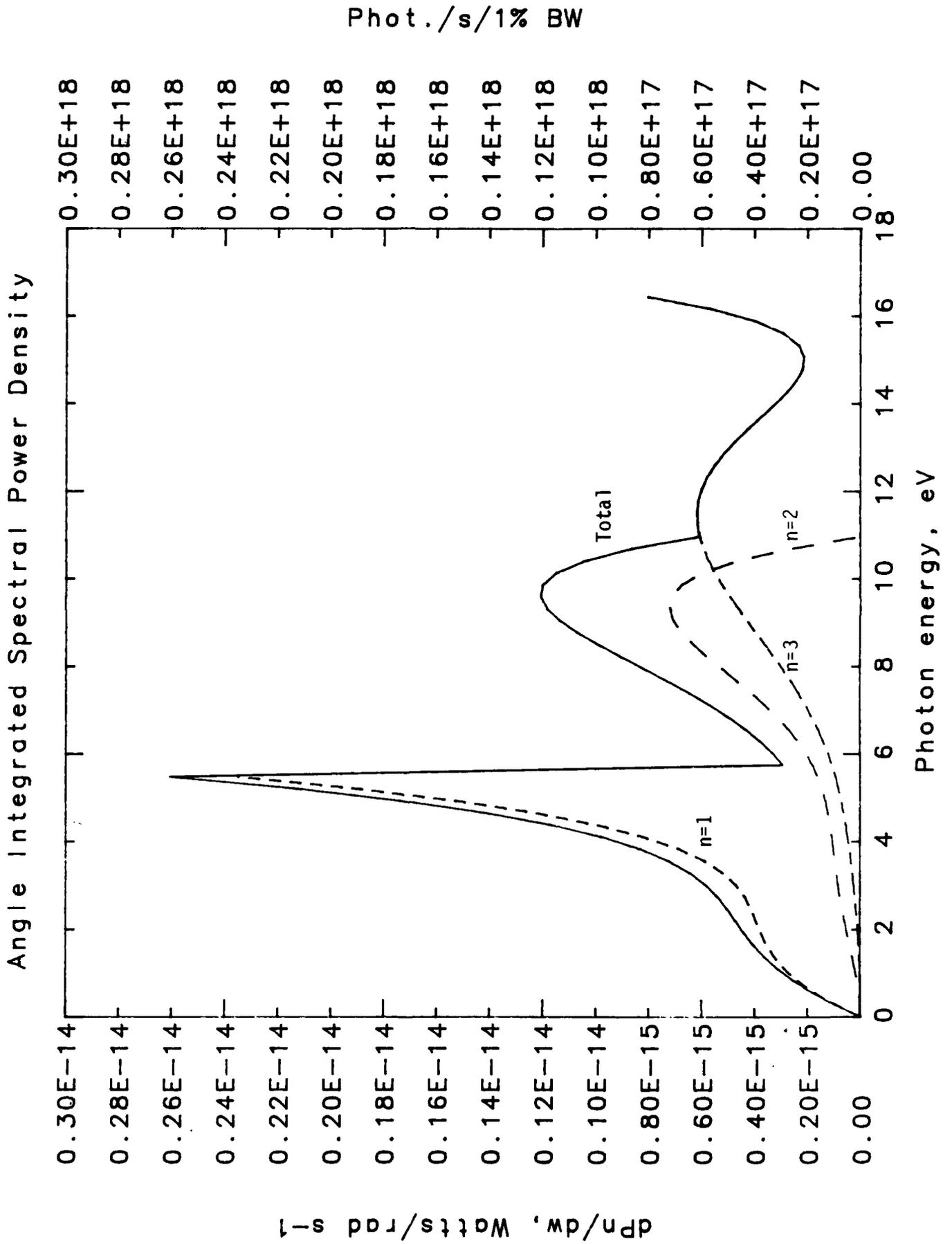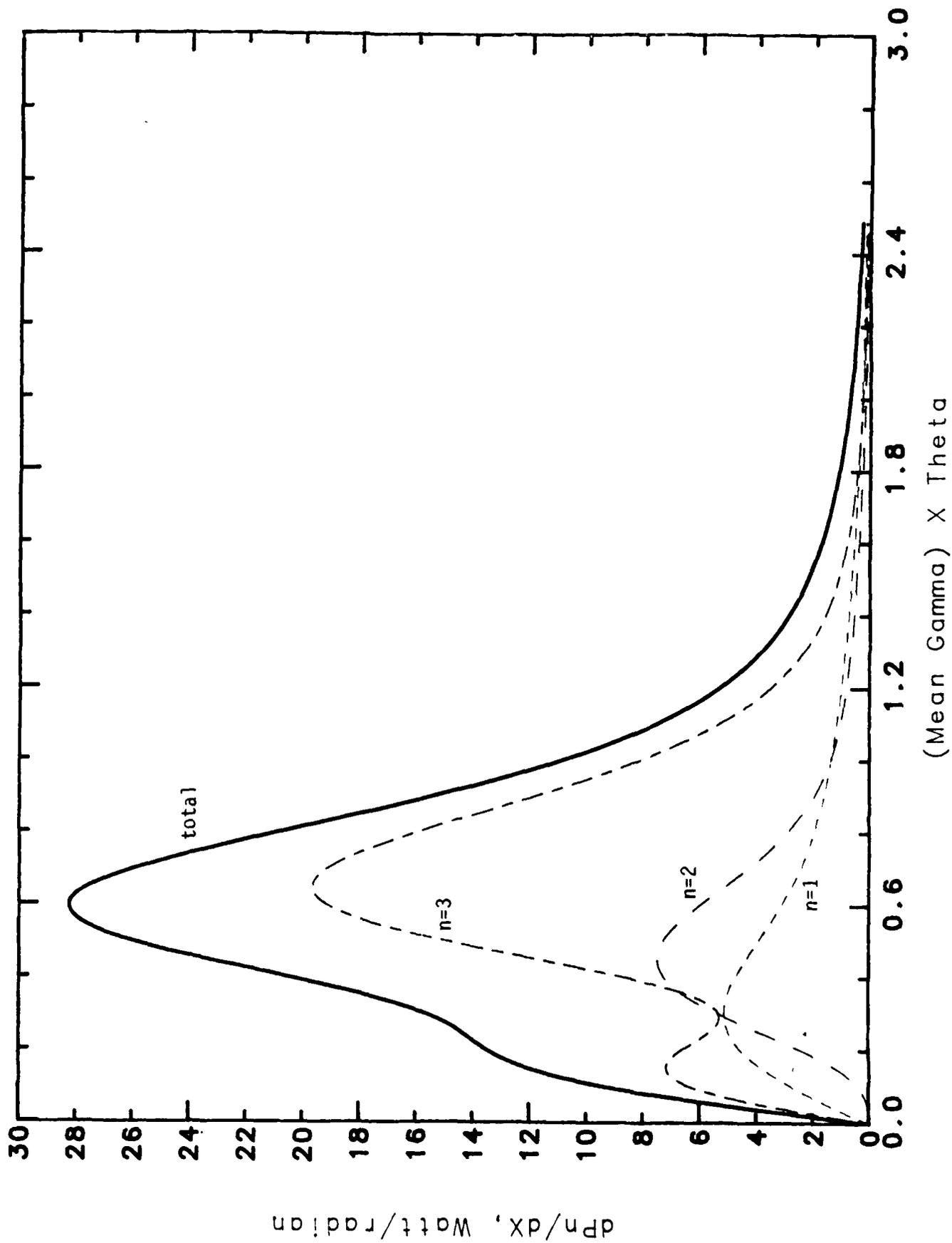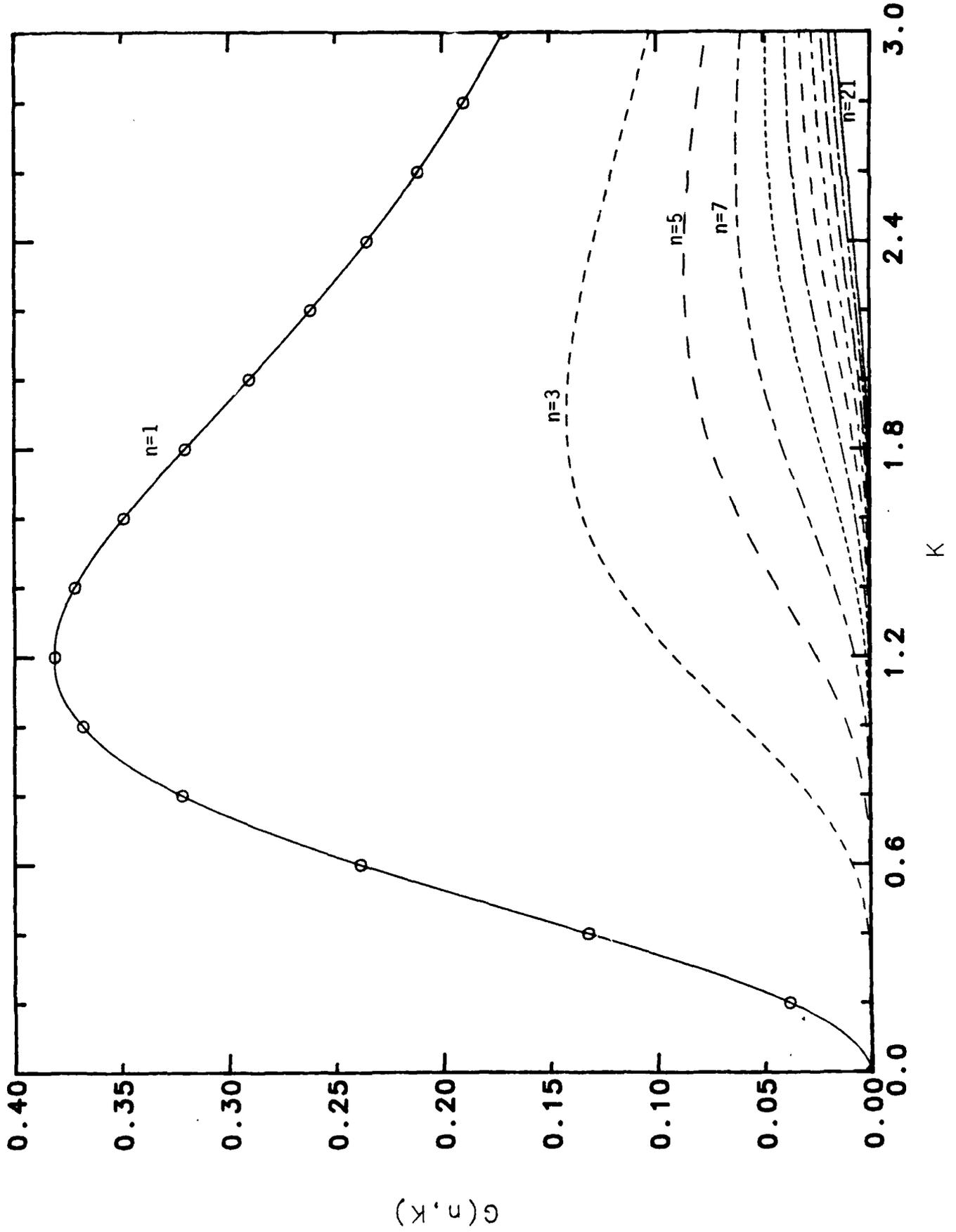
Appendix B

Design Note 11

Wiggler Field Errors

FEL Design Note 11

Wiggler Field Errors

R. G. Johnson
June 22, 1988

I.   Introduction

Errors in the wiggler magnetic fields can produce two deleterious

effects in an FEL. The electron beam can suffer a net deflection

(trajectory error), and the path length can be incorrect (phase

error). In the NBS wiggler the design and specifications are

probably sufficient that these inevitable errors will not cause

a serious problem in FEL operation. The purpose of this note is

to establish a basis for that conclusion.

The specifications which limit the integrated field errors to a

maximum of 92 G-cm (with field correctors at the beginning and

end of the full and half-length wiggler and, if necessary, at

intermediate points) effectively limit the trajectory errors.

The specification which limits the RMS field error to 0.5% is

important for both kind of errors but particularly so for phase

errors.

II. Types of Errors

In general, field errors can be divided into two classes, random

and correlated.[1,2] In this section the relative effects of

single errors of these types are compared. The effects due to a

distribution of (random) errors are considered in the next section. A random error is distinguished from a correlated error in that the excursion of the field is not compensated by nearby excursion(s) of the field in the opposite direction. Many of the sources of error in a hybrid wiggler produce correlated errors rather than the more serious random errors.[2] Note that fully correlated errors (i.e. exact cancellation) do not contribute to the field integral but do contribute to the RMS error. The division into random and correlated errors is of course an approximation. For example, errors which are correlated in a 2-D approximation may have a random component when 3-D effects are included.

The coordinate system is defined as: z - the axis of the wiggler, y - the direction of the magnetic field, and x - the direction of the electrons' oscillatory (wiggle) motion. The wiggler is considered as 2N half periods indexed by i. In this Note only field errors in the y-direction will be considered. To determine trajectory (displacement) and phase errors, the velocity and path length error must first be determined. They are given by

$$\Delta v_x = \int_o^z \Delta B_y(z)\,dz \tag{1}$$

$$\Delta l = \int_o^z (v_x \Delta v_x + \frac{1}{2}\Delta v_x^2)\,dz \tag{2}$$

From these the displacement and phase errors are given by

$$\Delta x = \int_o^z \Delta v_x\,dz \tag{3}$$

and

$$\Delta\phi = \frac{2\pi}{\lambda}[\frac{\Delta l}{\beta}] \tag{4}$$

where λ is the wavelength of FEL light. (Note: γ and β are
the usual relativistic quantities for the electron.) In the
remainder of this section three error type models are examined.
Equations are derived for Δx and Δl and numerical examples are
shown in Table 1. For the numerical examples the quantities
actually shown are $\Delta x/a$ and $\Delta l/s$ where a is the amplitude and s
is the extra one-period path length of the wiggle motion. These
quantities are given by

$$a = \frac{1}{2\pi}\lambda_w(K/\gamma) \tag{5a}$$

$$s = \frac{1}{4}\lambda_w(K/\gamma)^2 \tag{5b}$$

where λ_w is the length of a wiggler period and K is the wig-
gler constant. For example, for K = 1 and γ = 150 then
a = 29 μm and s = 0.31 μm.

Type I error: Assume a half-period sine function centered at
the i-th pole, i.e.

$$\Delta B_y = \Delta B_o \sin kz \qquad (i-1)\lambda_w/2 \le z \le (i)\lambda_w/2 \tag{6}$$

where $k = 2\pi/\lambda_w$. This is the only random error considered.
It is difficult to envisage how to physically produce such an
error but for modelling purposes it will be used. Brian Kincaid
suggests[1] that "there are errors, such as machining tolerances,
that are not necessarily correlated". Steve Benson reported[3]

that the STI Thunder wiggler had unexpectedly high random errors, probably due to near saturation of the pole pieces.

The consequences of this type of error (by integrating according to eqs. (1) - (3)) are given by

$$\Delta x = \frac{\Delta K}{\gamma} \lambda_w [2N - i] \qquad (7a)$$

$$\Delta l = \frac{1}{4} \lambda_w (K/\gamma)^2 [\Delta K/K + 2(\Delta K/K)^2 (2N - i - \frac{1}{4})]. \qquad (7b)$$

Note that because there is a net velocity error in this case, the trajectory error continues to grow from the point of occurence to the end of the wiggler.

Type II error: Assume a full-period sine function extending over the i-th and (i+1)-th poles, i.e.

$$\Delta B_y = \Delta B_o \sin kz \qquad (i-1)\lambda_w/2 \leq z \leq (i+1)\lambda_w/2. \qquad (8)$$

This is an approximation for the correlated field which would be produced if the magnet between two poles had a magnitude error. Actually the field would extend to several poles on each side of the magnet. However the assumed model is an adequate approximation.

For this case

$$\Delta x = 0 \qquad (9a)$$

$$\Delta l = \frac{1}{4} \lambda_w (K/\gamma)^2 [2\Delta K/K + (\Delta K/K)^2]. \qquad (9b)$$

Even if 3-D effects are included, the integrated field for this case is zero, by symmetry.

<u>Type III error</u> If a permanent magnet has a component of its field in the y-direction, the error field will peak at the center of the permanent magnet with lobes in the opposite direction on either side. For a hybrid wiggler the integrated field for such an error is nearly zero. (Not exactly zero because of the parts of the field not confined to the gap, i.e. 3-D effects.) As a model choose the following:

$$\Delta B_y{}^{(1)} = (\Delta B_0/2)\cos kz \quad (i-\frac{3}{2})\lambda_w/2 \le z \le (i-\frac{1}{2})\lambda_w/2 \quad (10a)$$

$$\Delta B_y{}^{(2)} = \Delta B_0 \cos kz \quad (i-\frac{1}{2})\lambda_w/2 \le z \le (i+\frac{1}{2})\lambda_w/2 \quad (10b)$$

$$\Delta B_y{}^{(3)} = (\Delta B_0/2)\cos kz \quad (i+\frac{1}{2})\lambda_w/2 \le z \le (i+\frac{3}{2})\lambda_w/2. \quad (10c)$$

Then

$$\Delta x = 0 \tag{11a}$$

$$\Delta l = \frac{1}{4}\lambda_w(K/\gamma)^2[\frac{3}{4}(\Delta K/K)^2]. \tag{11b}$$

Again this is an approximation for the real error which as in the previous case will extend over several half-periods on either side of the magnet in error.

The group at STI has made measurements[4] on both pure-REC and hybrid wiggler models with this type of error. For the pure-REC model the side lobes are very small and the velocity error on traversing the field is about 70% of that for a random error of the same magnitude. For the hybrid model the velocity error is at least a factor of 30 smaller. Using that ratio, an estimate

for $\Delta x/a$ is included in Table 1.

Table 1. Consequences of a single field error.

Error Type	Trajectory Error $\Delta x/a$	Path Error[a] $\Delta l/s$
I[b]	6.1	$\pm 0.005 + 0.01$
II	0	$\pm 0.01 + 2.5E-5$
III	0 (model) 0.2 (measured)[c]	1.9E-5

[a] The two terms are from the terms linear and quadratic in Δv_x.
[b] Field error assumed to occur at the center of the wiggler.
[c] From the results of Ref. 4.

The results shown in Table 1 form the basis for the conclusion that only random errors (i.e. Type I) are significant. For the correlated cases the trajectory errors are zero or nearly so. Although path length errors are of comperable size for single errors (Type I and II), terms linear in Δv_x (i.e. the mean of the error distribution is zero within the the tight field integral specifications. Consequently, the path errors from the correlated errors are a factor of about 1000 smaller than from the random errors.

III. Consequences of Random Errors

In the previous section the effects caused by single wiggler errors of various types were examined. To extend this analysis

to a complete wiggler is a difficult task. However Kincaid[1] has done this extension for the case of random errors which, as pointed out, are the worst case. In particular, because random errors produce a net velocity error, the resulting random walk of the trajectory can be extreme.

Kincaid uses the same definition of individual random errors as above. The distribution of such errors is assumed to be Gaussian with zero mean and standard deviation σ.

The calculated maximum trajectory error for a compensated (i.e. with steering) wiggler is given by

$$\Delta x/a = (2/3)^{1/2} \pi \sigma N^{3/2}. \tag{12}$$

For the NBS wiggler (N = 130, σ = 0.005) the maximum trajectory error is 19a (e.g. for K = 1 and γ = 150 then Δx = 0.55 mm). With steering at each quarter Δx = 2.4a (0.07 mm). Note that the optical waist for this example has a radius of 0.76 mm. Calculating the effect on the emission spectrum caused by random errors is more complicated and in general cannot be reduced to an anaylitical form. For wigglers with small errors and/or few periods (such that $\sigma^2 N^3 \leq 0.5$) a Gaussian approximation is valid. That is not the case for the NBS wiggler; however, a second approximation based on the Rice-Mandel function (see Ref. 1) does apply.

The loss in the spontaneous emission spectral peaks is parameterized by the quantity

$$q = n\sigma^2 N^2 (K^2/2)/(1 + K^2/2) \tag{13}$$

where n is the harmonic number. For the NBS wiggler (and for n = 1 and K = 1.0) q = 0.14. Using Figs. 10 and 11 in Ref. 1 the loss in peak intensity is estimated to be less than 8.5% and the peak broadening is negligible. Then by Madey's theorem the small signal gain will be reduced by less than 8.5%. Note that the loss is more severe for the higher harmonics. Actually this may be an over-estimate for the NBS wiggler. Although the calculation is for a compensated wiggler, it is compensated only at each end. Unfortunately it is not clear how to modify the analysis for a wiggler compensated at inter-mediate points. An educated guess is that the loss in small signal gain is inversely proportional to the number of segments. Thus if the NBS wiggler is compensated at each quarter, the small signal gain would be reduced by 2.2%, rather than 8.5% (for n = 1).

IV. Conclusions

Random errors in the magnetic fields of a wiggler can cause serious degredation in its performance. The effect is primarily due to the fact that the electrons passing a random error have a net velocity error which has the rest of the wiggler in which to act. Consequently the electron beam can walk excessively off its normal path. On the other hand, correlated errors are much less of a problem.

Although hybrid wigglers are much less prone to random errors than a pure-REC design, there may still be random errors due to

mechanical imprecision and magnetic material imperfections.
Both the specifications and the contractor's proposal should be
adequate to control these errors. At minimum gap a 0.5% error
is caused by a 2-mil gap error. The contractor has set toler-
ences on pole pieces and holders of ±0.5 mil. The design also
uses a larger volume of permendur than necessary to achieve the
required field strength. Although this was done to produce a
better field shape, it also means that the permendur is operated
at a low permanance coefficient (the ratio B/H).

A primary source of correlated errors, errors in the permanent
magnet blocks, also seems well under control in the contractor's
design. In the design, tolerances on H_c are ±2% and tolerances
on magnetization direction are ±2°. Although such variation
could cause RMS errors greater than 0.5%, sorting and matching
blocks will reduce the errors considerably.

A worst case scenario would occur if most of the field errors
were random and yet the field integral and RMS specifications
were met without the need for intermediate steering. In that
case the trajectory error and the loss in small signal gain
are marginal. However a small change in the design can help
reduce this problem. At present steering for half-length
wiggler operation is part of a removable end corrector. If
this steering is made a permanent part of the full-length wig-
gler, the trajectory errors can be reduced by 2.8 and loss of
small signal gain can be reduced by about 2 (for the full-
length wiggler).

Finally, more accurate calculations of the effects of wiggler field errors need to be done to check the results in this note.

References

1. Brian M. Kincaid, J. Opt. Soc. Am. B, <u>2</u>, 1294 (1985).

2. K. Halbach, Nucl. Instrum. Methods, <u>A246</u>, 77 (1986).

3. Steve Benson, private communication (1988).

4. K.E. Robinson, D.C. Quimby, and J.M. Slater, IEEE J. Quantum Electron., <u>QE-23</u>, 1497 (1987).

Appendix C

Deisgn Note 12

Optical Cavity Length Choice: Update

FEL Design Note   12

Optical Cavity Length Choice: Update

R. Johnson and C. Johnson
December 19, 1988

The issue of the length of the optical cavity was discussed in FEL Design Notes 1 and 3. We have decided recently to remove the entire shielding wall that is between the RTM room and the FEL room. Also, it appears that we will not use a laser-drive photocathode in the new high current injector. Therefore, the issue of the cavity length bears re-examination.

The design criteria are summarized here: 1) the optical cavity must fit in the allocated space; 2) the length of the optical cavity, L, is given by the relation $L = Mc/(2f_0)$, where M = integer, c = speed of light, and f_0 = the rf frequency of 2.38 GHz; 3) the frequency of the electron pulses in the RTM, f_I, is given by $f_I = mf_0/M$, where m and M/m are integers; 4) several values of m, which represent the number of independent optical pulses in the cavity, are available for the same value of M, so that the average power and/or the peak current can be varied; 5) it is possible to extract the full beam power of 100 kW over an "acceptable" range of electron beam parameters (energy, peak current, and pulsewidth); 6) the values of m and M are optimized for the performance of the new high-current injector; 7) the physical clearance between the optical cavity mirrors and the FEL electron beam transport magnets (D16 - D18) is maximized; and 8) diffraction losses and alignment problems in the optical cavity are minimized. The new high-current injector may also serve electron-beam users in MR1, but this requirement is not addressed here.

The original proposal had m = 5 and M = 120, so that L = 7.558 m and f_I = 99.167 MHz, which is the 24th sub-harmonic of f_0. The transverse distance from the center of the upstream cavity mirror to the electron beam axis was 1.87". With 3-ps wide pulses, the RTM would have delivered a 100 kW beam at

1.82 A peak current and 185 MeV.

Design Note 3 recommended $m = 4$ and $M = 128$, so that $L = 8.062$ m and $f_I = 74.375$ MHz, which is the 32nd sub-harmonic of f_o. The FEL could be operated a $m = 1$, 2, 8, or 16. Design Note 3 demonstrated that 2.42 A would be required to produce full beam power at 185 MeV and 3-ps wide pulses. For $m = 1$ and 2, it was shown to be impossible to deliver full beam power, since the peak current was limited to 4 A or less. With the 8-m cavity, the transverse distance from the center of the upstream cavity mirror and the electron beam axis was increased to 2.97". The longitudinal distance from the center of the upstream cavity mirror to the point where the 1"-OD vacuum beam pipes of the electron and optical axes would intersect was 16". There was 39" from the downstream side of D18 and the center of the downstream cavity mirror. The experimental layout is shown in Figures 2 and 3 of Design Note #3.

We are now recommending $m = 4$ and $M = 144$, so that $L = 9.067$ m and $f_I = 66.111$ MHz, which is the 36th sub-harmonic of f_o. The integer m could take on the values 1, 2, 3, 4, 6, 8, 9, or 12. For $m = 4$, $E = 185$ MeV, and $\tau = 3$ ps, it would require 2.73 A peak current to deliver 100 kW of electron beam power. Full beam power could also be delivered at high energy with $m = 3$ and 3.5 A $< I < 4$ A (see Figure 1). The transverse distance from the center of the upstream mirror to the electron beam axis would be about 4.5"; if the magnets D15 and D16 were relocated as shown in Figure 2, the distance would be 6.66". The longitudinal spacing between the center of the upstream mirror and the point where the 1"-OD vacuum beam pipes of the electron and optical axes intersect would be 45", and there would be 49" from the downstream side of D18 to the center of the downstream cavity mirror. The new layout is shown in Figures 2 and 3.

The proposed design meets the requirements 1) - 4). The number of actual

values for m is greater than before. Regarding beam power, requirement 5), the proposed design offers the advantage of higher peak current and therefore higher gain and less optical damage to the cavity mirrors (see Design Note 10). However, the injector performance may be compromised at high current; this issue is under study by R. Cutler and E. Lindstrom. The longer cavity reduces the average optical power density on the cavity mirrors. Regarding item 6), the 36th sub-harmonic is more convenient for the new chopper-buncher system. The physical clearances, item 7), are very comfortable with the proposed design. There is no increase in diffraction losses, item 8), if 2"-diameter substrates are used for the cavity mirrors.

Even larger values for the integer M/m are possible. However, to take advantage of the available electron beam power while holding m fixed, higher peak currents would be required. As an example, consider M = 192, m = 4 with m = 1, 2, 3, 6, 8, or 12. L would be 12.09 m and a peak current of 3.63 A would be required to produce 100 kW of beam power at 185 MeV. A 12-m cavity is physically possible, but just barely (it would involve moving the upstream cavity mirror back 3 meters to just inside the RTM room). Diffraction losses would require 4"-diameter optics for the upstream mirror.

We believe the point of diminishing returns has been reached with the 9-m optical cavity, and are recommending ~his design change for the NIST-FEL.

Figure Captions

1. Power limit curves for the RTM. The solid lines represent full beam power (100 kW) as a function of electron beam energy for M = 144 and several values of m. The BBU limit is estimated to be 2 mA at 100 kW.

2. Layout of components around the upstream cavity mirror. The dimensions are given in inches. The spacing between D15 and D16 was decreased to 12" in order to increase the transverse distance between the upstream cavity mirror and the electron beam axis.

3. Layout of the FEL room and a portion of the FEL electron beam transport. Two possible configurations are shown for the bend magnet D18.
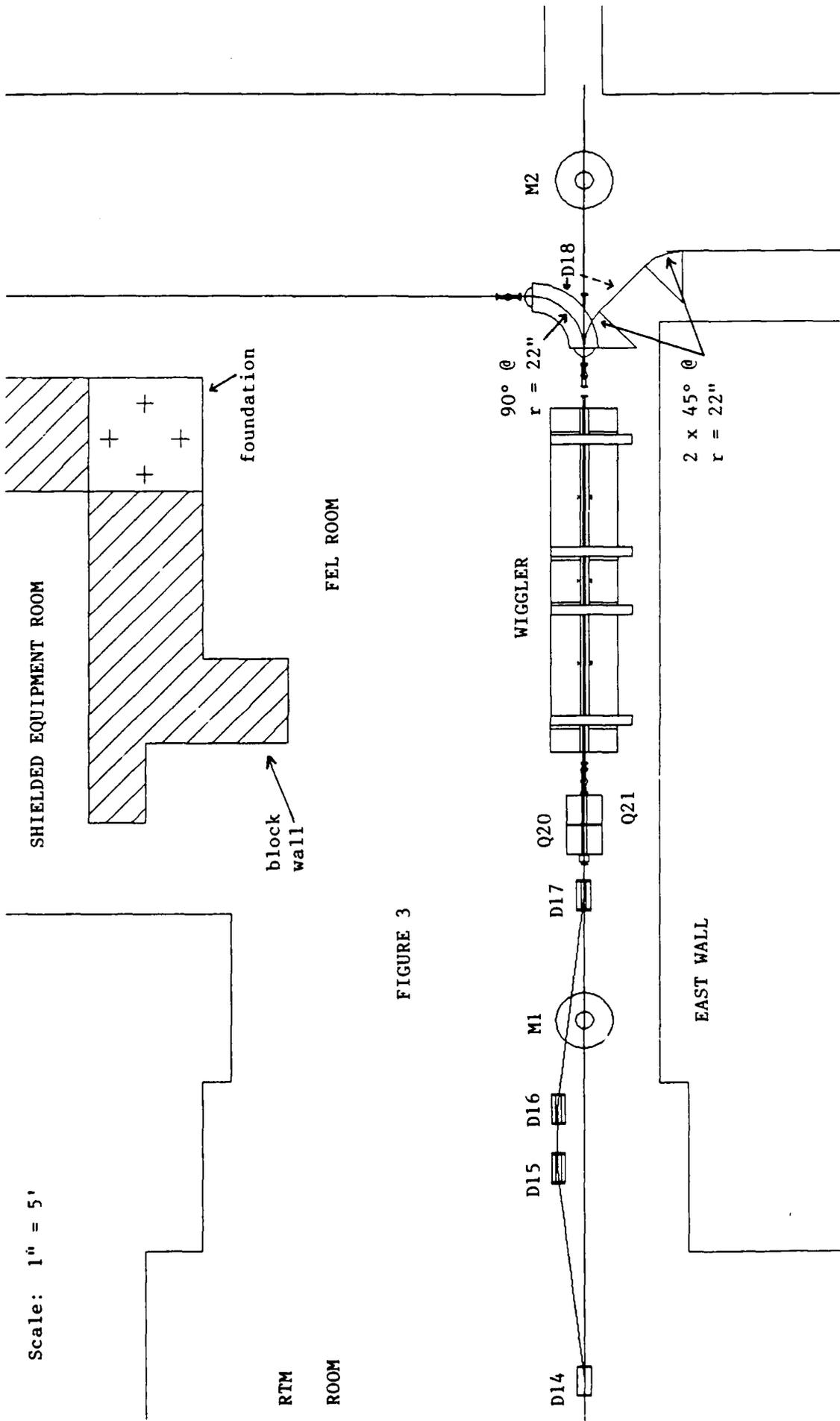
FIGURE 1

Figure 2
1″ = 16″

D17

Center of M1

7.11

12.00

31.50

46.92

31.49

ø7.50

D16

13

11.41

12

D15

EAST WALL

e- Beam

FEL AXIS

FIGURE 3

Scale: 1" = 5'

SHIELDED EQUIPMENT ROOM

foundation

block wall

FEL ROOM

RTM ROOM

D14

D15 D16

M1

D17

Q20

Q21

WIGGLER

90° @ r = 22"

D18

2 x 45° @ r = 22"

M2

EAST WALL
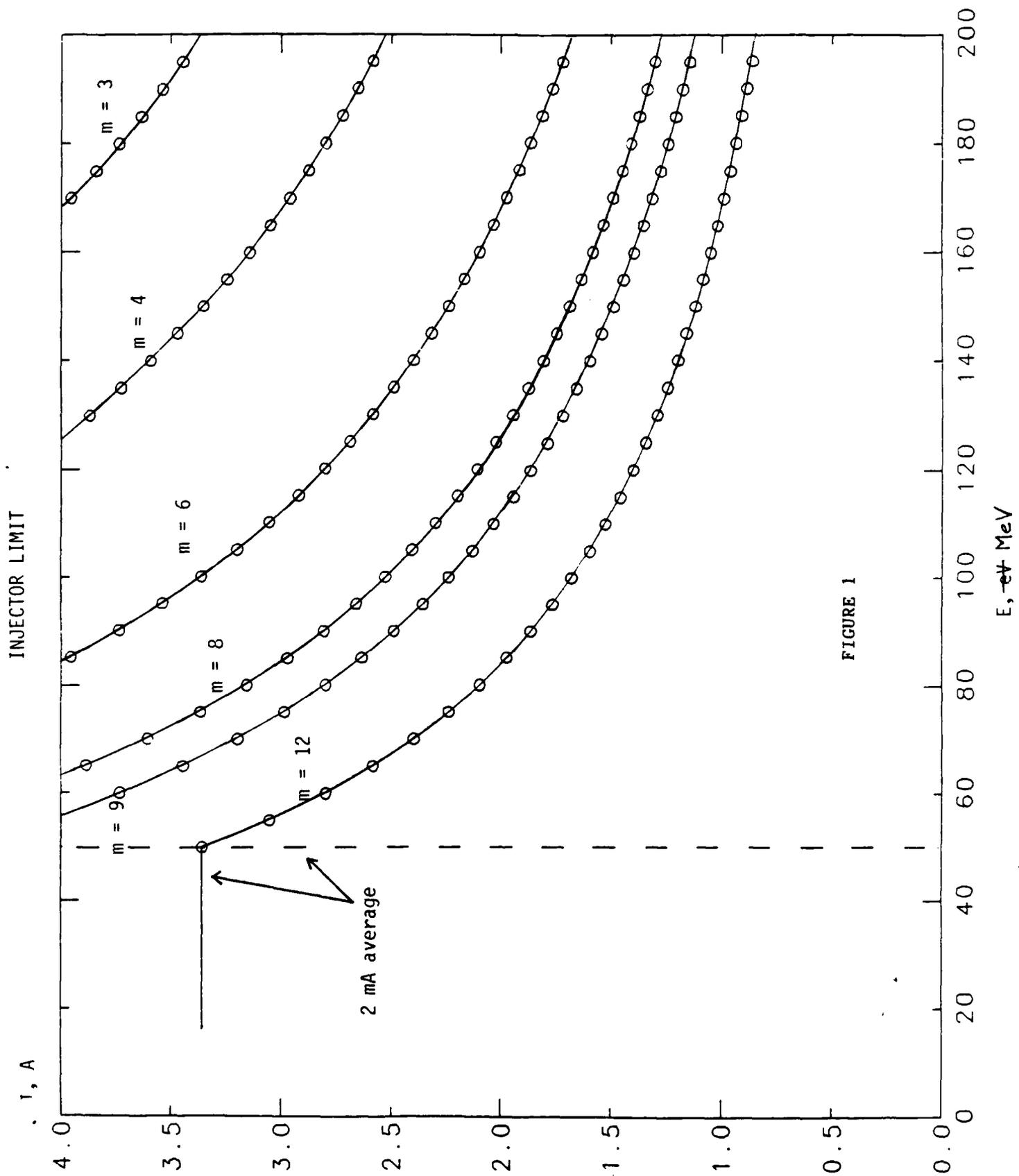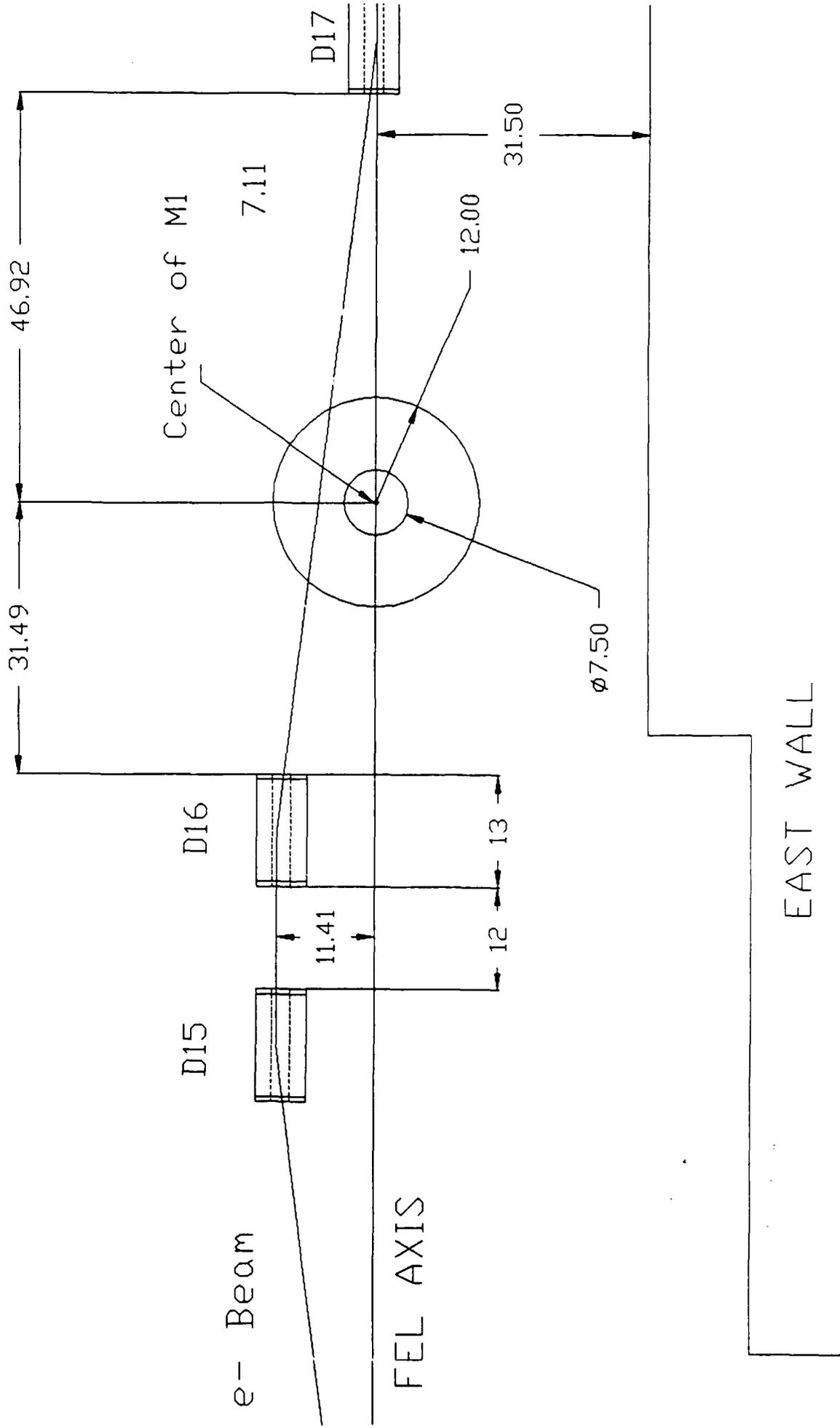
Appendix D

The NBS Free Electron Laser Facility

The NBS free electron laser facility

B Carol Johnson[†], P H Debenham[†], S Penner[†], C-M Tang[*], and P Sprangle[*]

[†]Center for Radiation Research, National Bureau of Standards, Gaithersburg,
MD 20899 and [*]Plasma Physics Division, Naval Research Laboratory, Washington, DC 20375

ABSTRACT: A free electron laser (FEL) user facility is being con-
structed at the National Bureau of Standards in collaboration with the
Naval Research Laboratory. The anticipated performance of the FEL is:
1) wavelength variable from approximately 150 nm to 10 μm; 2) continuous
train of 3 ps-wide pulses at 74.375 MHz; and 3) average power of 10 W to
200 W. One advantage of the NBS-FEL for RIS schemes is the ability to
select the wavelength at will. It is also possible to scan the wave-
length. The high repetition rate is an additional attractive feature.

1. INTRODUCTION

The National Bureau of Standards is building a free electron laser (FEL) as
a joint project with the Naval Research Laboratory. The FEL will be oper-
ated as an user facility for research in physics, chemistry, biophysics,
and biomedicine. The electron beam source for the FEL is the NBS-LANL cw
racetrack microtron (RTM). The combined characteristics of the RTM make it
an unique FEL driver. The other necessary ingredients for the FEL are the
magnetic structure, or wiggler, which couples the energy of the electrons
to that of the radiation field, and the optical cavity. We have calculated
the characteristics of the NBS-FEL, and anticipate operation from about 150
nm to 10 μm with an average power of 10 W to 200 W. The FEL can be
described as a high-power, picosecond, tunable, harmonically-mode-locked
laser.

2. FREE ELECTRON LASER

The NBS-LANL cw RTM consists of a 5 MeV injector section and a 12 MeV rf
linear accelerator, or linac (Penner *et al*. 1981). The linac is located
between two uniform-field end magnets that recirculate the beam. The beam
can be deflected out of the RTM after completing up to and including 15
passes through the linac, so that the final beam energy is 17 MeV to 185
MeV. The performance of the 5 MeV injector section exceeds the design
specifications (Wilson *et al*. 1987). The principal components of the RTM
are installed; a second series of beam tests is being done at 17 MeV before
the entire machine and the associated FEL transport system are completed in
1989.

When compared to other types of accelerators, there are several advantages
of an RTM as an FEL driver. The large energy range corresponds to optical
wavelengths from 200 nm to 10 μm. Because the transverse emittance and
longitudinal energy spread of the RTM are small, operation in the ultra-

violet is not limited by these electron beam parameters. The electron beam is a continuous train of pulses at a frequency of 74.375 MHz, which is the 32nd sub-harmonic of rf drive frequency of 2.38 GHz. The excellent energy stability and the continuous repetition rate will act to stabilize the FEL wavelength. Finally, in comparison with single-pass linacs, the RTM is an economical and compact device.

The wiggler will provide a linearly-polarized magnetic field with a peak amplitude of B_o = 0.54 T, a minimum gap of 1.0 cm, and a period of λ_w = 2.8 cm. These values give a "wiggler parameter", K_{rms}, of 1.0 (Tang *et al.* 1987). The wiggler, which is being obtained commercially, is actually two separate devices. Two 65-period-long sections are used together for lasing in the UV and visible, where large gain is required (gain $\propto N^3$, where N is the number of periods). In the IR, diffraction losses limit the useful length to N = 65.

The optical resonator of the FEL is designed to produce a waist at the center of the wiggler. The spherical cavity mirrors are multi-layer dielectrics; a partial transmitter is used as an output coupler. The length between the cavity mirrors will be 8.062 m, so that the inverse of the round trip light travel time is 18.594 MHz, which is the 128th sub-multiple of the rf drive frequency. At the 74.375 MHz repetition rate, there are four independent light pulses and two electron pulses in the cavity at a given time. For some experiments, it will be desirable to operate at a repetition rate of 18.594 MHz.

The optical wavelength depends on the electron beam energy and the strength of the magnetic field: $\lambda = \lambda_w(1 + K_{rms}^2)/(2\gamma^2)$, where $K_{rms} \propto B_o$. Here γ is the electron beam energy in units of the electron rest mass. We will select the optical wavelength by adjusting γ. The value of γ depends on the number of passes in the microtron and the energy gain per pass, ΔE = 12 ± 2.4 MeV. We will scan the wavelength by changing the gap between the wiggler poles, for values of K_{rms} between 1.0 and 0.6. See Figure 1.

Fig. 1. Possible lasing wavelengths with the NBS-FEL. The solid horizontal lines are for fixed γ and ΔE, with K_{rms} between 0.6 and 1.0.

3. PREDICTED PERFORMANCE

The characteristics of the FEL have been described in some detail (Penner *et al.* 1988). We have calculated the small-signal power gain using a three-dimensional numerical method that includes, among other things, the transverse beam emittance (Tang *et al.* 1987). The small signal power gain is between 10% and 35%. In the fundamental, the small value of the gain in the UV and decreasing mirror reflectivities determine the 200 nm cutoff. However, we expect to have adequate electron beam quality to allow for operation as an oscillator on the third harmonic down to about 150 nm.

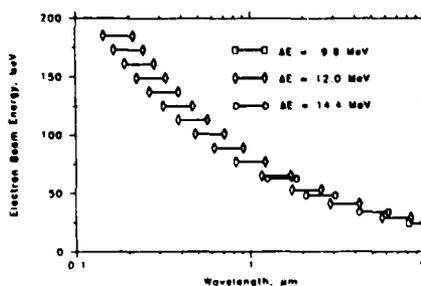For a saturated FEL in the ideal, one-dimensional, low-gain model, the

maximum power extraction efficiency from the electron beam is $1/(2N)$ (Sprangle, Smith, and Granatstein 1978). The maximum optical power as a function of wavelength is shown in Figure 2. The electron beam parameters were taken to be: repetition rate = 74.375 MHz, peak current = 2 A, and pulse width = 3 ps. The actual output power depends on the cavity losses. For the UV, visible, and most of the IR, diffraction losses are negligible. The power reflection coefficient of the high reflector, R_{HR}, and the power transmission coefficient of the output coupler, T, are given in Table 1.

Table 1
FEL Mirror Properties

Wavelength μm	Reflection Coefficient R_{HR}	Transmission Coefficient T
0.15 - 0.20	0.960	0.005
0.20 - 0.35	0.990	0.010
0.35 - 0.80	0.999	0.050
0.80 - 7.00	0.990	0.050
7.0 - 10.00	0.990	0.010

The output of the FEL will be linearly polarized. The spatial mode will be predominantly TEM_{00}. The degree of mode-locking in the FEL should be good; experiments with FELs driven by pulsed linacs indicate that the spectral bandwidth is Fourier-transform-limited (Benson 1985). A reasonable upper limit on the spectral bandwidth is found by assuming a Gaussian profile for the temporal pulse shape; for $\delta t = 3$ ps (FWHM), the Fourier-transform-limited bandwidth is 200 GHz, or about 7 cm^{-1}. At 200 nm, this corresponds to a resolution of $1.4 \cdot 10^{-4}$. The relative energy stability of the electron beam at this wavelength is expected to be $\pm 4 \cdot 10^{-5}$, and the fractional energy spread will be $\pm 1 \cdot 10^{-4}$, which is much smaller than the fractional width of the laser gain curve, $4 \cdot 10^{-3}$.
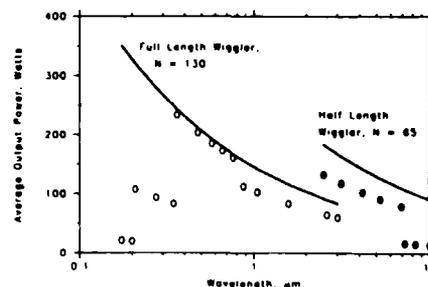

Fig. 2. Calculated average output power of the NBS-FEL as a function of wavelength. The solid lines are the maximum optical power. Note the dependence of the actual power on mirror properties (symbols).

The ability to select the wavelength makes an FEL an attractive RIS source. This is particularly true in the ultraviolet. The high repetition rate of the NBS-FEL may prove useful in RIS studies where high sensitivity is required, or multi-photon ionization is a strong background effect. As the energy in each pulse is moderate compared to that of low repetition rate, Q-switched lasers, the NBS-FEL is most suited to RIS processes involving single photon excitations. In two-color experiments, the other source(s) could be FEL-pumped tunable lasers, cw lasers, or cw, mode-locked lasers that are synchronized to the FEL repetition rate. The probability of excitation with a single pulse from the FEL can be estimated by comparing the time required for a π-pulse, t_π, to the optical pulse length, δt (Payne 1984). This is a reasonable estimate if the spectral bandwidth

is Fourier-transform-limited. The result is, for $g_1f_{12} = 1.0$, a 1-mm beam diameter, and the data shown in Figure 2, 0.3 ps $\leq t_\pi \leq 3$ ps. This time scales as $(g_1f_{12})^{-1/2}$, so it may be possible to saturate $(t_\pi > \delta t)$ strong transitions. In order to ionize the excited state, the product of the photoionization cross section and the photon fluence must be greater than unity. The photon fluence for the FEL for the data in Figure 2 is $3 \cdot 10^{13}$ photons cm^{-2} to $5 \cdot 10^{15}$ photons cm^{-2}. Typical photoionization cross sections are 10^{-16} cm^2 to 10^{-18} cm^2, so in a two-step, single-color experiment, the FEL would not produce 100% ionization in a single pulse.

4. USER FACILITY

There will be two experimental rooms in the user facility. The first, about 1600 square feet in area, is adjacent to the FEL, so that UV radiation can be delivered to users with a minimum of reflections. This room is located underground and is separated from the FEL by a 17 foot-thick shielding wall. The second room, about 2000 square feet in area, will be a new addition at ground level. The first operation of the FEL is scheduled for 1991. Administrative groups include an outside advisory panel, which reports to the Director of the Center of Radiation Research. The project is managed by the Chief, Radiation Source and Instrumentation Division. We are also forming a FEL user group, which will interact at the Division level.

5. ACKNOWLEDGEMENTS

6. REFERENCES

Benson S V 1985 Ph.D. Thesis, Stanford University

Payne M G 1984 in *Resonance Ionization Spectroscopy 1984* ed G S Hurst and M G Payne (The Institute of Physics: Bristol, England) pp 19-26

Penner S et al. 1981 *IEEE Trans. Nuc. Sci.* NS-28 1526

Penner S et al. 1988 to appear in the *Proceedings of the Ninth International Free Electron Laser Conference*

Sprangle P, Smith R A, Granatstein V L 1978 *NRL Memorandum Report 3911* (Naval Research Laboratory: Washington, DC)

Tang C-M, Sprangle P, Penner S and Maruyama X K 1987 *Proceedings of the 1987 IEEE Particle Accelerator Conference* (IEEE Cat. No. 87CH2387-9) 1 205

Wilson M A et al. 1987 *Proceedings of the 1987 IEEE Particle Accelerator Conference* (IEEE Cat. No. 87CH2387-9) 1 322

Appendix E

NIST-Los Alamos Racetrack Microtron Status

NIST-Los Alamos Racetrack Microtron Status

M.A. Wilson, R.L. Ayres, R.I. Cutler, P.H. Debenham, E.R. Lindstrom,
D.L. Mohr, S. Penner*, J.E. Rose
National Institute of Standards and Technology (formerly NBS)
Gaithersburg, MD 20899

L.M. Young
Los Alamos National Laboratory
Los Alamos, NM 87545

Introduction

The NIST-Los Alamos Racetrack Microtron (RTM) is designed to deliver a low-emittance electron beam of up to 0.5 mA cw over an energy range of 17 MeV to 185 MeV. Fed by a 5 MeV injector, the RTM contains two 180° end magnets that recirculate the beam up to 15 times through a 12 MeV RF linac. The linac, which operates in a standing-wave mode at 2380 MHz, has been tested to nearly full RF power. At present, the injector has undergone beam tests,[1] and the beam transport system is complete through the 12 MeV linac. A temporary beam line has been installed at the exit of one end magnet to measure the beam energy, energy spread, and emittance after one pass through the accelerator. Preliminary results indicate that the accelerated beam energy spread and emittance are within design goals.

Accelerator Description

The RTM and injector, shown in Figure 1, are connected by a 180° achromatic beam transport system (shown in Figure 2), which injects the 5 MeV beam onto the RTM accelerator axis. The two end magnets recirculate the beam through the 12 MeV linac up to 15 times by way of separated return lines. A single, 500 kW, cw klystron delivers RF power to four separate accelerating sections (two on the injector and two on the RTM axis) by way of a waveguide RF distribution system. The phase and amplitude of each linac section are independently controlled. Tests of the RF system[2] have confirmed that

phase and amplitude stability are well within design requirements.

To measure the effect on the electron beam of the first-pass acceleration through the RTM linac, a temporary beam line has been installed in place of the return lines at the exit of end magnet E1, parallel to the linac axis at a displacement of 66 cm. This configuration is shown in Figures 3 and 4. Included on this one-pass return beam line are three viewscreens, spaced three meters apart, to determine the beam position, shape, and approximate size. A wirescanner assembly[3] is included near each viewscreen for more precise measurements of the beam size. A Hall probe, calibrated by an adjacent NMR, is used to measure the end magnet field.

Beam Transport, Acceleration, and Measurement

Conditions calculated to provide achromatic beam transport have been verified experimentally for each 90° section of the 180° transport beam line between the 5 MeV injector and the RTM. The final dipole magnet in the transport system deflects the 5 MeV beam through an angle of 15° onto the RTM accelerator axis. Three low-field steering magnets (S16-S18, Figure 4), one located at each end of the linac and one between the two linac sections, are used to keep the beam on the accelerator axis over the 12.5-meter distance between end magnets. Quadrupole doublets ($Q_{6,7}$ and $Q_{8,9}$, Figure 4) are located at each end of the RTM linac.
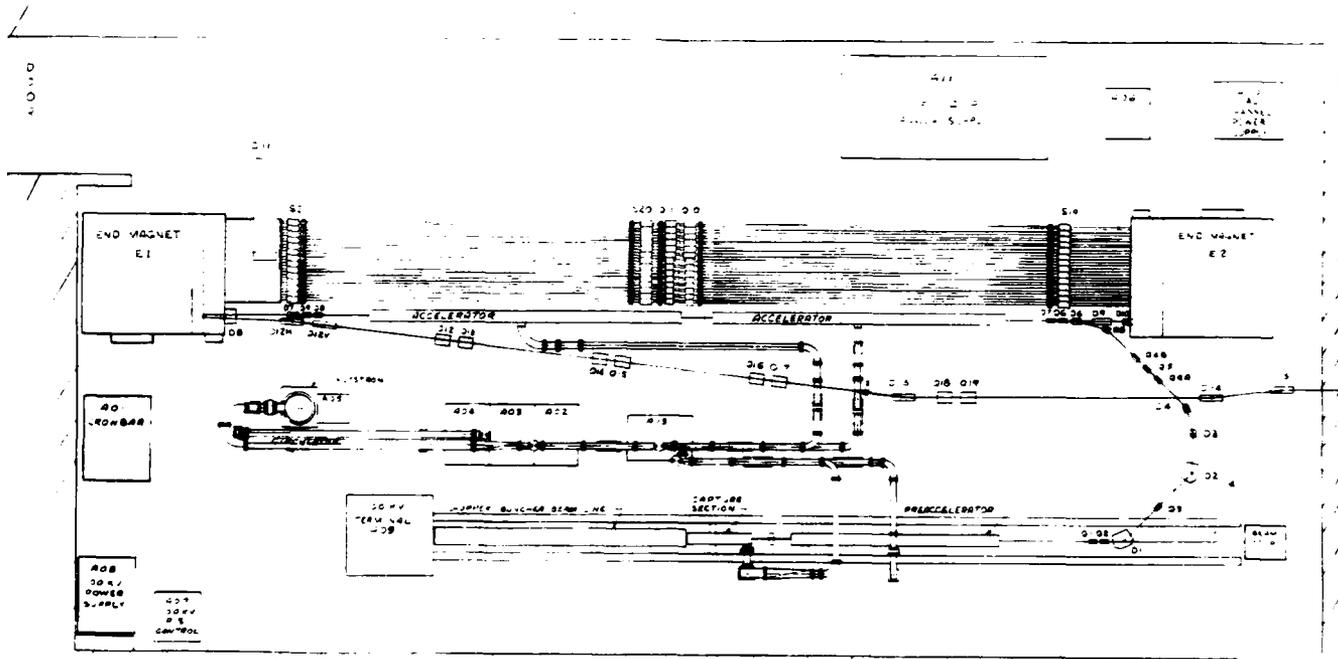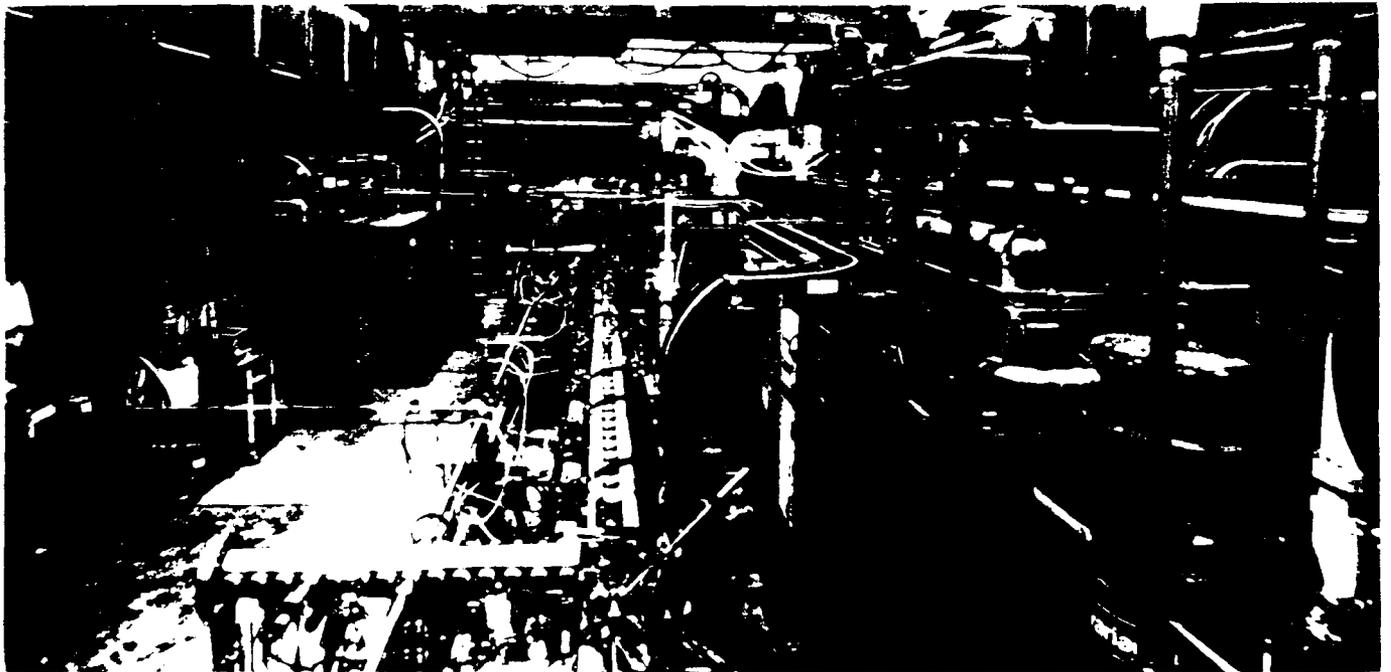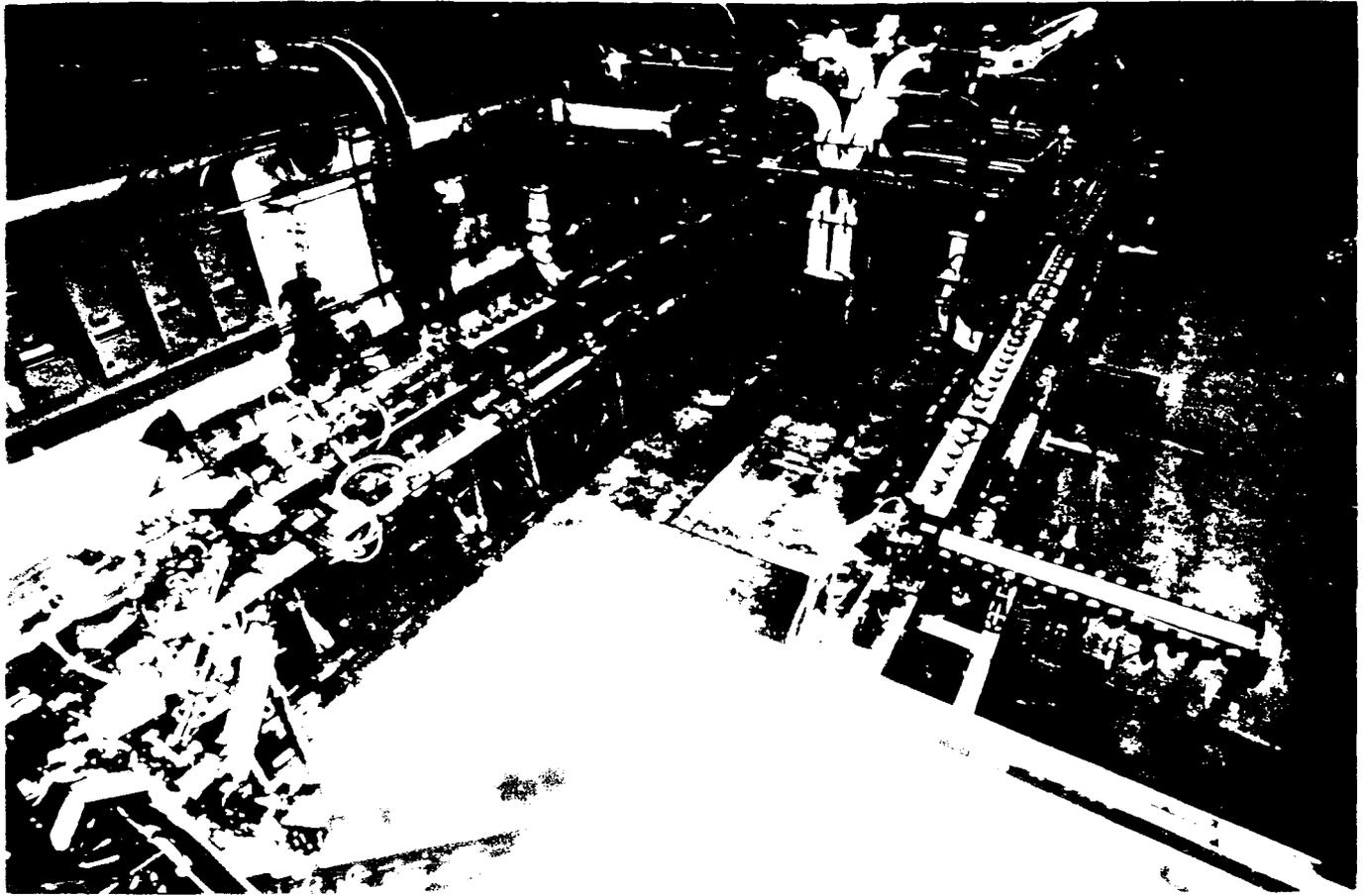

Figure 1. Plan view of the completed RTM.

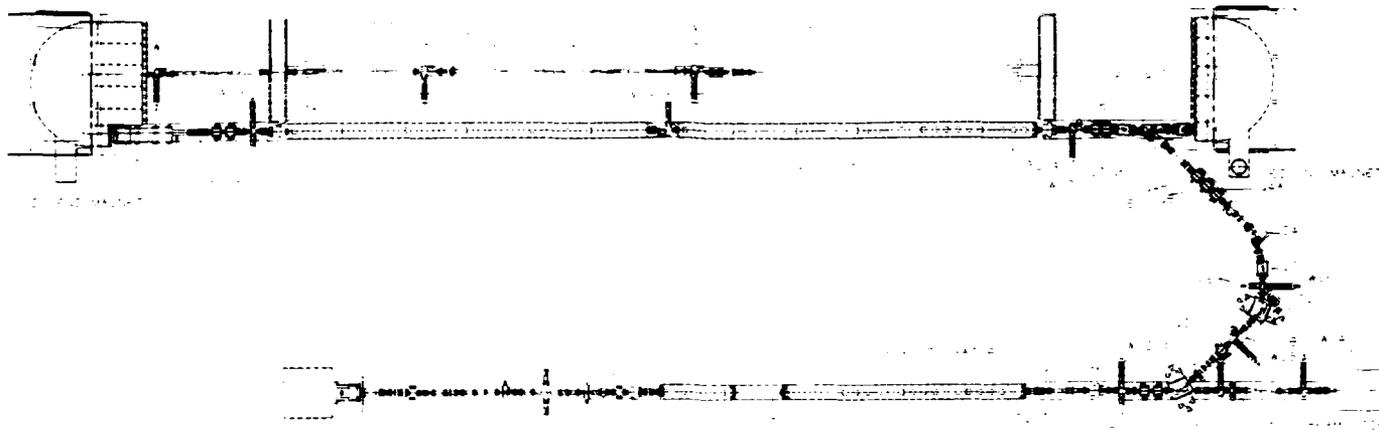*Present address: 10500 Pine Haven Terrace, Rockville, MD 20852.

Figure 4. Plan view of the RTM with the one-pass return line.

The 5 MeV beam was aligned on the RTM accelerator axis and deflected by end magnet E1 onto the one-pass return beam line. The RF power in the first linac section was raised to about 100 kW, and the accelerator RF phase was adjusted to maximize the beam energy gain, as determined by the magnetic field in E1. This sequence was repeated with the second linac section. The maximum beam energy attained with power in both accelerators was 16.2 MeV, limited during these preliminary beam tests by the voltage gradient sustainable in the second linac. This limit will be overcome as linac conditioning continues.

The power in the accelerating sections was reduced by about 10% for the sustained operation required to carry out the beam tests. Figure 5 shows the accelerated beam spot produced on viewscreens along the one-pass return beam line axis. The beam is about 1 mm high (y) by 2 mm wide (x). With no steering applied beyond the middle of the linac to the end of the one-pass return line, the beam passed within 1 mm of the center of each viewscreen, indicating good alignment of the beam with both the accelerating fields and magnetic guide fields.
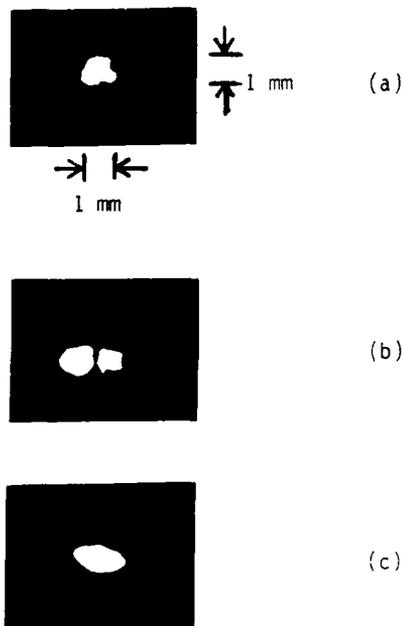
Figure 5. Image of accelerated beam on viewscreens located three meters apart on one-pass return line axis. a) 1 m from E1 exit, b) 3 m from (a), c) 6 m from (a).
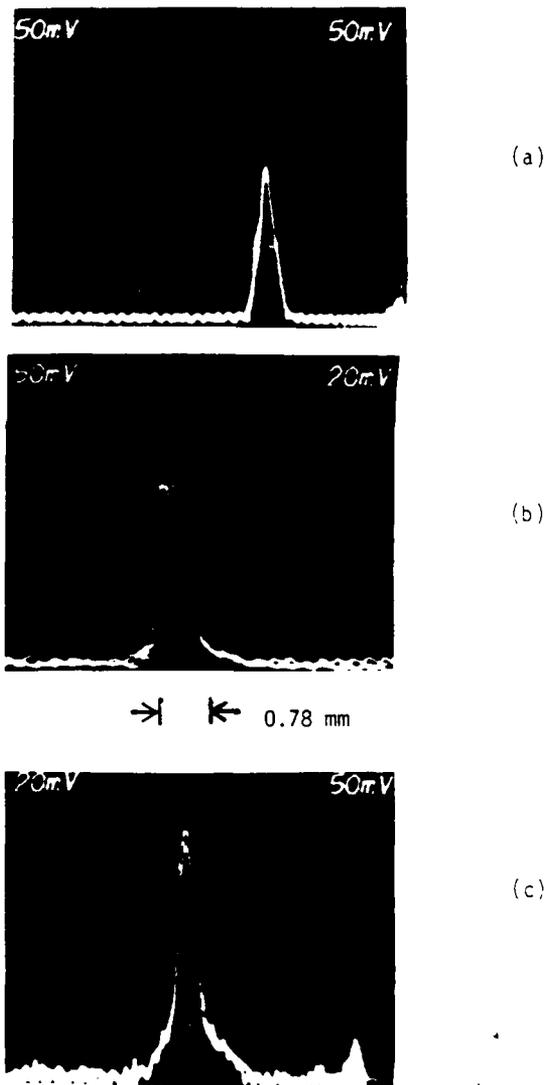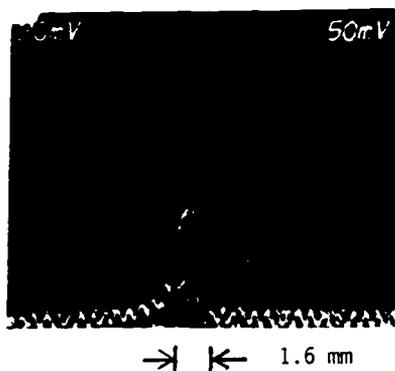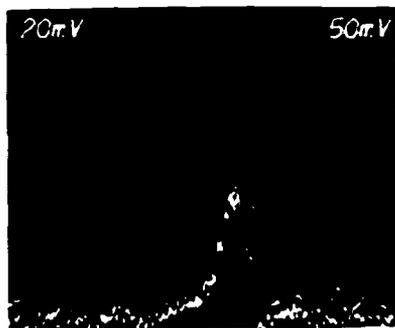

Figure 6. Oscilloscope traces of the signal produced as the y-scanning wires pass through the accelerated beam on the one-pass return line.
a) Beam y-profile about one meter from the exit of end magnet E1.
b) Beam y-profile 3 m from (a). The horizontal scale is magnified 2.5x relative to (a) and (c).
c) Beam y-profile 6 m from (a).

The quadrupole doublet, Q_8 and Q_9, located at the exit end of the RTM Linac (Figure 4), was adjusted to produce a waist in the y-direction near the middle of the one-pass return beam line to facilitate emittance measurements with the three wirescanners. Figure 6 shows the beam profile in the y-direction as measured by these wirescanners. The focusing produced a 0.8 mm vertical beam waist near the middle wirescanner. Following a technique described in an earlier paper,[1] the normalized transverse y-plane emittance[4] was determined from these beam size measurements to be 2.35 μm. The x-plane emittance was not determinable, from similar measurements, due to energy spread effects. Beam envelope measurements along the accelerator axis will be included during further planned beam tests, in order to measure the x-plane emittance and the beam energy spread independently.
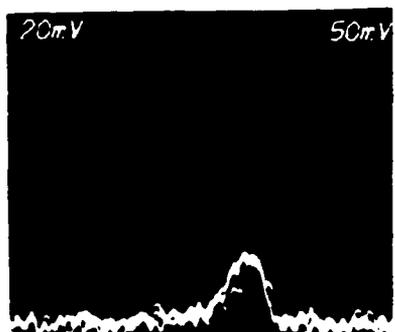
As a first estimate of the accelerated beam energy spread, the beam was focused to as small a size as possible in the x-direction near the first wirescanner on the one-pass return beam line by the quadrupole doublet, Q_8 and Q_9. Figure 7 shows the beam profiles at the three wirescanner positions along the one-pass beam return line under these conditions. The minimum beam envelope width was measured to be about 1.6 mm. From the minimum y-waist measured from the data in Figure 6, and assuming equal x- and y-emittance for the accelerated beam, the emittance part is estimated to contribute a little more than 1/2 to the beam envelope size. Therefore the momentum dispersion contribution to the beam size is estimated to be 0.7-0.9 mm, corresponding to a full energy spread of 16-20 keV.

Summary and Conclusions

Preliminary measurements of the electron beam after one acceleration through the RTM linac have been made. The maximum energy achieved thus far is 16.2 MeV. The measured normalized emittance after one pass is 2.35 μm and the estimated energy spread is 16-20 keV. The design goals for normalized emittance and energy spread at 185 MeV are 5 μm and 36 keV, respectively. The energy spread is not expected to increase significantly with multiple passes through the microtron because of phase focusing.

These tests were conducted with a 0.3 mA pulsed beam, with no indication of beam loss. It is evident from these preliminary results that the electron beam can be transported and accelerated through the RTM while beam quality is maintained well within design limits.

Additional one-pass beam tests are planned to include full voltage conditioning of the RTM linac sections, comprehensive beam envelope measurements to determine the x-emittance and for a more accurate energy spread determination, and the transport and acceleration of cw beams up to 0.55 mA average current.

References

1. M.A. Wilson, et al, "Performance of the 5 MeV Injector for the NBS-Los Alamos Racetrack Microtron," Proc. 1987 IEEE Particle Accelerator Conference, 322, December 1987.

2. R.I. Cutler and L.M. Young, "Performance of the High Power RF System for the NIST-Los Alamos Racetrack Microtron," this conference.

3. R.I. Cutler, et al, "Performance of Wire Scanner Beam Profile Monitors to Determine the Emittance and Position of High Power CW Electron Beams of the NBS-Los Alamos Racetrack Microtron," Proc. 1987 IEEE Particle Accelerator Conference, 625, December 1987.

4. For definition of emittance, see: S. Penner, "RF Linac Based Free Electron Lasers," Proc. 1987 IEEE Particle Accelerator Conference, 185, December 1987.

(a)

→| |← 1.6 mm

(b)

(c)

Figure 7. Oscilloscope traces of the signal produced as the x-scanning wires pass through the accelerated beam on the one-pass return line.
  a) Beam x-profile about one meter from exit of end magnet E1.
  b) Beam x-profile 3 m from (a).
  c) Beam x-profile 6 m from (a).
  The beam was focused to a waist near (a) by the quadrupole doublet, Q_8 and Q_9.

Appendix F

Performance of the High Power RF System

for the NIST-Los Alamos Racetrack Microtron

PERFORMANCE OF THE HIGH POWER RF SYSTEM FOR THE
NIST-LOS ALAMOS RACETRACK MICROTRON

R.I. Cutler
National Institute of Standards and Technology
Gaithersburg, Md. 20899

L. Young
Los Alamos National Laboratory
Los Alamos, NM. 87545

Introduction

The high power RF system of the NIST-LANL RTM has been tested at nominal full power levels and has accelerated electron beams successfully[1]. RF stability and calibration measurements have been made using the accelerated electron beam. These measurements have been used to calculate the effective shunt impedance of the side-coupled accelerator structure. RF stability measurements were also performed using power meters and phase detectors.

RF System Description and Operation

The high power RF system for the NIST-LANL RTM consists of a single 500 kW CW klystron at 2380 MHz that powers four separate linac sections. Two are in the injection line and two are in the microtron. The first linac section in the injection line is the capture section, a 1.1-meter long, tapered-β (0.55 to 0.95) section with an energy gain of 1.3 MeV. The nominal power level of the capture section with no beam

loading is 25 kW. The other linac section in the injection line is the preaccelerator section, a 2.7 meter long, tapered-β (0.95 to 0.99) section with an energy gain of 3.7 MeV. The nominal power level of this section with no beam loading is 63 kW. The two linac sections in the microtron are each 4 meters long, β = 1 sections with an energy gain of 6 MeV. Their nominal unloaded RF power levels are 100 kW each.

The RTM RF system uses two separate control methods for power and phase regulation, one for the capture section and the other for the remaining three accelerating sections. A block diagram of the high power RF control system is shown in figure 1. The feedback control loop of the capture section monitors the phase and power level in the capture section via a 50 dB coupling loop and varies the input signal to the klystron to reach the desired values. This control loop uses low-level (≈1 watt) amplitude and phase controls with an open loop gain bandwidth of 40 kHz. Details of this control system are in Reference 2. The
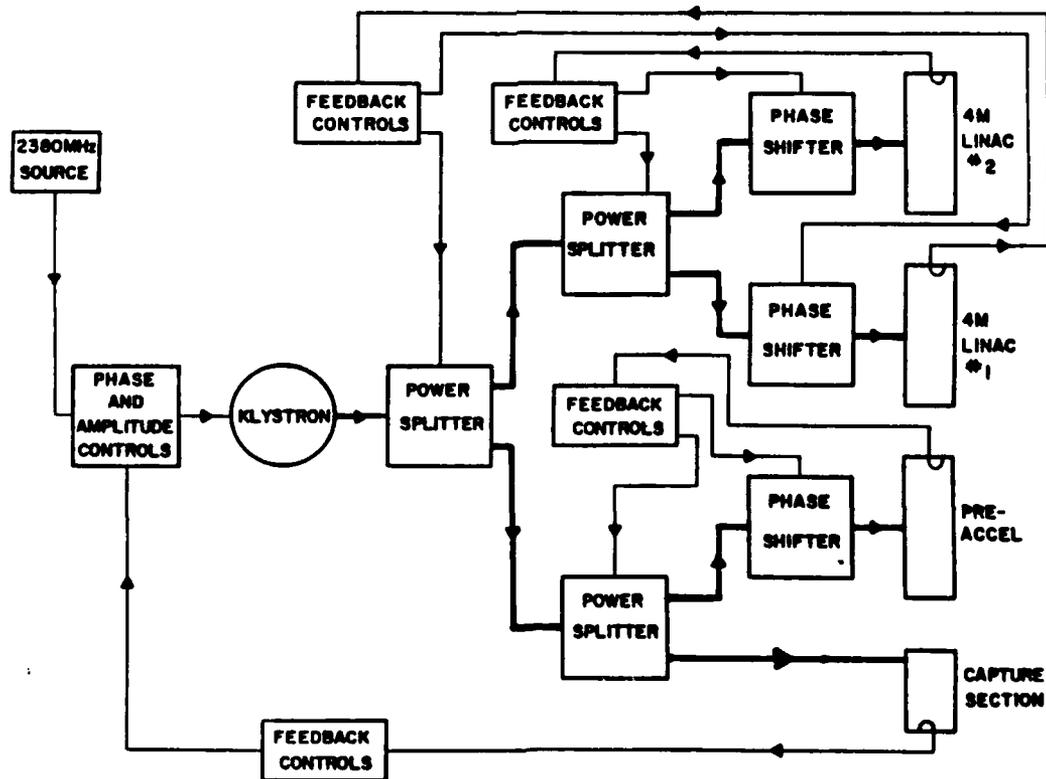

Figure 1. Block diagram of RTM RF control system.

other three linac sections use high power waveguide power splitters and phase shifters as their control elements. The waveguide power splitters allow a < 1% to 99% power split. The waveguide phase shifters have a 140° range. Since these waveguide elements employ large mechanical shifters with stepping motor drives, the control loops containing these elements have an open loop gain bandwidth of 3 Hz. As the power level in the preaccelerator or in either of the two microtron linacs is changed, the RF drive to the klystron is controlled by the capture section control loop to maintain the proper total power requirements of the RF system. Because the capture section control loop has a much faster response time than the other three linac sections, there are no control loop problems in increasing power. A complete description of the high power waveguide feedback system is presented in Reference 3.

A separate temperature control system is used on each linac section to maintain the RF resonance at the operating frequency of 2380 MHz. These temperature control systems vary the cooling water flow into each linac section to maintain resonance at all RF power levels. This keeps the reverse power at each accelerating section window to a minimum, typically less than 1 kW in steady state operation. A block diagram of this control system is shown in Figure 2. A description of this system is presented in Reference 4.

The RTM uses a computer control system[5] to monitor and control all accelerator parameters. All accelerator devices have hardware protection to prevent damage. The status of all hardware protection interlocks is monitored by the computer control system. Software may be written to allow computer automated monitoring and control of any combination of the accelerator parameters.

The program AUTORF ramps the power up from zero to preset values for all four linac sections simultaneously. The program usually can reach full power in less than 10 minutes.

RF Measurements

Measurements were made of phase and energy stability of the four accelerator sections at full power. Phase measurements were made by mixing a signal obtained from a 50 db coupling loop in each accelerating cavity with a reference signal in a double balanced mixer. The output of this mixer, near the null, is proportional to phase. The maximum phase deviation in a 20 minute period was found to be ±0.15°. Energy stability measurements were made using a low barrier Schottky diode detector at the output of the 50 db coupling loop. The voltage deviation of each accelerating section was measured to be less than 1 part in 1000, and the voltage variation of the 1.3 MV capture section was less than 1 part in 2000. Energy stability was also measured by observing energy variations in an electron beam accelerated by all four accelerating sections. This electron beam was then energy-analyzed by a 180° bending magnet and the position of the beam measured using a wire scanner[6]. The 15.5 MeV electron beam was found to have a width of about 20 keV. Also observed was a slow (approximately a few Hertz) energy fluctuation of ±10 keV, which is due to energy variations in the preaccelerator and the two RTM linac sections. This is illustrated by figures 3 and 4, which show several super-imposed wire scanner electron beam profiles for the X (energy analyzed) and Y (non-energy analyzed) planes. The wire scanner, which operates at 10 profiles per second, detects multiple images corresponding to energy shifts of ±10 keV in the X plane, but not in the Y plane. These data are consistent with the energy stability of each
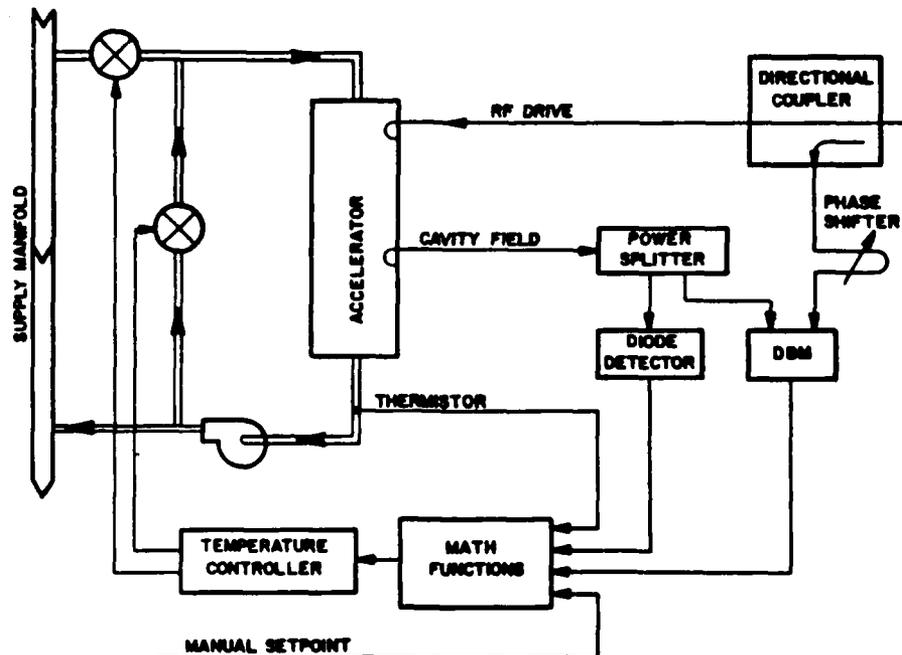

Figure 2. Block diagram of RF resonance control system.

accelerating section measured using the detection diode.

The energy gain of each accelerator as a function of input power was also measured using the 180° analyzing magnet and a wire scanner. The absolute energy calibration of the 180° analyzing magnet was ±1.5%. The input power was measured in several ways. Wave guide directional couplers were used with an RF power meter for one set of measurements. These measurements are only absolutely accurate to ±10% due to the uncertainty in the calibration of the waveguide couplers. Measurements of power were also made by using the RF power meter with the accelerating cavity field probes, which also have an absolute calibration of about ±10%. Finally, calorimetric measurements of the temperature rise of the cooling water were performed for each accelerating section. The calorimetric measurements, which were accurate to ±6%, agreed with the previous two measurements and were used to calculate the effective shunt impedance for the two RTM linac sections and the preaccelerator. The values obtained, 76±5, 77±5, and 80±5 MΩ/meter are in good agreement with the value of 82.5±1 MΩ/meter from low power measurements on the pre-accelerator[7].

References

1. M.A. Wilson, R.L. Ayres, R.I. Cutler, P.H. Debenham, E.R. Lindstrom, D.L. Mohr, S. Penner, J.E. Rose, "NBS-Los Alamos Racetrack Microtron Status", This proceedings.

2. L.M. Young and D.R. Keffeler, "The RF Power System for the Chopper/Buncher System on the NBS-Los Alamos RTM", IEEE Trans. Nucl. Sci., 32, 2165 (1985).

3. L.M. Young and R.S. Biddle, "High-Power Controls for the NBS-Los Alamos Racetrack Microtron", IEEE Trans. Nucl. Sci., 32, 2162 (1985).

4. L.M. Young and R.S. Biddle, "Resonance Control for a cw Accelerator", Proceedings of the 1987 Particle Accelerator Conference, 634.

5. R.L. Ayres, N.R. Yoder, E.R. Martin, R.E. Trout, and B.L. Wilson, "NBS/LANL Racetrack Microtron Control System", IEEE Trans Nucl. Sci., 32, 2086 (1985).

6. R.I. Cutler, D.L. Mohr, J.K. Whittaker and N.R. Yoder, "A High Resolution Wire Scanner Beam Profile Monitor with a Microprocessor Data Acquisition System", IEEE Trans. Nucl. Sci., 30, 2213 (1983).

7. L.M. Young and J.M. Potter, "CW Side Coupled Linac for the Los Alamos/NBS Racetrack Microtron", IEEE Trans. Nucl. Sci., 30, 3508 (1983).
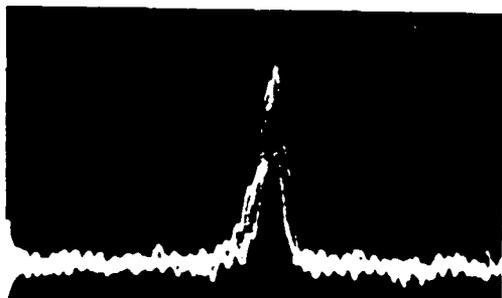
Figure 3. Wirescanner output X (energy analyzed) plane. Horizontal scale is 2.15 mm per division, or 50 keV. Vertical scale is current, in arbitrary units.
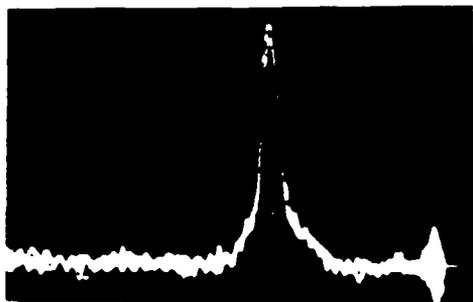

Figure 4. Wirescanner output Y (not energy analyzed) plane.

Appendix G

Conceptual Design of a High Current Injector

for the NIST-NRL Free Electron Laser

CONCEPTUAL DESIGN OF A HIGH CURRENT INJECTOR
FOR THE NIST-NRL FREE ELECTRON LASER

R.I. Cutler and E.R. Lindstrom
National Institute of Standards and Technology
Gaithersburg. Md 20899

S. Penner
10500 Pine Haven Terrace
Rockville, Md. 20852

Abstract

The NIST-LANL Racetrack Microtron (RTM) is to be used as a driver for a cw Free-Electron Laser. To achieve the peak currents of 2-4 A required for lasing, 15-ps, 120-keV electron pulses at 66.111 MHz with 7-14 pC per pulse will be accelerated to 5 MeV by the existing injector linac for injection into the RTM. The conceptual design of a high current injection system to produce this beam using a pulsed electron gun and sub-harmonic chopping and bunching is described, and the results of PARMELA calculations are presented.

Introduction

The 185-MeV cw Racetrack Microtron (RTM) at NIST, originally intended for nuclear physics research, is being modified to become a driver for a cw Free Electron Laser. It also must still provide low emittance electron beams for a variety of other accelerator physics related experiments, such as channeling and transition radiation, micro-undulators and dosimetry. The principal modification of the RTM consists of changing the 5-MeV injector to provide the diverse beams needed for these new experimental usages.

The present 5 MeV cw injector[1] consists of a 100-keV, 5-mA dc electron gun, followed by fundamental-frequency RF choppers and a buncher. This produces 15-ps, 23-mA electron pulses which are accelerated by two accelerating sections to provide ≈ 3.5-ps, 0.35-pC (.1 A) electron pulses at 2380 MHz (accelerator frequency). The transverse and longitudinal emittance of this electron beam are 0.7 μm (normalized) and 5 keV-degrees respectively, for 95 % of the current. This beam is well suited for some of the intended applications of the RTM, but the peak current, ≈0.1 A, is not high enough to initiate lasing in the FEL. For optimum performance, 2-4 A peak current is needed. Because the RTM is cw, we cannot simply increase the current injected, as this would increase the total average power in the electron beam from the present maximum of 100-150 kW, which is fixed by the amount of RF power available. The solution is to reduce the cw repetition rate of the injected beam while raising the current, keeping the average power in the electron beam fixed. The repetition rate has to be an integral sub-multiple of the accelerating frequency and a multiple of the frequency defined by the round trip optical transit time of the FEL cavity. For the 9.076 m long FEL cavity being built at NIST, this frequency is 16.528 MHz. The repetition rate to take advantage of the maximum available average RF power would be 66.111 MHz, which is 1/36 of the accelerating frequency and 4 times the optical cavity frequency. The goal of the new injector is to provide 5-MeV cw electron beams at these frequencies, 66.111 and 16.528 MHz, at a design emittance of 5 μm (normalized), transverse and 20 keV-degrees, longitudinal. The new injector also must supply cw electron beams similar to the ones provided by the existing injector, and low repetition rate (≈10-10000 Hz) beams for tune-up modes.

To produce such a wide variety of beams, we considered several different types of sources. Laser driven photocathode[2] sources were investigated, but were found to lack the flexibility to provide the many different repetition rates we required. Also, they have not demonstrated sufficient lifetimes and high enough average beam currents to be of practical use for our application. The other types of sources considered use conventional thermionic cathodes and RF chopping and bunching to produce the desired electron beams. Injectors using a variety of combinations of sub-harmonic RF bunching and chopping were modeled and optimized using the computer program PARMELA. The design of the new injector is to use existing injector components where possible to save cost and time.

PARMELA Calculations

The program PARMELA allowed the modeling of the new injector to minimize the space charge effects of the higher current. The starting point was our existing injector. Modifications investigated were different chopped beam lengths, buncher frequency changes and lens strengths. The design requirement of a longitudinal emittance of 20 keV-degrees proved to be the most difficult problem. The PARMELA calculations indicated that this could be best met by using a short pulse (70 ps) from the chopper and only a modest amount of bunching. Using a longer pulse from the chopper with greater bunching introduced unacceptable longitudinal emittance growth due to non-linear space charge effects. The longitudinal charge distribution in the chopped pulse was also found to be important in minimizing emittance growth. Best results were achieved by using a parabolic longitudinal charge distribution.

To meet our design longitudinal and transverse emittance goals, several changes were made in the electron optics. Some were quite simple, such as scaling beam sizes with current and varying lens strengths appropriately. Considerable reduction in emittance growth is achieved by raising the gun voltage from 100 kV to 120 kV. This presented problems, as the existing first accelerator tank is a tapered-β design, intended for 100 keV injection. However, by reducing the voltage gradient slightly (5%), and changing the beam entrance phase, this problem could be completely compensated. It was also discovered that because of space charge induced longitudinal spreading of the chopped 70-ps beam, an on-frequency buncher did not have sufficient linearity to bunch the beam without increasing the longitudinal emittance. This was solved by changing to a half-frequency buncher. The new buncher is to be operated at significantly higher voltage levels than the existing buncher, as longitudinal space charge effects tend to de-bunch the beam. Also, the higher bunching voltage compensates for the change in accelerator phase mentioned above, which produces less bunching by the first accelerator tank.

Figure 1 shows the PARMELA longitudinal and transverse beam sizes through the injector for 14-pC pulses. Table 1 lists the PARMELA-predicted emittances for the various beams.
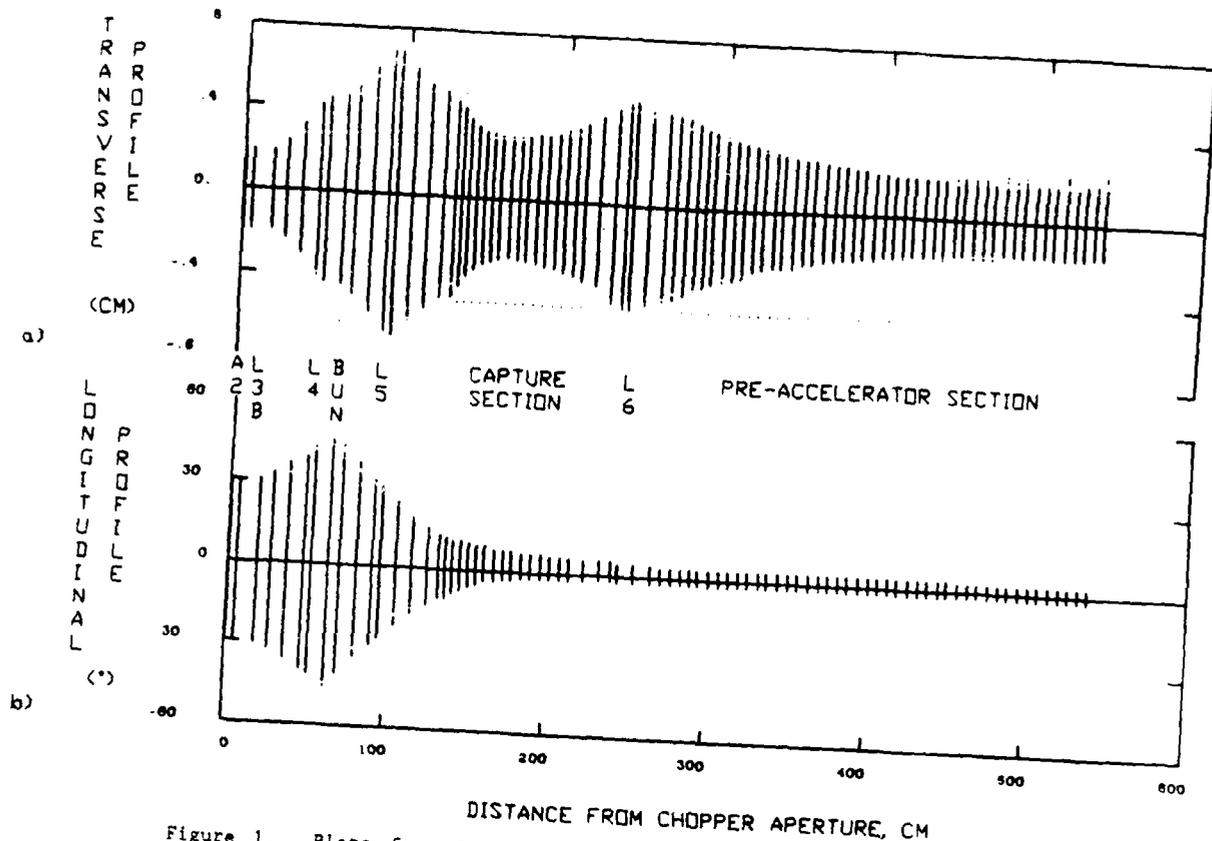
DISTANCE FROM CHOPPER APERTURE, CM

Figure 1. Plots from PARMELA calculations showing (a) transverse beam profile in cm. and (b) longitudinal beam profile in degrees of fundamental frequency, 2380 MHz, for a 14 pC electron pulse as a function of position along the injector beam line from the chopper aperture.

Table 1. Longitudinal and Transverse Emittances for 90 % of beam particles from PARMELA for New Injector.

Charge per Pulse, pC	Transverse Emittance, (Normalized) μm	Longitudinal Emittance, keV-degrees
0.35*	0.7*	5*
0.35	1.8	4.7
7	4.4	14
14	5.0	22

* Measured values for present injector (95% of beam)

New Injector Description

A schematic drawing of the proposed new injector is shown in figure 2. The major differences between the new injector and the existing injector are in the gun, the chopping scheme, and in the buncher. The two accelerating sections remain unchanged, although they are to be operated at slightly different power levels and phases than previously. Most lenses are also the same, and are to be near their original locations. The new injector is to work as follows: A 2.3 ns, 300-mA electron pulse is produced by the gun at 55.111 or 16.528 MHz by the use of a modulating anode or grid. These pulses are chopped to 70 ps by a sub-harmonic chopping system. As in the existing injector, the chopping system is followed by a buncher to compress the beam to 15 ps for injection into the injection linac. The system also has the ability to produce high repetition rate cw electron beams (at 1190 or 2380 MHz) similar to the existing injector.
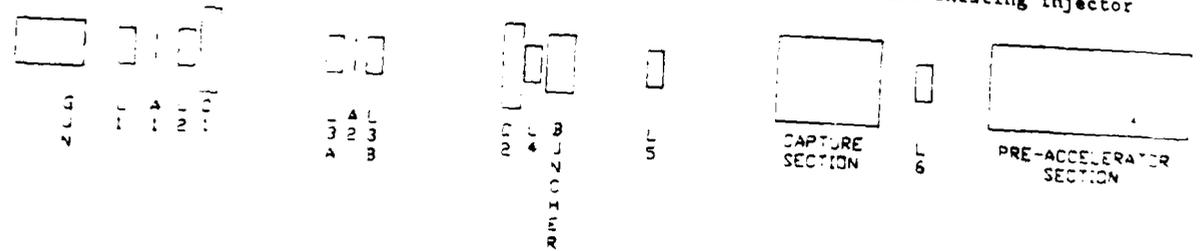

Figure 2 Schematic Representation of proposed injector (not to scale).
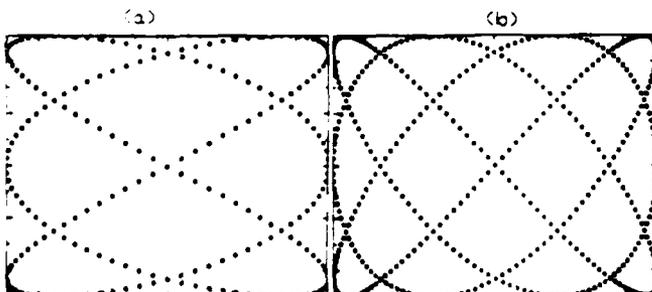
Electron Gun

The design emittance is to be less than 1.8 μm normalized at 120 keV with a maximum current output of 300 mA. Pulse synchronism for the 120 kV gun will be provided via optical links from a ground-potential solid-state laser-transmitter. The pulsing system will also have to accommodate low frequency pulsing for tune-up modes, and allow low current (<20 mA) operation for high frequency cw beams. A short pulse is desirable, as it simplifies the chopper system design. Short pulse guns with pulses less than 1 ns have been produced in the past[3], but not at these repetition rates. Provisions will be made to install our existing electron gun in place of the new gun should applications arise that require even lower emittance.

RF Chopping and Bunching System

The final design of the chopping system is dependent on the pulse length from the gun. If a 2-ns pulse is achievable, an RF deflecting cavity with 1/2 (X) and 1/3 (Y) of the fundamental frequency will be used to generate the lissajous figure shown in figure 3a at the chopper aperture location. This figure has a period of 2.5 ns. The lissajous figure shown in figure 3b will be used if the pulse from the gun is as long as 5 ns. This figure is generated by a 1/4 (X) and 1/3 (Y) deflecting cavity. In either case, a centrally located chopper aperture 8 mm in diameter (twice the beam diameter at this point) will subtend 40 degrees of primary-frequency phase. This will serve to approximate the parabolic longitudinal charge distribution used for the PARMELA calculations. A comparison of a parabolic and the actual longitudinal charge distribution is shown in figure 4. The chopped, RF deflected beam is then un-deflected by a second RF deflecting cavity identical to the first cavity. This chopping scheme is similar to that used successfully in the present injector, and in the case of the 1/2 by 1/3 RF deflector is identical to the one used by the University of Illinois[4]. The higher frequency deflection cavities are smaller, and the amount of deflection needed is less, so these cavities are more desirable than the lower frequency cavities. The shorter gun pulse used with the higher frequency cavities also reduces the total power dissipated on the aperture plate. In either case, the beam is next bunched by a half-frequency buncher, and accelerated by the injection linac.

To produce high repetition rate cw electron beams similar to those produced by the existing injector, the 1/3 frequency deflector is turned off and a 5 ma dc beam from the gun will oscillate back and forth in a straight line over the chopper aperture at either 1/2 or 1/4 the fundamental frequency, crossing the aperture twice per oscillation. This yields either 2380 or 1190 MHz chopped electron beam pulses. The RF chopper amplitude is adjusted to yield 70 ps pulses. In the case of the 2380 MHz beam (produced by the 1/2 by 1/3 chopping scheme), an on-frequency buncher will be added to bunch the beam to 15 ps. For the 1/4 by 1/3 chopping scheme, the 1/2 frequency buncher will be used.

The control circuits for the new RF components will be similar to existing controls. The timing accuracy of these circuits is sufficient for the new system. The timing accuracy needed for the gun pulser is about ± 200 ps, as the chopper selects only a small part of the gun pulse.

Conclusion

A conceptual design of an injector has been presented that will produce the desired electron beams for FEL and other planned usage of the RTM. The new injector uses conventional, proven technology similar to that used in the present injector, which has operated successfully.

Acknowledgment

References

[1] M.A. Wilson et al, "Performance of the 5 MeV Injector for the NBS-Los Alamos Racetrack Microtron", in Proceedings of the IEEE 1987 Particle Accelerator Conference, 1987, pp. 322-324.

[2] R.L. Sheffield "RF Photoelectron Gun Experimental Performance" to be published in Proceedings of the 1988 Linac Conference, 1988.

[3] R.F. Koontz, "One Nanosecond Electron Gun Systems", IEEE Trans. Nucl. Sci., vol. NS-26. pp. 4129-4130, June 1979.

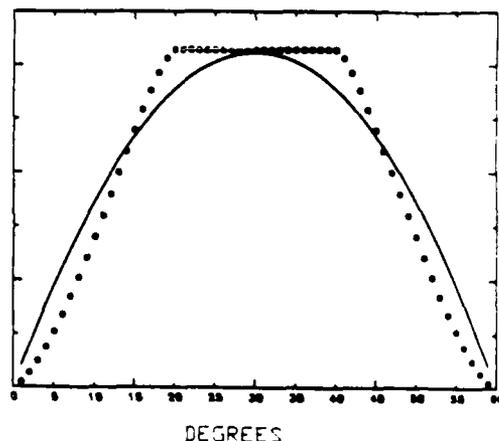[4] Nuclear Physics Research with a 450 MeV Cascade Microtron, March 1986, pp. IV 13-20.

DEGREES

Figure 4. A comparison of the longitudinal charge distibution used in the PARMELA calculations (solid line) and a longitudinal charge distribution produced by a uniform circular beam of diameter D, being chopped by a aperture of diameter 2D (open circles) Both distributions contain the same total charge

Figures 3a and 3b. Lissajous figures generated by sub-harmonic choppers at chopper aperture location. Figure 3a is generated by 1 2 (X) by 1/3 (Y) fundamental frequency chopper, and figure 3b by 1/4 (X) by 1/3 (Y) chopper. In both figures each point represents 10 degrees at the fundamental frequency.

Appendix H

The NIST/NRL Free Electron Laser Facility

The NIST/NRL Free-Electron Laser Facility

P.H. Debenham, R.L. Ayres, J.B. Broberg, R.I. Cutler, B.C. Johnson, R.G. Johnson,
E.R. Lindstrom, D.L. Mohr, J.E. Rose, J.K. Whittaker, N.D. Wilkin, and M.A. Wilson

National Institute of Standards and Technology
Gaithersburg, MD 20899, USA

C.-M. Tang and P. Sprangle

Naval Research Laboratory
Washington, DC 20375, USA

S. Penner, Rockville, MD 20852, USA

ABSTRACT

A free-electron laser (FEL) user facility is being constructed at the National Institute of Standards and Technology (NIST) in collaboration with the Naval Research Laboratory. The FEL, which will be operated as an oscillator, will be driven by the electron beam of the racetrack microtron (RTM) that is nearing completion. Variation of the electron kinetic energy from 17 MeV to 185 MeV will permit the FEL wavelength to be tuned from 200 nm to 10 μm. Performance will be enhanced by the high brightness, low energy spread, and continuous-pulse nature of the RTM electron beam. We are designing a new injector to increase the peak current of the RTM. A 3.6-m undulator is under construction, and the 9-m optical cavity is under design. The FEL will emit a continuous train of 3-ps pulses at 66 MHz with an average power of 10-200 W, depending on the wavelength, and a peak power of up to several hundred kW. An experimental area is being prepared with up to five stations for research using the FEL beam. Initial operation is scheduled for 1991.

1. INTRODUCTION

We are building a free-electron laser at the National Institute of Standards and Technology (NIST) to provide a powerful, tunable source of light for research in biomedicine, materials science, physics, and chemistry.[1] The planned research facility is shown in Figure 1. In a free-electron laser (FEL), the static, sinusoidal, magnetic field of an undulator (or wiggler) causes an electron beam to follow a sinusoidal trajectory and hence emit electromagnetic radiation. Radiation with a particular wavelength, λ, remains in phase with the electrons and stimulates additional emission; i.e., the device lases. The resonant wavelength is given by the expression

$$\lambda = (\lambda_w/2\gamma^2) \cdot (1+K^2), \tag{1}$$

where λ_w is the wavelength of the wiggler magnetic field, and γ is the electron energy in units of the electron rest energy, E_0. The wiggler parameter, K, that appears in Equation 1 is proportional to the root-mean-square (rms) magnetic field of the wiggler, B_w:

$$K = |eB_w\lambda_w/2\pi E_0|. \tag{2}$$

Our FEL will be driven by the electron beam of the NIST/LANL racetrack microtron (RTM), a continuous-wave (cw) accelerator that is scheduled for completion in 1990. The FEL can be characterized as a high-power, tunable, picosecond, mode-locked laser. By varying the kinetic energy of the electron beam between 17 MeV ($\gamma = 34$) and 185 MeV ($\gamma = 363$), we will be able to vary λ between 200 nm and 10 μm, from Equation (1). For our wiggler, $\lambda_w = 28$ mm, and B_w can be varied between 0.23 T and 0.38 T by varying the gap. This will allow us to tune λ by $\pm 20\%$ without changing γ. The laser output, like the electron beam, will be a continuous train of 3-ps long pulses at a frequency of 66 MHz. The expected properties of the output radiation are given in Table 1, and the average output power is shown in Figure 2 as a function of λ.

FEL radiation will be available for research applications in the 160-m^2 FEL user area shown in Figure 1. The photon beam will be transported in vacuum from the FEL to any of up to five experimental stations in the user area. The user area will be shielded from the electron beam and inhabitable at all times. Thus experimenters will be able to make manual adjustments to experiments in progress, as well as set up experiments when the photon beam is delivered to other stations. In the remainder of this paper we discuss the physics of microtrons and the status of our FEL project.

2. MICROTRONS

Racetrack microtrons have several properties that make them excellent sources of electrons for free-electron lasers. In this section we discuss the physics of the racetrack microtron and its predecessor, the classical microtron.
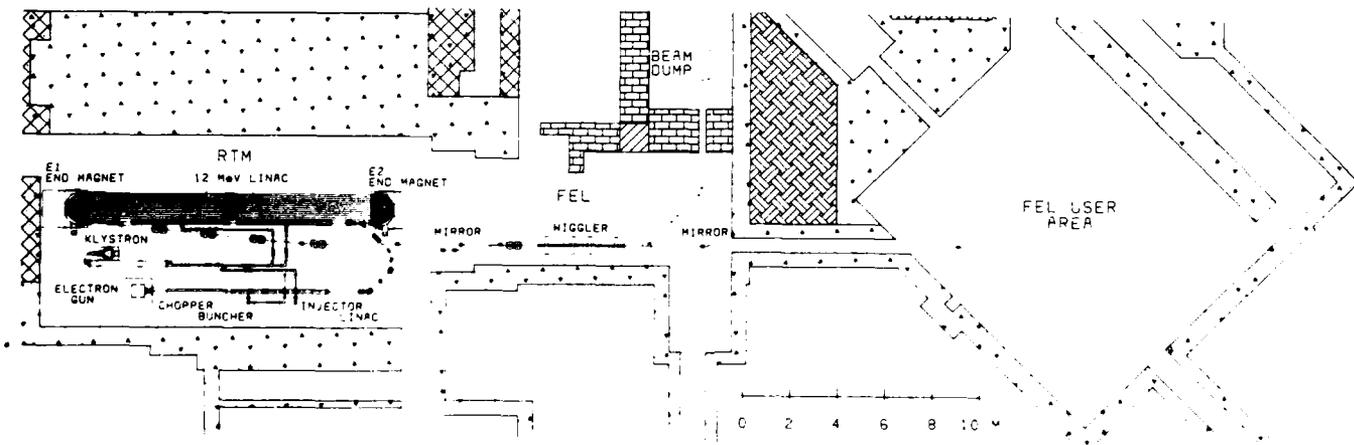

Figure 1. Plan view of the NIST/NRL FEL facility.

Table 1. Output Light Properties of the NIST/NRL FEL

Wavelength	200 nm - 10 μm
Average Power (W)	10 - 200
Repetition Rate (MHz)	16.528 and 66.111
Peak Power (kW)	40 - 1000
Peak Energy (μJ)	0.1 - 3.0
Photon Flux ($cm^{-2} \cdot s^{-1}$)	10^{25} - $2 \cdot 10^{27}$
Photon Fluence (cm^{-2}, 1mm-diam spot)	$3 \cdot 10^{13}$ - $6 \cdot 10^{15}$
Pulse Width (ps)	3
Spectral Resolution	$1.4 \cdot 10^{-4}$ - $7 \cdot 10^{-3}$
Polarization	Linear
Spatial Mode	TEM_{00}
Beam Diameter (mm, at 1/e amplitude)	0.4 - 1.6
Beam Divergence (mrad, full angle)	0.3 - 5

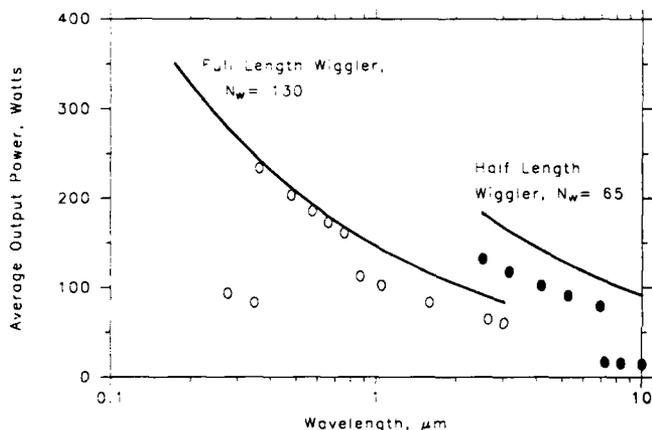Figure 3. Classical microtron (left) and racetrack microtron.

Figure 2. Predicted average output power of the NIST/NRL FEL. The solid curves show the maximum power that can be extracted from the electron beam. The circles are calculated values of output power for realistic values of mirror reflectivity and output coupling.

2.1 Classical microtron

The racetrack microtron evolved from the conventional, or classical, microtron, which was proposed by Veksler[2] in 1944. (Reference 3 provides a thorough discussion of the classical microtron.) As indicated in Figure 3, the classical microtron consists of a microwave* cavity with an accelerating gap located in a uniform magnetic field, B. An electron that originates at one side of the gap with negligible kinetic energy crosses the gap at rf phase ϕ and in doing so gains energy $\Delta T = V \cdot \cos\phi$, where V is the peak gap voltage. The electron is returned to the gap on a circular orbit with a radius of curvature that is proportional to its momentum. The values of B and ΔT are chosen such that the circumference of the first orbit is an integral multiple of the rf wavelength, λ, and each subsequent orbit is an integral number of wavelengths, $\nu\lambda$, larger in circumference than the one before. This choice of energy gain, ΔT_r, defines a resonant phase angle, ϕ_r, such that $V \cdot \cos\phi_r = \Delta T_r$. Electrons at this phase remain in resonance with the accelerating voltage and

*Hence the name microtron.
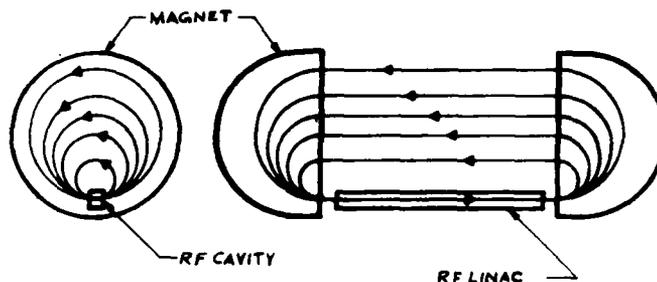†These are called end magnets.

gain energy ΔT_r each time they cross the gap. The resonant parameters are related by the microtron resonance condition,

$$2\pi \cdot \Delta T_r / c = \nu\lambda B. \qquad (3)$$

Conventional microtrons are used to produce pulsed electron beams at energies of 5 MeV to 45 MeV. The resonant energy gain per pass, ΔT_r, is limited to approximately 1 MeV. The maximum energy is limited by the need to use a relatively large, low-field magnet ($0.1 \text{ T} \leq B \leq 0.3 \text{ T}$). The microwave cavity is limited to operation in the pulsed mode by cooling limitations[4].

2.1.1 Phase focusing.
Like other resonant accelerators, the microtron benefits from phase focusing, an important mechanism which results in good energy resolution and stability. Phase focusing comes from operating on the falling side of the microwave, so that an electron that crosses the accelerating gap before the central electron (i.e., with $\phi < \phi_r$) gains more energy than ΔT_r. The extra energy of this electron increases the length of the next orbit, and the extra distance traveled delays its next gap crossing. In this way, the phase is restored toward ϕ_r. The restoring force produces phase oscillations around ϕ_r with an amplitude equal to the initial phase spread in the electron bunch, so the phase spread remains constant as the electrons are accelerated.

Likewise, electrons that begin at the resonant phase with excess energy will arrive at the gap late the next time and gain less than ΔT_r. Thus, the initial energy spread in the beam is preserved.

2.2 Racetrack microtron

Reference 4 is a comprehensive study of the racetrack microtron and other recirculating electron accelerators. The racetrack microtron, shown in Figure 3, can be thought of as a classical microtron with its circular magnet separated into two semicircular ones† and its microwave cavity replaced by a multi-cavity linear accelerating structure, viz., a linac. The electron orbits resemble a nested series of racetracks having a common homestretch and increasingly distant backstretches. The space between the magnets is exploited for several improvements. A linac can provide an energy gain on the order of 10 MeV and can be cooled adequately for cw operation. Focusing elements can be included on the straight sections.

Racetrack as well as conventional microtrons are governed by Equation 3 and benefit from phase focusing. From Equation 3 it can be seen that the increased ΔT_r allows the use of a higher magnetic field (approximately 1 T) and therefore smaller, more efficient magnets.

A racetrack microtron with N passes through a linac of energy gain ΔT_r can be compared with a single-pass electron linac of energy gain $N \cdot \Delta T_r$, to which we will refer as a "straight" linac. The RTM linac is shorter than the straight linac by a factor of N, which is typically between 10 and 50. This can lead to a significant reduction in the initial cost of the linac, its enclosure, and radiation shielding, which more than compensates for the cost of the end magnets and return beam lines. Moreover, the power dissipated in the shorter linac is lower by a factor of N, a saving that can make cw operation affordable. Finally, the straight linac does not provide phase focusing and consequently tends to have a larger beam energy spread and poorer energy stability than the RTM.

3. THE NIST/LANL RTM

The NIST racetrack microtron arose from the need for cw electron accelerators for nuclear physics in the late 1970's. Existing pulsed accelerators were not suitable for doing experiments in which several subatomic particles are detected coming from a nuclear reaction initiated by a single electron. High event rates during the pulse increase the probability of detecting unrelated but coincident particles from separate reactions to the point where the signal from true coincidences is obscured. One solution to this problem is to reduce the peak electron current without reducing the average current (hence the true event rate) by increasing the duty factor of the accelerator.

Existing US cw electron accelerators based on cryogenic, superconducting linacs[5] were limited in average current by the phenomenon of beam breakup, or BBU[†]. Encouraged by the successful RTM at Mainz[6], we began in 1980 the construction of a high-current, 185-MeV, cw RTM with a room-temperature linac at NIST. This was a joint project with Los Alamos National Laboratory (LANL), funded by the US Department of Energy (DoE), to determine the feasibility of a 1 to 2 GeV, cw, high-current, room-temperature, recirculating electron accelerator for nuclear physics. The design of the NIST/LANL RTM was thus strongly influenced by requirements for a 1 to 2 GeV accelerator. For example, the product of the number of passes (N) and the average beam current (I) is the same in the two machines, close to the threshold for beam breakup.

[†]BBU is self-destructive deflection of the beam by unwanted modes of the accelerating structure that are excited by the beam. Superconducting, low-loss structures are especially vulnerable to BBU because the unwanted modes can be excited by relatively low-current beams.

When the DoE project ended in 1987, we realized that the RTM would make an excellent FEL driver and began the present project.

3.1 Design

The NIST/LANL RTM is described in Reference 7. Table 2 gives the design parameters of the accelerator and some measured beam properties. Shown in Figure 4, the accelerator comprises a 5-MeV injector connected to

Table 2. NIST/LANL RTM Parameters

	Original Design	Observed as of 3/89	Modified Design for FEL
Injection energy (MeV)	5	5.5	5
Energy gain per pass (MeV)	12	11.2	12
Number of passes	1-15	1	1-15
Output energy (MeV)	17-185	16.2	17-185
Average current (μA)	10-550	630	10-550
Accelerating frequency (MHz)	2380	2380	2380
End magnet field (T)	1.0	1.0	1.0
Peak current (A)	<0.066	–	2-4
Micropulse length (ps)	3.5	–	3.5
Micropulse frequency (MHz)	2380	2380	66.111 16.528
Macroscopic duty factor	1.0	1.0	1.0
Energy spread (keV)	<40	18	<40
Normalized emittance* (μm)	<10	2.4	<10

*In the two-dimensional phase space of beam size and beam divergence, the emittance, ϵ, is the area which contains 95% of the beam, divided by π. Normalized emittance = $\beta\gamma\epsilon$, where β is the electron velocity divided by c.
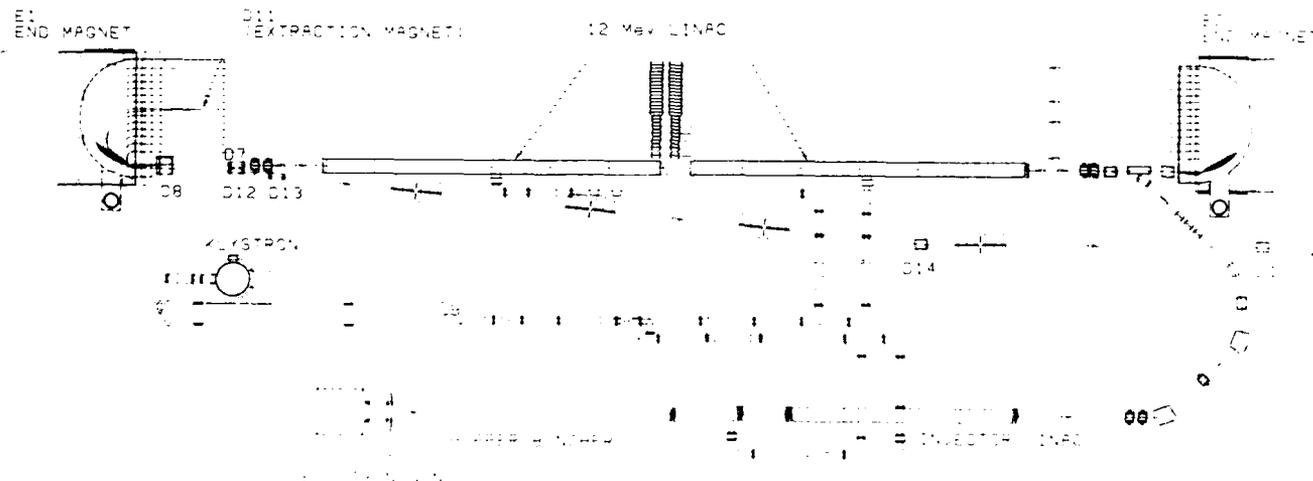

Figure 4. Plan view of the NIST/LANL RTM.

a racetrack microtron by a 180-degree beam transport system. With a floor area of 5 m by 16 m, the RTM is compact for a 185-MeV, cw accelerator. The average beam power at full energy is 100 kW.

The injector consists of a 100-keV, dc electron gun followed by a transverse-emittance-defining system, a chopping and bunching stage, and a 5-MeV, cw linac. In the microtron, 5-MeV electrons from the injector are recirculated for up to 15 passes through an 8-m long, 12-MeV, cw linac for a total energy gain of up to 180 MeV. The first pass is from right to left in Figure 4, following which the 17-MeV beam is given a parallel displacement by dipole magnets D7 and D8, deflected counter-clockwise through 180 degrees by end magnet E1, and returned to the linac axis by D8 and D7. With the length of the 17-MeV orbit adjusted to a half-integral multiple of λ, the 17-MeV beam enters the left end of the standing-wave linac with a 180-degree phase shift and is accelerated to the right. From this point on the beam circulates counter-clockwise through the microtron. Quadrupole magnet doublets are located at the middle of each beam-return line to provide adjustable focussing.

Beam can be extracted from the RTM after any number of passes simply by moving extraction magnet D11 to the appropriate beam-return line. The magnet deflects the beam inward, causing it to emerge from end magnet E1 outside the racetrack orbit. It is then removed from the accelerator by dipole D12 and the ensuing beam line. In this fashion the energy can be varied in steps of 12 MeV by changing nothing in the accelerator but the position and field strength of magnet D11*. Continuous energy variation is achieved by changing ΔT_r and B.

Microwave power from a single, 450-kW-output cw klystron is delivered to the injector linac and the RTM linac through a waveguide distribution system that can be seen in Figure 4. With a dissipation of approximately 50 kW in the distribution system, 100 kW in the injector linac and 200 kW in the 12-MeV linac, there is 100 kW available to accelerate the beam. Overall, the accelerator uses 1.1 MW, of which 9% is converted into beam power. By contrast, an equivalent 185-MeV linac would be 124 m long, dissipate 3.1 MW, and consume roughly 8.8 MW for the same beam power. The power saved by recirculating the beam through a relatively short linac makes cw operation feasible.

3.2 High-Current Injector

The injector produces beam pulses at the accelerating frequency, f_0, of 2380 MHz with a maximum of 0.35 pC per pulse. A peak beam current of 2-4 A is necessary for adequate gain in the FEL, corresponding to 7-14 pC per pulse. We must increase the peak current without increasing the average beam power, which is limited by the amount of rf power available. This will be done by reducing the beam pulse frequency to 66.111 MHz, the 36th subharmonic of f_0. We plan to replace the present, 4-mA, dc, thermionic, electron gun with a 200-mA, thermionic gun pulsed at 66.111 MHz. Subharmonic chopping and bunching will be used to prepare the beam for the injector linac. The new injector, which is also designed to operate at 16.528 MHz, the 144th subharmonic of f_0, is described in detail in Reference 8. Design parameters for the RTM with the new injector are given in the last column of Table 2.

3.3 Status and Plans

The present configuration of the RTM is with a single temporary beam line in place of the 14 beam-return lines in order to study performance with one pass through the 12 MeV linac for a nominal beam energy of 17 MeV. The beam line contains three beam profile monitors (wirescanners[9]) spaced three meters apart. After one pass, the beam is deflected clockwise by end magnet E1 through 180 degrees into the beam line for energy analysis and emittance measurement. Preliminary results are given in Table 2 and in Reference 10. The full, vertical width of the beam at 20% maximum[†] is about 1 mm throughout the 6-m beam line. The normalized emittance in the vertical plane is less than 2.4 μm, better than the design goal of 5 μm at 17 MeV.

The observed horizontal beam width of 1.6 mm includes the dispersion of electrons with different energies by the magnet. Assuming equal horizontal and vertical emittance, the width from dispersion is 0.8 mm, corresponding to a full energy spread of 18 keV. The observed energy spread is consistent with the measured voltage stability of the linacs of 0.1%[11]. Because the microtron is phase-focused, the energy spread should not increase significantly with recirculation, so we expect to surpass the design goal of 40 keV at full energy. By comparison, the energy spread from a 185-MeV linac with similar voltage stability would be 370 keV. In view of Equation 1, the RTM-driven FEL will have much better wavelength stability than one driven by a linac.

After completion of single-pass beam tests this spring, we will install the microtron beam-return lines. Concurrently, we will install the beam transport line between the microtron and the beam stop shown in Figure 1, without the mirror chicane (dipoles D15-18, shown in Figures 4 and 5) or the following quadrupole doublet. This arrangement will be used to commission the accelerator at full energy with the present injector in 1990. Three wirescanners spaced approximately six meters apart will provide beam size measurements for determining the transverse emittance, and a wirescanner following the 45-degree bending magnet D19 (see Figure 5) will be used to measure energy spread.
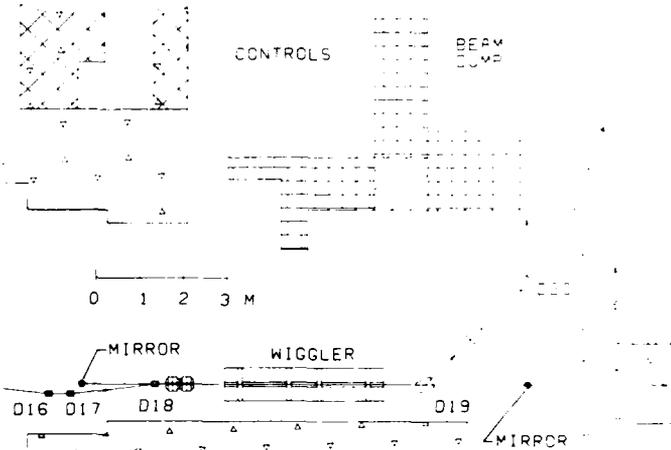

Figure 5. Plan view of the NIST/NRL FEL.

Operation of the RTM for the FEL requires a peak current of up to 40 times the original design value. The stronger wake fields that the increased peak current induces is estimated to have a non-negligible effect on beam quality. We plan to perform more detailed calculations of these effects. Operation with a decreased beam pulse frequency for the FEL could reduce the threshold current for beam breakup, I_s. This is because the accelerating structure may support BBU modes that are resonant with harmonics of the lower frequency that are not harmonics of the higher

---

*Of course, the magnetic fields in the beam transport line must be changed with the beam energy.

†This includes about 95% of the beam.

frequency. Preliminary calculations indicate that operation at 66.111 MHz will reduce $N \cdot I_s$ from approximately 9 mA (average) to approximately 6 mA[12]. More accurate calculations are underway. Small adjustments in focusing can produce large improvements in I_s. We are developing the high-current injector for installation in 1990, after the RTM is commissioned with the present injector. We plan to commission the new injector in 1991.

4. THE NIST/NRL FEL

4.1 Electron-beam transport

The planned electron-beam transport line from the RTM to the FEL is shown in Figures 1, 4, and 5. Following extraction from the RTM, the beam will be deflected onto the wiggler axis by dipole D14 without dispersion, i.e., with no correlation between electron energy and position or angle. Dipole magnets D15 through D18 will form an achromatic chicane to guide the beam around the upstream mirror of the FEL optical cavity and back onto the wiggler axis without dispersion.

The vertical aperture of the wiggler vacuum chamber will be 8.4 mm. The length of the wiggler will be 3.64 m for optical wavelengths between 200 nm and 2 μm. For wavelengths between 2 μm and 10 μm, we will use only the first 1.82 m of the wiggler to reduce diffraction losses. In both cases we will put the waist of the optical beam at the active center of the wiggler. The size of the waist will depend on λ. The Rayleigh length* will be half the active wiggler length to optimize transmission through the wiggler vacuum chamber. To optimize coupling between the electron and optical beams, we will use the two quadrupole magnet doublets on the wiggler axis to match the size and location of the electron-beam waist to those of the optical beam.

The spent electron beam will be removed from the FEL after the wiggler by an achromatic, 90-degree deflection system consisting of two 45-degree dipole magnets, D19 and D20, and an intermediate quadrupole magnet. The deflection system will focus the beam into a shielded beam dump behind a thick shielding wall. The energy distribution in the spent beam is an important diagnostic for lasing. This information will be obtained from a beam profile monitor located between the 45-degree magnets, where the beam will be dispersed.

4.2 Optical cavity design

The FEL optical cavity, shown in Figure 5, consists of an upstream mirror, the wiggler, and a downstream mirror. We will use a partially-transmissive downstream mirror to extract a small fraction of the optical beam from the cavity. The extracted light will be transported in vacuum to the user area. We have chosen the cavity length to be 9.070 m, twice the distance between electron pulses at 66.111 MHz, so four independent light pulses will build up in the cavity in synchronism with the electron pulses. Because the electron pulse train is continuous, the light pulses will persist in the cavity indefinitely. This eliminates the start-up problems of a pulsed FEL. For the most stable optical output, we will operate at 16.528 MHz to form a single light pulse in the cavity. Approximately four meters of electron-free length will be available for optical devices in the cavity.

4.3 Status and Plans

We have a contract with a vendor to design, construct, install and test the wiggler, including vacuum chambers, supports, controls, and a magnetic-field-mapping apparatus. The design is complete, and the main structure has been constructed. The vendor built a full-scale model of one period of the magnetic structure and performed magnetic field measurements on it to verify the design. The measured field met or exceeded all specifications. Installation of the completed wiggler at NIST is scheduled for the end of this year.

Operation of the FEL is scheduled to begin in 1991. Initially, we plan to operate at visible wavelengths, where good optical components are available. Damage to the cavity mirrors from the relatively high intracavity power is a potential problem. Multi-layer dielectric mirror coatings are available for visible wavelengths that can withstand the irradiance and fluence expected in the cavity. The absorption of these coatings is initially about 10 ppm, but is expected to increase with exposure to harmonic radiation in the FEL. While our situation is somewhat unique, experience at the LURE/ACO FEL[13] suggests that increased absorption will result in mirror failure after several days of lasing.

5. REFERENCES

1. S. Penner et al, Nucl. Inst. and Meth. in Phys. Res. A272 (1988) 73.

2. V.I. Veksler, Proc. USSR Acad. Sci. 43 (1944) 346 and J. Phys. USSR 9, (1945) 153.

3. S.P. Kapitza and V.N. Melekhin, The Microtron, Harwood, London (1978).

4. R.E. Rand, Recirculating Electron Accelerators, Harwood, London (1984).

5. P. Axel et al., IEEE Trans. Nucl. Sci. NS-24 (1977) 1133.

   C.M. Lyneis, IEEE Trans. Nucl. Sci. NS-26 (1979) 3246.

6. H. Aufhaus et al., Proc. of the 1981 Linear Accelerator Conference LA-9234-C (1981) 22.

7. S. Penner et al., IEEE Trans. Nucl. Sci. NS-32 (1985) 2669.

8. R.I. Cutler et al., "Conceptual Design of a High-Current Injector for the NIST-NRL Free-Electron Laser," to be published in Proceedings of the 1989 Particle Accelerator Conference.

9. R.I. Cutler et al., Proc. 1987 IEEE Particle Accelerator Conference (1987) 625.

10. M.A. Wilson et al., "NIST-Los Alamos Racetrack Microtron Status," to be published in the Proceedings of the 1988 Linear Accelerator Conference.

11. R.I. Cutler and L.M. Young, "Performance of the High-Power RF System for the NIST-Los Alamos Racetrack Microtron," to be published in the Proceedings of the 1988 Linear Accelerator Conference.

12. S. Penner, "BBU in Microtrons with Subharmonic Injection," to be published in Transactions of the 1989 IEEE Particle Accelerator Conference.

13. M. Billardon et al., J. de Physique C1 (1983) 29.

*The distance from the waist to the point where the cross section of the optical beam doubles.

Appendix I

BBU in Microtrons with Subharmonic Injection

BBU IN MICROTRONS WITH SUBHARMONIC INJECTION[*]

S. Penner
10500 Pine Haven Terrace
Rockville, Maryland 20852

Abstract

The current in recirculating electron accelerators is limited by the recirculating regenerative type of beam breakup (BBU).[1] Existing calculations of the BBU threshold current, I_s, average over the relative phase between the beam bunch and the RF mode causing the blowup. This averaging is invalid if the BBU frequency is an integral or half-integral multiple of the beam frequency, in which case I_s may be substantially reduced. This effect is not important when the beam frequency equals the accelerating mode frequency, f_0, because the RF structure can be designed to avoid the harmonic condition. When the beam frequency is a large submultiple of f_0, this may not be possible. Calculations for the NIST RTM[2], which will inject at the 36th subharmonic of f_0, are presented. Our calculations also include the effects of the reversed first return orbit and the variable return-path focusing of the RTM.

Introduction

The basic mechanism of recirculating regenerative BBU is illustrated in figure 1. In addition to the accelerating mode, most RF structures support many other modes, including some (e.g., TM_{11}- and TE_{11}-like modes) which can deflect the beam transversely, even if the beam is on axis. A beam deflected by this interaction will, in general, return to the accelerator on subsequent passes off axis, where the beam can exchange energy with the deflecting mode. If, on average, the mode extracts energy from the off-axis beam, the deflection will grow until the beam is lost, unless the energy in the mode is removed from the structure. The mechanism for energy removal in room temperature structures is resistive dissipation of the structure. Since the rate of energy input is proportional to beam current while the rate of dissipation is independent of current, recirculating regenerative BBU will exhibit a threshold current, I_s, above which the accelerator will not operate stably, and below which there is little, if any, perturbation of the beam.

The BBU phenomenon in recirculating accelerators has been studied extensively. In reference 1, it is estimated that $I_s > 0.83$ mA in the NBS RTM. The original proposal[3] for the development of the NIST RTM envisioned an experimental study of BBU, but it was not believed to be a limiting factor in machine performance since the design maximum average current is 0.55 mA, well below the predicted threshold.

It is necessary to reexamine the BBU problem as it applies to the NIST RTM because of the plan to inject beam into the RTM at a subharmonic of the accelerating frequency, f_0. Subharmonic injection is used to increase the peak beam current and thus increase the gain of the Free Electron Laser which is the primary planned user of the RTM, without increasing the average current, which is limited by available RF power.[2] All existing calculations of recirculating BBU (to the best of our knowledge) make use of an average over the phases of the electron beam bunches relative to the blowup mode. This averaging process is valid in the every-bucket-filled case unless $f/f_0 = n/2 \pm O(1/Q)$, where f is the blowup-mode frequency, n is an integer, Q is the (loaded) quality factor of the blowup mode, and O indicates "of the order". If the beam is injected at subharmonic h of the accelerating frequency (so that the beam repetition frequency is f_0/h), the averaging process is invalid when

$$f/f_0 = n/(2h) \pm O(1/Q) \quad . \tag{1}$$

Existing data on the mode pattern of the side-coupled structure used in the RTM indicates that the harmonic condition probably occurs for two modes in the TM_{11} band.[4] It is therefor necessary to include this possibility in the BBU calculations.

The goals of the present study are to predict the BBU threshold current for the RTM and to find practical methods to raise the threshold, if necessary. A realistic computer model of BBU must include:

1. the ability to calculate I_s when an harmonic condition, as defined by equation (1), exists;
2. the effect of the reversed-first-return geometry of the RTM;
3. the full effect of the focusing system of the RTM; and
4. the effect of the coupled-cell nature of the RF structure, which is expected to affect the width of the resonances as well as influence the value of I_s.

The model is being developed in stages to facilitate comparison with previous work, and to allow assessment of the importance of the various effects. As the computer model is developed, it will be used as a guide to the experimental program of determining I_s and to choosing operating conditions which will raise the BBU threshold.

Formulation of the Problem

The present computer model contains the following major approximations:

1. The accelerating section of the RTM is represented by a single, short cavity in which the energy gain per pass is ΔW. This cavity supports several BBU modes, such that the ratios of the BBU mode frequencies to the accelerating mode frequency are
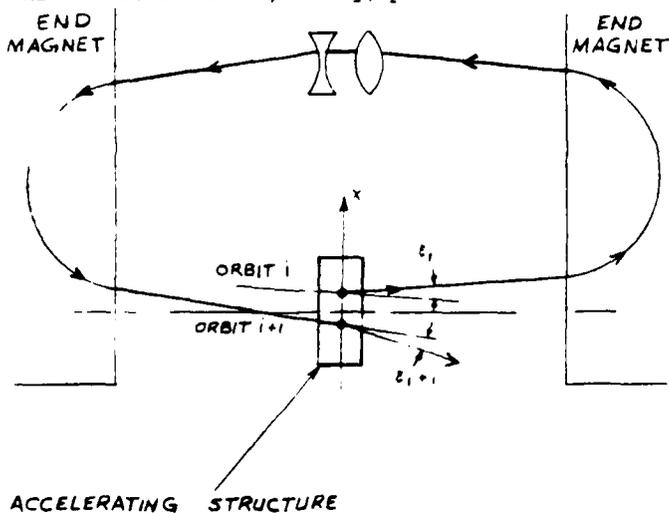

ORBIT i

ORBIT i+1

ℓ_i

ℓ_{i+1}

x

END MAGNET

END MAGNET

ACCELERATING STRUCTURE

Figure 1. Schematic drawing of the basic mechanism of recirculating regenerative BBU.

$\eta = f/f_0$. The different BBU modes are assumed to act independently on the beam, so that each has its own value of I_s. The lowest calculated I_s is taken to be the actual BBU threshold.

2. The focusing of the RIM is represented by a set of 2 X 2 transfer matrices, R_{jk}, representing the motion, in one of the transverse planes, between the center of the accelerating section on passes j and k. Together with approximation 1, this implies that the beam-accelerator interaction on pass j occurs at energy

$$W_j = W_0 + (j-1/2) \Delta W \quad . \qquad (2)$$

Transverse-longitudinal coupling, which can affect the transverse position of the beam centroid when focusing elements are used on the RIM return paths, is ignored. Subject to these approximations, I_s is calculated as outlined below.

The stored energy, U, in the cavity, <u>in the BBU mode</u> at time t is governed by the equation

$$\frac{dU}{dt} + \frac{2\pi f}{Q} U = P(t) \quad , \qquad (3)$$

where P(t) is the power input to the mode by the beam, averaged over a time of order $\tau = Q/(2\pi f)$, the decay time of the BBU mode (when P=0). U is related to the electric field amplitude, E, (in a pillbox cavity of length l) by the shunt impedance, R, given by

$$R = E^2 l^2 Q/(8\pi f U) \quad . \qquad (4)$$

The axial electric field, E_z, and the transverse magnetic field, B_y, are given by

$$E_z = -(\pi f E x/c) \sin 2\pi f t \qquad (5)$$

and

$$B_y = (E/2c) \cos 2\pi f t \quad , \qquad (6)$$

where x is the transverse coordinate measured from the cavity axis. The angular deflection of the beam centroid on pass j due to B_y is

$$\xi_j = -(eEl/2W_j) \cos 2\pi f t \quad . \qquad (7)$$

The beam centroid displacement on any later pass, k, due to ξ_j, is $x_k = (R_{jk})_{12} \xi_j$. The energy transferred from a pulse of electrons (which passes through the cavity at displacement x and at time t) to the cavity is $\Delta U(t) = q(t) l E_z(x,t)$.

We must sum the energy inputs over all passes for each pulse. The result is

$$\Delta U = \frac{\pi e l^2 f \alpha E^2}{2c} \sum_{k=2}^{J} \sum_{j=1}^{k-1} F_{jk} \sin(\phi + \theta_k) \cos(\phi + \theta_j) \quad , \qquad (8)$$

where: J = number of passes through the cavity, $F_{jk} = (R_{jk})_{12}/W_j$, $\phi = 2\pi f t_1$ is the arbitrary initial phase of the beam pulse (on pass 1 relative to the phase of the blowup-mode RF field),

$\theta_j = 2\pi \eta \sum_{i=1}^{j-1} N_i/\beta_i$ is the beam phase advance relative to the blowup mode from pass 1 to pass j ($\theta_1 = 0$ and β_i is the velocity of the beam on pass i, in units of the speed of light), and N_i is the circumference of the orbit on pass i in units of the accelerating mode free-space wavelength $\lambda = c/f_0$.

In obtaining equation (8) we have used the fact that the total transit time,

$f_0^{-1} \sum_{i=1}^{J-1} N_i/\beta_i$, is much less than τ, so that E can be taken to be time-independent. The beam consists of a series of infinitesimally short pulses, each containing charge q, at the repetition frequency f_0/h, so that the time-averaged beam current is $I = qf_0/h$. Time averaging equation (8) leads to

$$P = el^2 f I E^2 S(\phi)/(4c) \quad , \qquad (9)$$

where

$$S(\phi) = \frac{2}{M} \sum_{m=1}^{M} \sum_{k=2}^{J} \sum_{j=1}^{k-1} F_{jk} \sin(\phi_m + \theta_j) \cos(\phi_m + \theta_k) \quad . \qquad (10)$$

In equation (10), $\phi_m = \phi + 2\pi \eta h m$, and M is the number of beam pulses over which the average is taken. Substituting equation (9) in equation (3), and using equation (4) to eliminate E, we obtain

$$\frac{dU}{dt} = \frac{2\pi f}{Q} \left(\frac{I}{I_s} - 1\right) U \quad , \qquad (11)$$

where we have defined

$$I_s = \lambda/(\pi \eta R S) \quad . \qquad (12)$$

It is clear from the form of equation (11) that if $I > I_s$, the power in the blowup mode will grow exponentially, whereas if $I < I_s$, any excitation of the mode will damp.

Harmonic vs non-Harmonic Case

We next address the dependence of S on the initial phase, ϕ. Equation (10) can be rewritten as

$$S(\phi) = \sum_{k=2}^{J} \sum_{j=1}^{k-1} F_{jk} [\sin(\theta_k - \theta_j) + \langle \cos 2\phi_m \rangle \sin(\theta_k + \theta_j) + \langle \sin 2\phi_m \rangle \cos(\theta_k + \theta_j)] \quad , \qquad (13)$$

where $\langle \ \rangle$ indicates averaging over m. If ηh is any integer or half-integer, $\langle \cos 2\phi_m \rangle = \cos 2\phi$ and $\langle \sin 2\phi_m \rangle = \sin 2\phi$. For any other value of ηh, these averages vanish. In the latter (non-harmonic) case

$$S = S_0 = \sum_{k=2}^{J} \sum_{j=1}^{k-1} F_{jk} \sin(\theta_k - \theta_j) \quad , \qquad (14)$$

and $I_{s0} = \lambda/(\pi \eta R S_0)$. In the harmonic case,

$$S(\phi) = S_0 + S_1 \sin 2\phi + S_2 \cos 2\phi \quad , \qquad (15)$$

where

$$S_1 = \sum_{k=2}^{J} \sum_{j=1}^{k-1} F_{jk} \cos(\theta_k + \theta_j) \quad , \qquad (16)$$

and

$$S_2 = \sum_{k=2}^{J} \sum_{j=1}^{k-1} F_{jk} \sin(\theta_k + \theta_j) \quad . \qquad (17)$$

In the harmonic case, since the buildup of the blowup mode starts from noise, it will tend to assume that phase which minimizes I_s, $I_{smin} = \lambda/(\pi \eta R S_{max})$, where, from equation (15)

$$S_{max} = S_0 + |S_1 \sin \psi + S_2 \cos \psi| \quad . \qquad (18)$$

and $\psi = \tan^{-1}(S_1/S_2)$.

General Form of the Starting Current

In both harmonic and non-harmonic cases, I_s is very sensitive to the value of η because the phase, θ_j, reaches values of the order $2\pi \eta N_j J$. For the NIST RIM, $N_1 = 101$, $N_2 = 204$, $N_j = N_2 + 2(j-2)$, and J=15. The blowup mode frequency ratios, η, are in the range 1.5 to 2. Thus, θ_j is of order 2×10^4. A change of η by one part in 10^4 can change I_s drastically. This is clearly unphysical when the blowup-mode Qs are of order 10^4. In evaluating I_s, for each value of η we find the smallest value of $I_s(\eta') \exp[2Q(\eta - \eta')/\eta]^2$, and take this to be the starting current for the mode with frequency ratio η.

The transverse time of the RIM enters the calculation via the $(R_{jk})_{12}$. These could all be made zero,

but this corresponds to a half-integer resonance condition, and is not practical, especially when the extended length of a real accelerating section is considered. However, transverse tunes, μ, in the range of 45 to 90 degrees of betatron phase per pass are possible. Thus, the F_{jk} can change sign several times in the summations, resulting in a large increase in the BBU starting current, compared to a weakly focused microtron.

From the form of equation (18), it is obvious that I_s for any given mode will be lower if the harmonic condition, equation (1), is satisfied for that mode. In our numerical studies for the NIST RTM, the harmonic-case threshold is lower than in the non-harmonic case by a factor of about two, typically, and occasionally by as much as a factor of five. However, when there are several blowup modes, one of the modes which does not satisfy the harmonic condition may have the lowest threshold. In such cases, subharmonic injection has no effect on the BBU threshold.

Results

A computer program has been written to calculate I_s in both the harmonic and non-harmonic cases. Two versions of the program are available. The more general one uses transfer matrices R_{jk} obtained from measurements or calculations. The simplified version of the program uses

$$(R_{jk})_{12} = (W_j/W_k)^{1/2} \beta \sin(k-j)\mu , \qquad (19)$$

where β and μ are constants. In this case we also use

$$N_j = N_1 + \nu(j-1) . \qquad (20)$$

Figure 2 illustrates the behavior of I_s in this simplified model as a function of μ. The parameters chosen for these sample calculations, $W_0=5$ MeV, $\Delta W=12$ MeV, and $J=15$ are appropriate for the NIST RTM. We use equation (20) for N_j, with $N_1=202$ and $\nu=2$.

In these sample calculations we use a model for the properties of the RF structure of the main accelerating section of the NIST RTM in which there are six blowup modes at frequencies near the intersections of the TM_{11} band frequencies (as a function of phase shift per cell) with a line representing the condition that the phase shift per cell be $\pm\pi\eta$ so that the beam encounters all cells at the same blowup-mode phase. This condition is used in the absence of a calculation of the effects of the finite extent of the accelerating structure, and should correspond to a lower BBU threshold than any other phase shift per cell (which would not be synchronous with the beam).

The six modes are all assigned a transverse shunt impedance of $R=20$ MΩ, and $Q=10^4$. The frequencies are known approximately from measurements made on the preaccelerator section of the NIST RTM.[4] Two of these frequencies are very close to satisfying the harmonic condition for 36th subharmonic injection, and were arbitrarily shifted to exactly satisfy equation (1). R and Q are estimates, since they have not been measured, but are believed to be conservative.

The calculations shown in figure 2 are in general agreement with the estimates in reference 1 for the magnitude of I_s and its trend to increase with stronger focusing (increasing μ and decreasing β). The decrease in blowup threshold for a subharmonically bunched beam is a new result.

The more general version of the program has been used to investigate the effect on BBU threshold of a number of particular features of the NIST RTM design. With the design parameters given above, in the particular case of a betatron tune of 45 degrees/pass, the effect of the reversed first return path (which changes N_1 from 202 to 101 leaving all other N_j unchanged and reduces β by a factor of two for the first pass only) is to reduce I_s by a factor of about
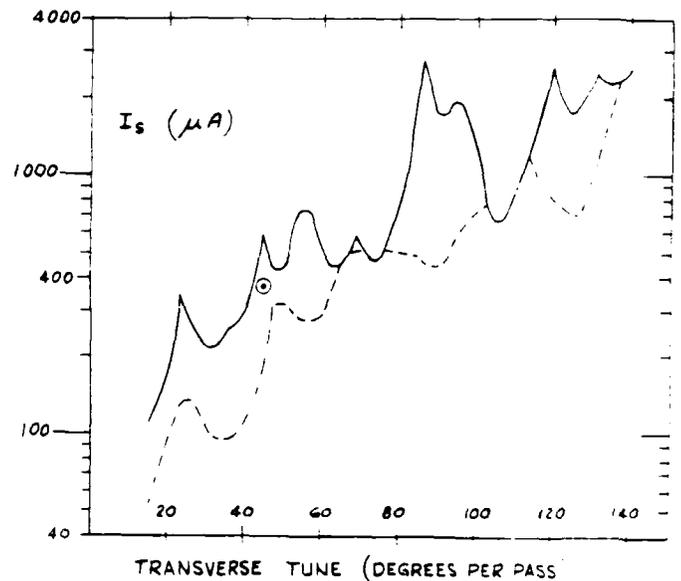

TRANSVERSE TUNE (DEGREES PER PASS

Figure 2. Predicted BBU threshold current as a function of transverse tune. The solid curve is the every-bucket-filled case, and the dashed curve is for a beam injected at the 36th subharmonic of the accelerating-mode frequency. Discontinuities in the slopes of the curves are due to changes in the mode having the lowest threshold. The circled dot at a tune of 45 degrees is the result using the more general formulation, which includes the calculated transfer matrices of the NIST RTM.

two in both the subharmonic and every-bucket-filled cases. We next used a full set of calculated transfer matrices corresponding to the nominal design of the RTM. This design uses a betatron tune of approximately 90 degrees/pass on the first three passes and 45 degrees/pass on all others. This change increased I_s, to about the original value of the simplified version of the calculation for the non-harmonic case. In this particular numerical example, there is no decrease in I_s due to bunching at the 36th subharmonic. There would have been a reduction (of about 12%) if bunching were at the 32nd subharmonic. The tendency for stronger focusing on the early passes to increase the threshold should be quite general.

The most significant omission from these calculations is the effect of the 8-m length of the accelerating structure. However, since we have chosen blowup frequencies which are synchronous with the beam, and transfer matrices for vertical motion (which corresponds to the TM_{11} polarization which couples cell-to-cell by the coupling cells of the side-coupled structure), the predicted blowup thresholds are probably conservative. By choosing an appropriate transverse tune, the threshold is expected to be above 0.5 mA in the subharmonic beam case, and above 1.0 mA in the every-bucket-filled case.

References

1. Roy E. Rand, _Recirculating Electron Accelerators_, Harwood, N. Y., 1984, Ch. 9.
2. P. Debenham, "NIST/NRL FEL Program", invited paper, this Conference.
3. _A Proposal for Research on CW Electron Accelerators Using Room Temperature RF Structures_, submitted to DoE by NBS and LANL, 1979 (unpublished).
4. _Radio Frequency Structure Development for the Los Alamos/NBS Racetrack Microtron_, Los Alamos National Laboratory report LA-UR-83-95, unpublished.

Appendix J

Analysis of Free Electron Laser Performance

Utilizing the National Bureau of Standards'

CW Microtron

Analysis of free electron laser performance utilizing the National Bureau of Standards' cw mictrotron

Cha-Mei Tang and Phillip Sprangle
Plasma Physics Division, Naval Research Laboratory, Washington, DC 20375-5000

Samuel Penner
Center for Radiation Research, National Bureau of Standards, Gaithersburg, Maryland 20899

Xavier K. Maruyama
Department of Physics, Naval Postgraduate School, Monterey, California 93943

The National Bureau of Standards' (NBS) cw racetrack microtron (RTM) will be utilized as a driver for a free electron laser (FEL) oscillator. The NBS RTM possesses many exceptional properties of value for the FEL: (i) cw operation; (ii) energy from 20–185 MeV; (iii) small energy spread and emittance; (iv) excellent energy stability; and (v) high average power. The 1D FEL gain formula predicts that the FEL would oscillate at the fundamental approximately from 0.25–10 μm when upgrading the peak current to $>$2 A. In this paper, we present 3D self-consistent numerical results including several realistic effects, such as emittance, betatron oscillations, diffraction, and refraction. The results indicate that the design value of the transverse emittance is small enough that it does not degrade the FEL performance for intermediate to long wavelengths, and only slightly degrades the performance at the shortest wavelength under consideration. Due to the good emittance, the current density is high enough that focusing, or guiding, begins to manifest itself for wavelengths > 2.0 μm.

I. INTRODUCTION

A FEL facility for applications, primarily in biomedical and material science research as well as for basic physics and chemistry, is to be situated at the National Bureau of Standards.[1,2] A cw 185-MeV racetrack microtron (RTM)[3] is under construction. The NBS Accelerator Laboratory consists of a series of interconnected, individually shielded, underground halls. The updated layout is indicated in Fig. 1. The FEL is expected to be operational by 1990.

The major limitation of a RTM as a FEL driver is that its peak current capability is lower than electron linacs which operate in the same energy range. However, the RTM is superior to pulsed linacs in energy spread and emittance. The RTM is comparable to a storage ring in terms of beam emittance and energy spread, but there is no restriction on insertion length or "stay clear" aperture. The beam energy can be varied continuously over a wide range without significant loss of performance. In addition, microtrons are compact and energy efficient. Because of the cw nature of the RTM, the generation of coherent photons is not hindered by a finite macropulse length.

The original design parameters of the NBS RTM are given in Refs. 1–3. The design calculations indicate a longitudinal emittance $\epsilon_L < 30$ keV degrees and a normalized transverse emittance[1,2] $\epsilon_N < 10$ mm mrad. Based on recent measurements of the performance of the 5-MeV injector linac, the actual values of both the longitudinal and transverse emittance are expected to be smaller than the design values. The injector system must be upgraded to provide a peak current of $>$2 A in 3.5-ps micropulses, giving electron pulse length $l_{eb} \simeq 0.1$ cm. In order to keep the average electron beam power within the capability of the existing rf power system, the new injector will fill only a small fraction of the rf buckets (e.g., 1/24, 1/120 depending on electron beam

energy). We are proceeding with a design of a photocathode injector system for this upgrade.

II. 1D FREE ELECTRON LASER ANALYSIS

A first-order evaluation of the FEL performance of the NBS RTM can be obtained from the 1D small-signal low gain formula.[4] The results indicate that sufficient gain can be obtained at fundamental wavelengths in the range from 10 μm $> \lambda > 0.25$ μm. The formula for the electric field amplitude gain G in the small-signal, low-gain regime, can be written as

$$G = F_1^2 \frac{\pi^2}{\sigma_R} \frac{I}{I_A} \frac{\lambda_w^2}{\gamma_0^3} K^2 N^3 \frac{\partial}{\partial \nu} \left(\frac{\sin \nu}{\nu} \right)^2,$$

where N is the number of wiggler periods, γ_0 is the initial relativistic gamma factor, $\sigma_R = \pi r_0^2$ is the cross-sectional
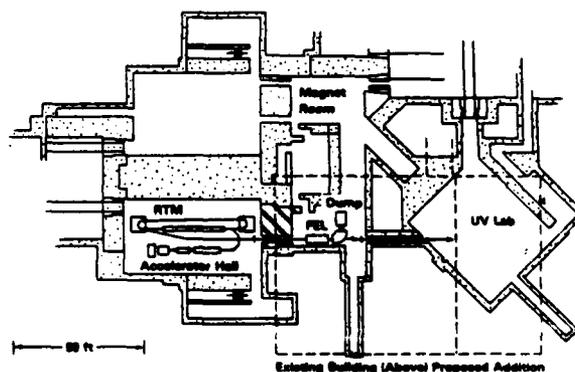

FIG. 1. Updated configuration for accelerator and FEL halls. The entire shielded complex is located 40 ft below ground level. Visible and infrared radiation will be directed to a ground level laboratory (indicated by the dashed lines) above the UV laboratory.

area of the radiation, r_0 is the minimum $1/e$ radius of the Gaussian radiation field amplitude, $I_A = 17 \times 10^3$ A, I is the current in amperes, $K = (|e|B_w\lambda_w/2\pi m_0 c^2)_{\rm RMS}$ is the wiggler parameter, B_w is the magnetic field in the wiggler, λ_w is the wavelength of the wiggler, $F_1 = J_0(b) - J_1(b)$ for a linearly polarized wiggler, $b = K^2/2(1 + K^2)$, $v = -N\lambda(w - w_0)/2c$ is the normalized frequency mismatch, and $w_0 \sim 2\gamma^2 c(2\pi/\lambda_w)/(1 + K^2)$ is the resonant angular frequency. The function $\partial/\partial v(\sin v/v)^2$ has a maximum value of 0.54 when $v = -1.3$.

The power gain can be obtained by

$$G_p = (1 + G)^2 - 1.$$

In the low-gain regime, $G_p \simeq 2G$. The FEL will oscillate when the power gain is greater than the losses per pass in the resonator. The 1D gain formula is only a rough estimate. It is sensitive to the choice of filling factor.

The conceptual design consists of a linearly polarized wiggler with a period of $\lambda_w = 2.8$ cm, and a nominal magnetic field amplitude of $B_{u0} = 5400$ G. This can be constructed with a hybrid wiggler design with the gap separating the wiggler poles of $g = 1.0$ cm. A wiggler can be constructed conceptually in more than one section, such that a wiggler of shorter length can also be available. A shorter wiggler and a corresponding vacuum chamber may be necessary for long-wavelength operation.

Figure 2 is a plot of the 1D maximum small-signal power gain versus wavelength, assuming a conservative peak current of 2 A. The open circles (O) are obtained with electron beam energies of 25, 50, 75, 125, and 175 MeV. The solid curves are obtained for the same electron beam energies, but varying the wiggler amplitude from $0.6B_{u0}$ to B_{u0}. The magnetic field in the wiggler is to be changed by varying the gap between the poles from 1.4 to 1.0 cm. As the magnetic field decreases, the wavelength of the radiation decreases, and the gain is reduced.

III. 3D EFFECTS ON THE GAIN

Since FELs are not actually 1D, 3D effects will change the gain. Some of the 3D effects that we will examine in this paper are finite transverse emittance, radiation diffraction and refraction, and some effects associated with finite-length electron pulses.
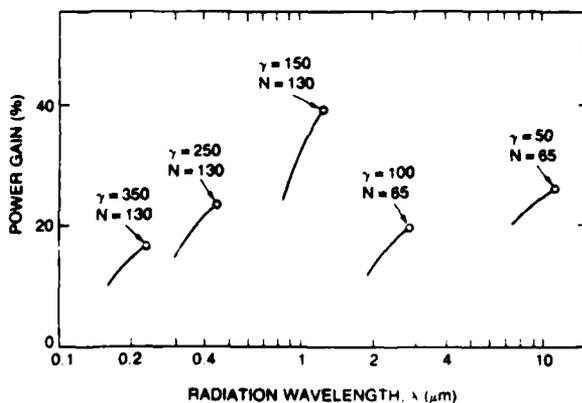
We will assess these three-dimensional effects using a fully 3D self-consistent computer code, SHERA, developed at the Naval Research Laboratory. The formulation of the wave equation is based on the source dependent expansion[5] of the radiation field, and the electron dynamics[6] are evaluated self-consistently. We assume a waterbag distribution in the 4D transverse emittance space, which leads to a parabolic profile for the electron beam density. Since the energy spread of the NBS RTM is very small, it will not be considered; and we will also not treat the effects of pulse slippage on the gain. The radiations are taken to have a Rayleigh length of 175 cm with the minimum radiation waist located at the center of the wiggler. Results for two different operating regimes will be presented.

The effect of the emittance on the performance of the FEL will be more important for short wavelength operations. Thus, our first example will be for $\lambda = 0.23$ μm with $\gamma_0 = 350$. The pulse slippage distance, $N\lambda = 0.003$ cm, is much shorter than the electron pulse length l_{eb}. The minimum $1/e$ radiation field amplitude waist is $r_o = 3.57 \times 10^{-2}$ cm. Plots of the power gain G_p versus the normalized frequency mismatch v are shown in Fig. 3. Curve (a) gives the 1D estimate of the gain. Curves (b)–(d) are the gains calculated from the computer code for normalized transverse emittance of $\epsilon_N = 5$, 10, and 20 mm mrad, respectively. the radii of the electron beams were determined by properly matching the beam into the wiggler, i.e., the radii of the beams inside the wiggler is uniform. The matched beam radius condition is

$$r_{eb} = (\epsilon_N/\gamma K_\beta)^{1/2},$$

where $K_\beta = \sqrt{2}\pi K/\lambda_w\gamma$ is the betatron wave number for the wiggler with parabolic pole faces,[7] where the focusing in
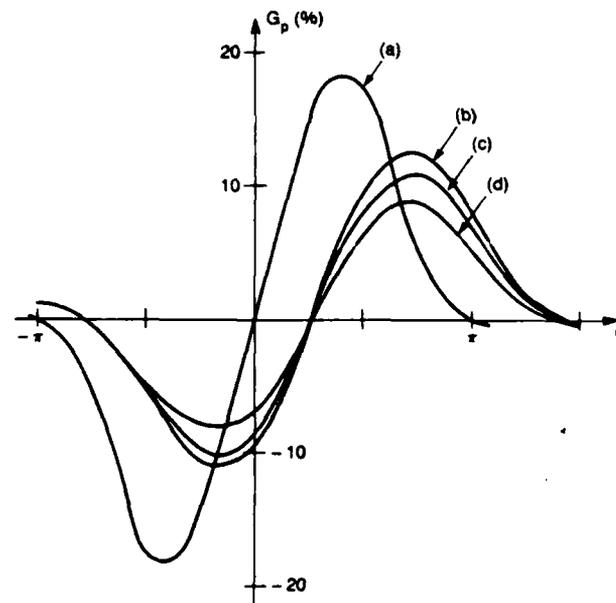

FIG. 2. Small-signal power gain vs wavelength based on 1D calculation.

FIG. 3. Power gain G_p vs frequency mismatch v at $\lambda = 0.23$ μm with $\gamma_0 = 350$. Curve (a) is based on 1D gain formula. Curves (b)–(d) are obtained from simulations with normalized transverse edge emittances of ϵ_N = 5, 10, and 20 mm mrad, respectively.

both transverse directions is equal. The matched edge radius of the electron beam can be rewritten as

$$r_{eb} = (\lambda_w \, \epsilon_N / \sqrt{2}\pi K)^{1/2},$$

independent of the beam energy. The matched edge radii of the electron beam are $r_{eb} = 1.77 \times 10^{-2}$, 2.50×10^{-2}, and 3.54×10^{-2} cm for normalized edge transverse emittances of $\epsilon_N = 5$, 10, and 20 mm mrad, respectively. If the emittance becomes larger than 20 mm mrad, the radius of the electron beam will become larger than the radiation spot size, and the gain will be substantially reduced.

The effect of finite emittance on the gain is negligible for $\lambda = 1.25 \, \mu m$ with $\gamma_0 = 150$. The pulse slippage distance in this case is 0.016 cm, and it is still unimportant. Figure 4 shows plots of the power gain G_p versus the normalized frequency mismatch ν, similar to Fig. 3. Again, curve (a) gives the 1D estimate of gain. Curves (b), (c), and (d) are the gains calculated from the computer code for normalized emittance of $\epsilon_N = 5$, 10, and 20 mm mrad, respectively. Since the wavelength is longer, the minimum $1/e$ radiation field amplitude waist becomes $r_0 = 8.3 \times 10^{-2}$ cm, and the electron beam radii are much smaller than the radiation waist. The gain at $\lambda = 1.25 \, \mu m$ is insensitive to the design value of the finite transverse emittance.

Figures 3 and 4 also show a shift of the zero crossing of the gain curves obtained from 3D simulation. This shift comes from the change in the phase of the diffracting radiation field. It has no real important effect on the oscillation criteria for the examples under consideration.

Figure 5 plots the maximum 3D power gain versus wavelength with a peak current of 2 A, for normalized emittances of 5, 10, and 20 mm mrad. Each curve is obtained for the identified electron beam energy, but varying the magnetic wiggler amplitude from B_{w0} to $0.6B_{w0}$, where the longer
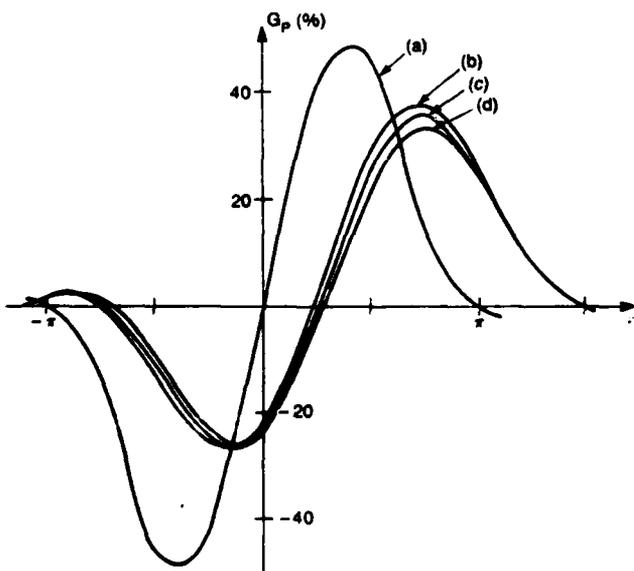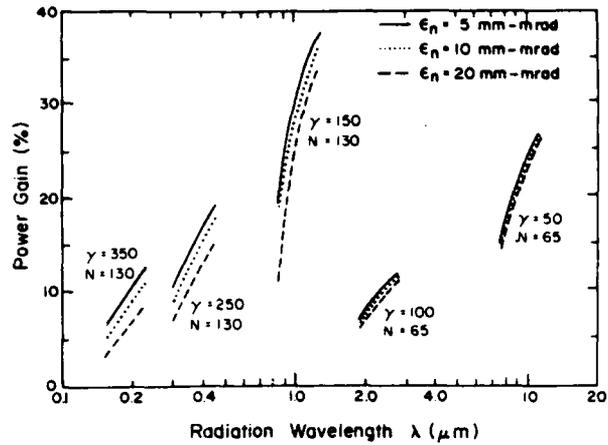

FIG. 5. Power gain vs wavelength based on a fully 3D self-consistent simulation by varying energy and emittance of the electron beam, and the magnetic field of the wiggler.

wavelength corresponds to the larger magnetic field. Normalized emittance is very good in the long-wavelength operating regime. In the shortest-wavelength operating regime, the normalized emittance larger than 5 mm mrad should be avoided.

Since the current is a function of axial position in a finite length electron pulse, and pulse slippage is unimportant, the local gain is a function of the local current in the electron pulse. For the first example at $\lambda = 0.23 \, \mu m$ with normalized transverse edge emittance $\epsilon_N = 10$ mm mrad, the simulations indicate that the gain is proportional to the local current, consistent with the 1D formula. For the second example at $\lambda = 1.25 \, \mu m$, the gain increases faster than the linear power of the current. Figure 6 is a plot of normalized power gain, i.e., power gain from simulation divided by the maxi-
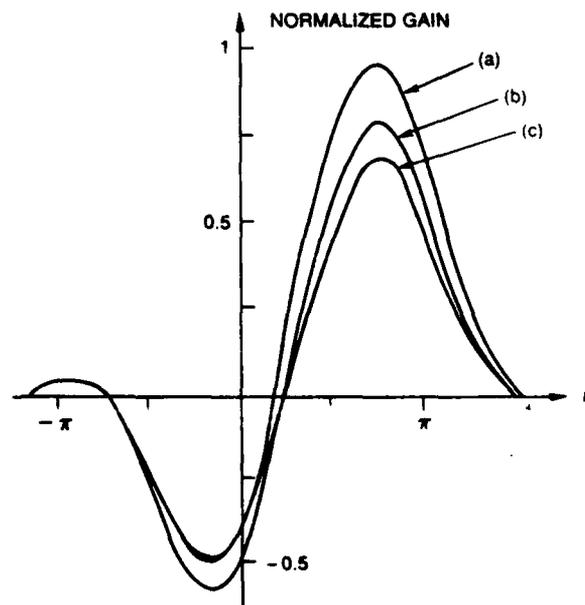

FIG. 4. Power gain G_p vs frequency mismatch ν at $\lambda = 1.25 \, \mu m$ with $\gamma_0 = 150$. Curve (a) is based on 1D gain formula. Curves (b)–(d) are obtained from simulations with normalized transverse edge emittances of $\epsilon_N = 5$, 10, and 20 mm mrad, respectively.

FIG. 6. Normalized gain vs frequency mismatch for $\lambda = 1.26 \, \mu m$ and edge emittance of $\epsilon_N = 10$ mm mrad. Curves (a)–(c) correspond to results obtained with currents of $I = 4.0$, 2.0, and 0.5 A, respectively.
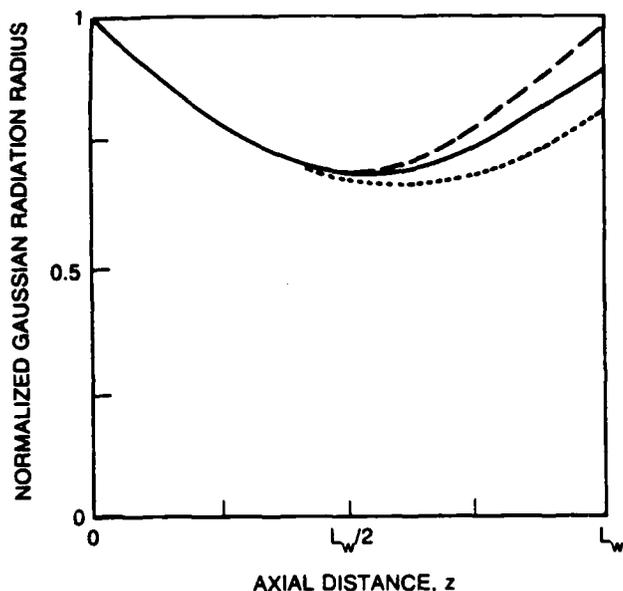
FIG. 7. Normalized 1/e Gaussian radiation field amplitude radius as a function of distance z in the wiggler with $\lambda = 1.25\,\mu$m and edge emittance $\epsilon_N = 10$ mm mrad for three different currents: dashed line: $I = 0.5$ A; solid line: $I = 2$ A; and dotted line: $I = 4$ A.

mum 1D power gain, versus the frequency mismatch at $\lambda = 1.25\,\mu$m with normalized transverse edge emittance $\epsilon_N = 10$ mm mrad for three different currents: (a) $I = 4.0$, (b) $I = 2.0$, and (c) $I = 0.5$ A. We find that the normalized gain increases as current increases. This can be explained by the self-focusing or guiding phenomenon[5,8-11] of the FEL. This is most easily observed in the plots of the normalized 1/e Gaussian radiation field amplitude radius, shown in Fig. 7. For $I = 0.5$ A, the radiation radius behaves like a free space resonator radiation field, shown by the dashed curve. For $I = 2$ A, the radiation radius is less than the free space radius at the end of the wiggler as self-focusing begins to show (solid curve). If the current can be increased to 4 A, the radiation becomes even more focused (dotted curve). The reason that self focusing is evident at such low current is that the emittance is very good and current density is high throughout the interaction region, i.e., high beam brightness

$$B_N = 2I/(\pi^2 \epsilon_N^2) > 4 \times 10^9 \text{ A}/(\text{m}^2 \text{ rad}^2) , \qquad (1)$$

where $I > 2$ A and edge emittance $\epsilon_N = 10$ mm mrad.

IV. CONCLUSIONS

The 3D self-consistent simulation results from the computer code SHERA indicate that the design value of the transverse emittance is very good, so that it does not degrade the FEL performance for intermediate to long wavelengths. For the shortest wavelength under consideration, emittance larger than 5 mm mrad should be avoided. Due to the good emittance, the current density is high enough that focusing, or guiding, begins to manifest itself for wavelengths > 2.0 μm.

ACKNOWLEDGMENT

[1] C. M. Tang, P. Sprangle, S. Penner, B. M. Kincaid, and R. R. Freeman, Nucl. Instrum. Methods A 250, 278 (1986); Free Electron Lasers, Proceedings of the 7th International Conference on FELs, edited by E. T. Scharlemann and D. Prosnitz (North-Holland, Amsterdam, 1986), p. 278.

[2] X. K. Maruyama, S. Penner, C. M. Tang, and P. Sprangle, in Free Electron Lasers, Proceedings of the 8th International FEL Conference, edited by M. W. Poole (North-Holland, Amsterdam, 1987), p. 259.

[3] S. Penner et al., IEEE Trans. Nucl. Sci. NS-32, 2669 (1985).

[4] P. Sprangle, R. A. Smith, and V. L. Granatstein, Infrared Millimeter Waves, edited by K. J. Button (Academic, New York, 1979), Vol. I, p. 279.

[5] P. Sprangle, A. Ting, and C. M. Tang, Phys. Rev. Lett. 59, 202 (1987); Phys. Rev. A 36, 2773 (1987); Free Electron Lasers, Proceedings of the 8th International FEL Conference, edited by M. W. Poole (North-Holland, Amsterdam, 1987), p. 136.

[6] C. M. Tang and P. Sprangle, IEEE J. Quantum Electron. QE-21, 970 (1985).

[7] E. T. Scharlemann, J. Appl. Phys. 58, 2154 (1985).

[8] P. Sprangle and C. M. Tang, Appl. Phys. Lett. 39, 677 (1981) See also C. M. Tang and P. Sprangle, Free-Electron Generator of Coherent Radiation, Physics of Quantum Electronics, edited by S. F. Jacobs, G. T. Moore, H. S. Piloff, M. Sargent III, M. O. Scully, and R. Spitzer (Addison-Wesley, Reading, MA, 1982), Vol. 9, p. 627.

[9] E. T. Scharlemann, A. M. Sessler, and J. S. Wurtele, Phys. Rev. Lett. 54, 1925 (1985).

[10] G. T. Moore, Opt. Commun. 52, 46 (1984); 54, 121 (1985).

[11] M. Xie and D. A. G. Deacon, Free Electron Lasers, Proceedings of the 7th International Conference on FELs, edited by E. T. Scharlemann and D. Prosnitz (North-Holland, Amsterdam, 1986), p. 426.

5236   J. Appl. Phys., Vol. 63, No. 11, 1 June 1988

Tang et al.   5236